



The anti-ageing potential of Rooibos: preserving preadipocyte function.

Anna C. Hattingh - 207017852

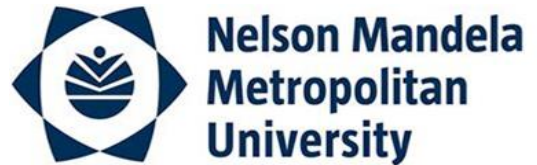
Submitted in partial fulfilment of the requirements for the degree of *Magister Scientiae* (MSc) in the Department of Biochemistry and Microbiology, in the Faculty of Science, at the Nelson Mandela Metropolitan University.

January 2015

Supervisor: Prof. Maryna van de Venter.

Co-Supervisor: Dr. Trevor Koekemoer.

**DEPARTMENT OF ACADEMIC ADMINISTRATION
EXAMINATION SECTION
SUMMERSTARND NORTH CAMPUS**



PO Box 77000
Nelson Mandela Metropolitan University
Port Elizabeth
6013

Enquiries: Postgraduate Examination Officer

DECLARATION BY CANDIDATE

NAME: Anna Cornelia Hattingh

STUDENT NUMBER: 207017852

QUALIFICATION: *Magister Scientiae* (MSc) Biochemistry

TITLE OF PROJECT: The anti-ageing potential of Rooibos: preserving preadipocyte function.

DECLARATION:

In accordance with Rule G4.6.3, I hereby declare that the above-mentioned treatise is my own work and that it has not previously been submitted for assessment to another university or for another qualification.

SIGNATURE: _____



DATE: 13 March 2015 _____

Acknowledgements

Professor Maryna van de Venter – Thank you for all your support, guidance and most importantly, patience with me during this project. It has yet again been a pleasure to work with, and learn from you. I am eternally grateful that you supported me in taking an extended “sabbatical” from my masters by accepting the EMA2SA scholarship to study at the Katholieke Universiteit Leuven in Belgium. Thank you for the extensive planning and organization that enabled me to attend the IPUF conference, as well as the GA conference in Portugal. It was an amazing experience for which I am truly thankful.

Doctor Trevor Koekemoer – Firstly, thank you for laying groundwork on which this study was built. Thank you for all your patience, ideas, advice, and for allowing (?) us to go “shopping” in your office for whatever we may have needed ☺. Thank you for ensuring that our lab always had all the required consumables and that everything ran relatively smoothly.

My family – I am sincerely grateful for your endless encouragement, support and prayers, not to mention all the “care packages” and endless supply of rusks!! Your daily phone calls and messages always brightened my day. Thank you for allowing me to follow my dreams by providing me with an education of which I can be proud.

Richard Davis – I truly cannot thank you enough for all your support and encouragement throughout this difficult year. Thank you for putting up with a part-time girlfriend, and for absolutely always being there for me, as well as making sure I remained a functional human being throughout these last few months.♥

My “maatjies” Luanne Venables & Kaitlin Sprong – Thank you for the support, encouragement and all the much needed afternoon tea sessions.

Julie Davis – I sincerely apologise for my permanent zombie-like state and for using our excessively loud kettle in the early morning hours throughout these last few months.

Professor Elizabeth Joubert – Thank you for all your assistance, as well as the preparation and characterisation of the green and fermented Rooibos extracts used in this study.

Imtiaz Khan – Thank you very much for your continued assistance and guidance with all my bursary applications.

Finally, I would like to thank the National Research Foundation, Dormehl Cunningham trust, South African Rooibos Council and the Nelson Mandela Metropolitan University for the financial support, without which none of this would have been possible.

Note to self: "Write-as-you-go".

TABLE OF CONTENTS

| | |
|---|-----------|
| List of Figures | v |
| List of Tables | ix |
| List of Abbreviations | x |
| Abstract | xiii |
| CHAPTER 1: Research rationale, aims and objectives | 1 |
| CHAPTER 2: Introduction to this study | 4 |
| 2.1 Ageing process | 4 |
| 2.1.1 Introduction | 4 |
| 2.1.2 Reactive Oxygen Species (ROS) | 5 |
| 2.1.3 The role of mitochondria in ageing | 6 |
| 2.2 Adipose tissue and ageing | 7 |
| 2.2.1 Introduction | 7 |
| 2.2.2 Regulation of adipogenesis | 8 |
| 2.3 Plant phenolic compounds | 9 |
| 2.3.1 Flavonoids | 11 |
| 2.3.2 Non-flavonoid phenolic compounds | 13 |
| 2.3.3 Health benefits and mode of action | 13 |
| CHAPTER 3: Methodology | 16 |
| 3.1 Culture conditions | 16 |
| 3.2 Endotoxin analysis | 17 |
| 3.3 Cell counts and viability | 20 |
| 3.4 Cell viability, cytotoxicity and IC ₅₀ determination | 20 |
| 3.5 Flow cytometry | 21 |
| 3.5.1 Introduction | 21 |
| 3.5.2 Flow cytometer | 23 |
| 3.5.3 Data collection and analysis | 24 |
| 3.5.4 Applications of flow cytometry | 26 |

| | | |
|---|---|-----------|
| 3.6 | Cell cycle analysis | 27 |
| 3.7 | Mitochondrial membrane potential | 28 |
| 3.8 | Mitochondrial mass determination | 30 |
| 3.9 | Metabolic assays | 31 |
| | 3.9.1 Glucose utilization assay | 31 |
| | 3.9.2 Lactate production assay | 32 |
| 3.10 | Data analysis and statistics | 33 |
| CHAPTER 4: Mitochondrial dysfunction | | 34 |
| 4.1 | Introduction | 34 |
| | 4.1.1 The mitochondria | 34 |
| | 4.1.2 Mitochondrial dysfunction | 38 |
| | 4.1.3 Role of mitochondrial dysfunction in disease and ageing | 40 |
| | 4.1.4 Cell culture models of mitochondrial dysfunction through mtDNA depletion | 41 |
| 4.2 | Methods and materials | 43 |
| | 4.2.1 Establishment of an mtDNA depleted 3T3-L1 preadipocyte cell line | 43 |
| | 4.2.2 Characterization of ρ^0 3T3-L1 preadipocytes | 44 |
| | 4.2.2.1 Cell growth characteristics | 44 |
| | 4.2.2.2 Cell cycle analysis | 44 |
| | 4.2.2.3 Mitochondrial membrane potential | 45 |
| | 4.2.2.4 Metabolic parameters: glucose utilization and lactate production | 46 |
| | 4.2.2.4.1 Glucose utilization assay | 46 |
| | 4.2.2.4.2 Lactate production assay | 46 |
| | 4.2.2.5 Confocal microscopy | 47 |
| 4.3 | Results and discussion | 49 |
| | 4.3.1 Characterization of ρ^0 3T3-L1 preadipocytes | 50 |
| | 4.3.1.1 Cell growth characteristics | 50 |
| | 4.3.1.2 Cell cycle analysis | 54 |
| | 4.3.1.3 Mitochondrial membrane potential | 56 |

| | | |
|---|---|-----------|
| 4.3.1.4 | Metabolic parameters: glucose utilization and lactate production | 59 |
| 4.3.1.5 | Confocal microscopy | 61 |
| 4.4 | Conclusion | 67 |
| CHAPTER 5: Anti-ageing properties of Rooibos: Effects on mitochondrial dysfunction | | 71 |
| 5.1 | Introduction | 71 |
| 5.1.1 | Rooibos (<i>Aspalathus linearis</i>) | 71 |
| 5.1.1.1 | Geographical distribution, classification and identification | 72 |
| 5.1.1.2 | History and commercial importance | 74 |
| 5.1.1.3 | Processing of plant material | 74 |
| 5.1.1.4 | Anecdotal and biological properties | 75 |
| 5.1.1.5 | Chemical composition | 77 |
| 5.1.1.5.1 | Factors affecting the phenolic composition of rooibos | 78 |
| 5.1.1.5.2 | Preparation and characterization of rooibos extracts | 79 |
| 5.2 | Methods and materials | 81 |
| 5.2.1 | Extract preparation and characterisation | 81 |
| 5.2.2 | Endotoxin analysis | 82 |
| 5.2.3 | Cell line maintenance | 82 |
| 5.2.4 | Experimental design | 83 |
| 5.2.5 | Cell viability and IC ₅₀ determination | 83 |
| 5.2.6 | Cell growth characteristics | 84 |
| 5.2.7 | Cell cycle analysis | 84 |
| 5.2.8 | Mitochondrial membrane potential | 85 |
| 5.2.9 | Metabolic parameters: glucose utilization and lactate production. | 86 |
| 5.2.9.1 | Glucose utilization assay | 86 |
| 5.2.9.2 | Lactate production assay | 86 |
| 5.2.10 | Confocal microscopy | 87 |

| | | |
|--------------------------------------|---|------------|
| 5.3 | Results and discussion | 88 |
| 5.3.1 | Endotoxin analysis | 88 |
| 5.3.2 | Cell growth characteristics | 89 |
| 5.3.3 | Cell cycle analysis | 93 |
| 5.3.4 | Mitochondrial membrane potential | 98 |
| 5.3.5 | Metabolic parameters: glucose utilization and lactate production | 102 |
| 5.3.6 | Confocal microscopy | 107 |
| 5.4 | Conclusion | 110 |
| CHAPTER 6: Concluding remarks | | 111 |
| References | | 115 |
| Appendices | | 138 |

List of Figures

CHAPTER 2

- | | | |
|-----|---|----|
| 2.1 | Diagram illustrating the process of adipocyte formation. | 8 |
| 2.2 | Overview of the association between primary and secondary metabolism in plants. | 10 |

CHAPTER 3

- | | | |
|------|---|----|
| 3.1 | Basic structure of LPS produced by gram negative bacteria. | 17 |
| 3.2 | Diagrammatic illustration of the principle of the Pierce LAL Chromogenic Endotoxin Quantitation Kit. | 19 |
| 3.3 | Chemical structure of Trypan blue. | 20 |
| 3.4 | Illustration of the principle reaction in the CellTiter-Blue™ cell viability assay. | 21 |
| 3.5 | Diagram illustrating the light-scattering characteristics of a cell. | 22 |
| 3.6 | Examples of single and dual parameter plots obtained from flow cytometric analysis of blood leukocytes. | 25 |
| 3.7 | Examples of the gating selection process utilized in all flow cytometry analysis experiments in this study. | 25 |
| 3.8 | Illustration of a typical eukaryotic cell cycle. | 27 |
| 3.9 | Chemical structure of propidium iodide. | 28 |
| 3.10 | Chemical structure of JC-1. | 29 |
| 3.11 | Chemical structure MitoTracker® Green FM. | 30 |
| 3.12 | Principle of the glucose oxidase assay. | 31 |
| 3.13 | Principle of the lactate oxidase assay. | 32 |

CHAPTER 4

| | | |
|------|---|----|
| 4.1 | ATP production through oxidative phosphorylation. | 35 |
| 4.2 | Organization of human mitochondrial DNA. | 37 |
| 4.3 | Phase contrast images illustrating the contrasting growth kinetics between untreated wildtype (left) and EtBr treated (ρ^0) 3T3-L1 preadipocytes (right). | 50 |
| 4.4 | Comparison of the growth rate of wildtype and EtBr treated (ρ^0) 3T3-L1 preadipocytes. | 51 |
| 4.5 | Percentage (%) cell viability of ρ^0 mutant and wildtype cells observed over 5 days in the presence of EtBr. | 52 |
| 4.6 | Representative cell cycle histograms illustrating DNA distribution for wildtype and ρ^0 mutants. | 54 |
| 4.7 | Histogram overlay representing the decreased mitochondrial membrane potential in ρ^0 mutants compared to wildtype cells as well as valinomycin treated wildtype and ρ^0 mutant cells. | 57 |
| 4.8 | Glucose utilization by ρ^0 mutants after 24, 48 and 72 hours, represented as a percentage of the wildtype control (100%). | 59 |
| 4.9 | Lactate production by ρ^0 mutants after 24, 48 and 72 hours, represented as a percentage of the wildtype control (100%). | 60 |
| 4.10 | Representative confocal microscopy images of JC-1 stained mitochondria in individually characterised wildtype and ρ^0 mutant cells. | 62 |
| 4.11 | Confocal microscopy images of MitoTracker [®] Green FM stained mitochondria in wildtype and ρ^0 mutant cells. | 63 |
| 4.12 | Confocal microscopy image of MitoTracker [®] Green FM stained mitochondria in ρ^0 mutant cells (left) accompanied by the corresponding bright field image (right). | 65 |

CHAPTER 5

| | | |
|------|---|-----|
| 5.1 | Geographical distribution of Rooibos in South Africa. | 72 |
| 5.2 | The rooibos (<i>Aspalathus linearis</i>) plant. | 71 |
| 5.3 | Comparison of the growth rate of untreated and rooibos treated wildtype cells. | 89 |
| 5.4 | Cell density of rooibos treated (100 µg/mL) wildtype cells represented as a percentage of the untreated wildtype control (100%). | 90 |
| 5.5 | Comparison of the growth rate of untreated and rooibos treated (100 µg/mL) ρ^0 mutant cells. | 91 |
| 5.6 | Cell density of rooibos treated (100 µg/mL) ρ^0 mutants represented as a percentage of the untreated ρ^0 mutant control (100%). | 92 |
| 5.7 | Representative cell cycle histograms illustrating DNA distribution for untreated and rooibos treated (100 µg/mL) wildtype cells. | 93 |
| 5.8 | Representative cell cycle histograms illustrating DNA distribution for untreated and rooibos treated (100 µg/mL) ρ^0 mutants. | 95 |
| 5.9 | Mitochondrial membrane potential of rooibos treated (100 µg/mL) wildtype cells after 24, 48 and 72 hours, represented as a percentage of the untreated wildtype control (100%). | 99 |
| 5.10 | Mitochondrial membrane potential of rooibos treated (100 µg/mL) ρ^0 mutants after 24, 48 and 72 hours, represented as a percentage of the untreated ρ^0 mutant control (100%). | 100 |
| 5.11 | Normalised glucose utilization by rooibos treated (100 µg/mL) wildtype cells after 24, 48 and 72 hours, represented as a percentage of the untreated wildtype control (100%). | 102 |
| 5.12 | Normalised lactate production by rooibos treated (100 µg/mL) wildtype cells after 24, 48 and 72 hours, represented as a percentage of the untreated wildtype control (100%). | 103 |
| 5.13 | Normalised glucose utilization by rooibos treated (100 µg/mL) ρ^0 mutant cells after 24, 48 and 72 hours, represented as a percentage of the untreated ρ^0 mutant control (100%). | 104 |

- 5.14 Normalised lactate production by rooibos treated (100 µg/mL) ρ^0 mutant cells after 24, 48 and 72 hours, represented as a percentage of the untreated ρ^0 mutant control (100%). 104
- 5.15 Representative confocal microscopy images of JC-1 stained mitochondria in individually characterised untreated (U) as well as green (G) and fermented (F) rooibos treated wildtype (left) and ρ^0 mutant cells (right). 109

List of Tables

CHAPTER 2

- 2.1 Overview of flavonoid subclasses and commonly associated dietary sources. 12

CHAPTER 4

- 4.1 Summary of cell cycle analysis results obtained for wildtype and ρ^0 mutants. 55
- 4.2 Summary of results obtained for analysis of mitochondrial membrane potential for wildtype and ρ^0 mutants. 58

CHAPTER 5

- 5.1 Characterisation of secondary metabolites in green and fermented rooibos extracts used in this study. 80
- 5.2 Summary of cell cycle analysis results obtained for untreated and rooibos treated (100 $\mu\text{g}/\text{mL}$) wildtype cells. 94
- 5.3 Summary of cell cycle analysis results obtained for untreated and rooibos treated (100 $\mu\text{g}/\text{mL}$) ρ^0 mutants. 96
- 5.4 Results obtained from post-acquisition confocal microscopy image processing indicating the $\Delta\Psi_m$ for wildtype and ρ^0 mutant cells. 107

List of Abbreviations

| | |
|-------------------|---|
| AMPK | 5' adenosine monophosphate-activated kinase |
| ATP / ADP | Adenosine triphosphate / Adenosine diphosphate |
| Bcl-2 | B-cell lymphoma 2 |
| BP | Band pass filter |
| BrdU | 5-bromo-2'-deoxyuridine |
| Ca ²⁺ | Calcium ion |
| CDK | Cyclin dependent kinase |
| CO ₂ | Carbon dioxide |
| DAPI | 4'6-diaminidine-2'-phenylindole dihydrochloride |
| DMEM | Dulbecco's Modified Eagle's Medium |
| DMSO | Dimethyl sulfoxide |
| DNA / nDNA | Deoxyribonucleic acid / nuclear deoxyribonucleic acid |
| DPBS | Dulbecco's phosphate buffered saline |
| e ⁻ | Electron |
| <i>E. coli</i> | <i>Escherichia coli</i> |
| EDTA | Ethylenediaminetetraacetic acid |
| E _m | Emission wavelength |
| ER | Endoplasmic reticulum |
| EtBr | Ethidium bromide |
| EU | Endotoxin unit |
| E _x | Excitation wavelength |
| FADH ₂ | Flavin adenine dinucleotide (reduced) |
| FBS | Foetal bovine serum |
| FOXO | Mammalian forkhead transcription factor |
| FS | Forward scatter |

| | |
|-------------------------------|---|
| G protein | Guanine nucleotide-binding protein |
| GSH | Glutathione |
| H ₂ O ₂ | Hydrogen peroxide |
| HIV | Human immunodeficiency virus |
| IC ₅₀ | Half maximal inhibitory concentrations |
| IFN-γ | Interferon gamma |
| IL-6 | Interleukin-6 |
| IR | Infrared |
| IRS-1 | Insulin receptor substrate-1 |
| JC-1 | 1 st J-aggregate-forming cationic dye: 5,5',6,6'-tetrachloro-1,1',3,3'-tetraethylbenzimidazolylcarbo-cyanine iodide |
| JNK | c-Jun-N-terminal kinase |
| K ⁺ | Potassium ion |
| LAL | <i>Limulus</i> Amebocyte Lysate |
| LDH | Lactate dehydrogenase |
| LPS | Lipopolysaccharide |
| MCP-1 | Monocyte chemoattractant protein-1 |
| MEK1/2-ERK1/2 | Mitogen-activated protein kinase/extracellular signal-regulated kinase kinase 1/2 - Extracellular signal-regulated protein kinase 1/2 |
| Mg ²⁺ | Magnesium ion |
| mtDNA | Mitochondrial DNA |
| MTT | 3-(4,5-dimethylthiazol-2-yl)-2,5-diphenyltetrazolium bromide |
| NA | Numerical aperture |
| NAD ⁺ | Nicotinamide adenine dinucleotide (oxidized) |
| NADH | Nicotinamide adenine dinucleotide (reduced) |
| NCS | Newborn calf serum |
| NF-κB | Nuclear factor κ-light-chain-enhancer of activated B cells |

| | |
|------------------------------|----------------------------------|
| NO | Nitric oxide |
| O ₂ | Molecular oxygen |
| O ₂ ^{-•} | Superoxide |
| OH [•] | Hydroxyl radical |
| ONOO ⁻ | Peroxynitrite |
| P/S | Penicillin / streptomycin |
| PI | Propidium iodide |
| PKC | Protein kinase C |
| PMT | Photomultiplier tube |
| pNA | p-Nitroaniline |
| P-nucleic acid | Cytoplasmic nucleic acid |
| RNA | Ribonucleic acid |
| ROS | Reactive oxygen species |
| SD | Standard deviation |
| SOD | Superoxide dismutase |
| SS | Side scatter |
| TCA | Tricarboxylic acid cycle |
| TLR 2/4 | Toll-like receptors 2 / 4 |
| TNF-α | Tumour necrosis factor alpha |
| USA | United States of America |
| ΔΨ _m | Mitochondrial membrane potential |
| ρ ⁰ | P-nucleic acid depleted |

Abstract

Treatments with natural products rich in anti-oxidants have attracted remarkable interest in the cosmetic and pharmaceutical industry to combat oxidative stress and reverse the effects of ageing. Rooibos (*Aspalathus linearis*) is a South African fynbos plant, well-known for its strong anti-oxidant capacity and use in many cosmetic products. However, little published research exists on its potential as an anti-ageing treatment. The anti-ageing properties of fermented and green rooibos were investigated using an *in vitro* cell culture model designed to evaluate the involvement of mitochondrial dysfunction in the age related decline in preadipocyte function. Mitochondrial DNA (mtDNA) deficient preadipocytes, ρ^0 3T3-L1 preadipocytes, were generated following continuous long-term exposure to sub lethal concentrations of ethidium bromide (EtBr). Depletion of the mtDNA resulted in a significantly reduced mitochondrial membrane potential, rate of proliferation in culture, as well as an increased glucose utilization and lactate production. Treatment with the green rooibos (100 $\mu\text{g/mL}$) stimulated cell growth rates for both the wildtype and mutant cell lines. MtDNA depleted cells showed arrest in the G1 phase ($48.8 \pm 3.34\%$) compared to wildtype cells ($44.6 \pm 1.38\%$), which was significantly attenuated after treatment with green rooibos for mutant ($42.0 \pm 0.83\%$) and wildtype ($36.5 \pm 5.80\%$) treated cells. The results obtained for glucose utilization and lactate production, indicated a significant increase in glucose utilization along with a concomitant increase in lactate production after treatment with both green and fermented rooibos for wildtype and mutant cell lines. A significant improvement in mitochondrial membrane potential was also later observed after treatment with green and fermented rooibos on both the wildtype and mutant cell lines. The results obtained indicate that rooibos extracts, particularly the green rooibos, exhibit effects which preserve the functional capacity of preadipocytes exposed to ageing related insults, and indicate that rooibos could cause a metabolic shift in cells redirecting carbon flow away from mitochondrial metabolism, and towards lactate production and consequently, cells become resistant to mitochondrial dysfunction.

Keywords: ageing, preadipocytes, rooibos, mitochondrial dysfunction.

CHAPTER 1: Research rationale, aims and objectives

The natural process of ageing in multicellular organisms is associated with the progressive accumulation of deleterious changes in the functional capacity of biological systems, which subsequently leads to an exponential decrease in the ability of cells to maintain homeostasis and ultimately increases the probability of death (Lui *et al.*, 2010; Ashok & Ali, 1999; Sohal *et al.*, 2002). Numerous molecular pathways have been identified in the ageing process however, apart from improvements in the longevity of model organisms such as mice and worms, and the fact that these pathways seem to be conserved in humans, no real advancements have been made in the field of anti-ageing. Nonetheless humans are living longer than ever, and it is predicted that by 2050 the number of people aged 65 years and older, will far exceed the number of younger people, which has numerous social, political and economic implications (Fontana *et al.*, 2014).

Although population statistics reveal that South Africa has a relatively young population, with 48.5% of the population under 24 years of age and 38.2% between the ages of 25 – 54, and that the average life expectancy has increased from 52.7 years in 2002 to 59.6 in 2013, the occurrence of age related diseases such as heart disease, diabetes, and neurodegenerative diseases has shown an even greater increase (Stats SA, 2014; The World Factbook, 2013). Ultimately, research into the ageing process is not aimed at increasing the lifespan of our species, but to rather increase the quality of life in ageing populations.

The free-radical hypothesis first proposed by Denham Harman in 1956 (Harman, 1956) is currently considered as the most accepted, and most widely tested theory of ageing. Since then, it has evolved and been modified to include the concept of oxidative stress, and therefore it is now believed that the process of ageing is induced at least in part, by an imbalance between endogenous reactive oxygen species (ROS) and anti-oxidant defences (Calabrese *et al.*, 2011). Treatment with anti-oxidants such as vitamin C, -E and polyphenols have been shown to be effective in improving resistance to oxidative stress, and subsequently prevent or improve cellular ageing (Masaki, 2010; Queen & Tollefsbol, 2010; Baret *et al.*, 2013).

Therefore it is not surprising that natural products rich in anti-oxidants have attracted remarkable interest in the cosmetic and pharmaceutical industry for its potential to restore and reverse the effects of ageing.

Rooibos (*Aspalathus linearis*) is a South African fynbos plant, well-known for its strong anti-oxidant capacity, yet little published research exists on its precise molecular and cellular involvement against ageing. Recent studies have demonstrated that preadipocytes lose their ability to replicate and differentiate during ageing (Zamboni *et al.*, 2014). Therefore it is possible that preventing preadipocyte dysfunction may slow down or even reverse age related adipose dysfunction and its associated risks.

The aim of this study was to investigate the potential anti-ageing properties of rooibos using an *in vitro* cell culture model and molecular mechanisms involved in the ageing process.

To meet the aims of this study, the objectives were:

- To establish an *in vitro* cell culture model representative of the age related decline in preadipocyte function.
- To characterise the biochemical indicators of the ageing cell culture model relative to normal cells.
- To determine the effects of rooibos on the biochemical indicators defined in the ageing and normal cell models.
- To provide evidence to substantiate the anti-ageing properties of Rooibos beyond that of its already known anti-oxidant capacity.

Overview of chapters

Key concepts, such as characteristics of ageing, adipose tissue and its involvement in ageing, as well as an overview of plant phenolic compounds, their associated health benefits and involvement in the ageing processes are reviewed in Chapter 2.

Chapter 3 provides a comprehensive description of all the principles and other background information relating to the methods used in this study, including: cell culture conditions, experimental principles, as well as a brief overview of flow cytometry which was primarily used throughout this study. Chapter 4 describes the development and characterisation of the mtDNA depleted ρ^0 3T3-L1 preadipocyte cell line as an *in vitro* cell culture model representative of mitochondrial dysfunction observed in preadipocytes during the ageing process. The ρ^0 and wildtype 3T3-L1 preadipocytes were then used, as described in Chapter 5, to determine the *in vitro* effects of green and fermented rooibos extracts on mitochondrial dysfunction through parameters such as: cell growth, mitochondrial membrane potential and metabolic parameters. Chapter 6 summarizes the findings of this study and describes considerations for its improvement. Prospective for future studies are also presented.

CHAPTER 2: Introduction to this study

2.1 Ageing process

2.1.1 Introduction

The natural process of ageing in multicellular organisms is associated with the progressive accumulation of deleterious changes in the functional capacity of numerous biological systems, including cellular function (Lui *et al.*, 2010). This subsequently leads to an exponential decrease in the ability of cells to maintain homeostasis, increasing the probability of disease and ultimately death (Lui *et al.*, 2010; Ashok & Ali, 1999; Sohal *et al.*, 2002). Even though humans have arguably been around for thousands of years, no real advancements have been made to improve the maximal lifespan of our species, or at least slow down the detrimental effects of ageing, whether it is related to our physical appearance (sagging skin, wrinkles, hair loss etc.) or age related diseases such as osteoporosis, diabetes, cancer, cardiovascular diseases, and neurodegenerative diseases such as Alzheimer's and Parkinson's (Lui *et al.*, 2010; Calabrese *et al.*, 2011).

The fundamental reason for this lies in the fact that the ageing process is extremely complex, and even though hundreds of theories have been proposed to explain the phenomenon of ageing, it is clear that not one specific theory or concept adequately describes the complete physiology and mechanisms of ageing in humans (Ashok & Ali, 1999). Currently the most accepted and widely tested theory of ageing is based on the free-radical hypothesis first proposed by Denham Harman in 1956 (Harman, 1956). Gradually, the free radical hypothesis has evolved and been modified to include the concept of oxidative stress, and therefore it is now believed that the process of ageing is induced by an imbalance between endogenous reactive oxygen species (ROS) and anti-oxidant defences, consequently allowing the accumulation of structural damage from free-radical reactions (Calabrese *et al.*, 2011; Ashok & Ali, 1999; Sohal *et al.*, 2002).

2.1.2 Reactive oxygen species (ROS)

ROS such as superoxide ($O_2^{\cdot-}$), hydrogen peroxide (H_2O_2) and peroxynitrite ($ONOO^-$), can be defined as ubiquitous, highly reactive molecules that are continuously derived both exogenously through environmental factors (environmental pollutants, solar radiation, physical stress etc.) and endogenously as by-products of normal cellular pathways through:

- Mitochondria: by product of aerobic respiration through oxidative phosphorylation (Chapter 4),
- Endoplasmic reticulum (ER): cytochrome P450 catalytic cycle in which enzymes generate ROS in order to metabolize and degrade hydrophobic toxic substances, steroids, drugs etc.,
- Phagocytes: produce ROS as a defensive response to infectious microorganisms, bacteria- and virus-infected cells, cancer cells etc.,
- Peroxisomes: by product of oxidative metabolic processes such as fatty acid β -oxidation,
- Enzymatic reactions: by-products of oxygenases such as lipo-oxygenase and COX, as well as oxidases such as NADPH- and xanthine oxidase (Barbieri *et al.*, 2003; Le Bras *et al.*, 2005; Núñez-Sellés, 2005; Alfadda & Sallam, 2012).

At low concentrations, these small, rapidly diffusing molecules play a vital role as second messengers in numerous intracellular signalling pathways including: regulation of cell growth, differentiation, proliferation, cell death through apoptosis or necrosis, induction or suppression of gene expression (AP-1, NF- κ B transcription factors), activation of cell signalling pathways (MAPK, Erk and guanylyl cyclase), energy production, as well as phagocytosis and defence against invading pathogens (Page *et al.*, 2010; Le Bras *et al.*, 2005). At slightly more elevated levels however, ROS initiates pathways for the adaptation to stress, and at even higher levels ROS can result in cell death or senescence (Chandel, 2014).

The activity of ROS is tightly regulated by intracellular anti-oxidants through preventive, repairing and scavenger mechanisms using enzymatic (superoxide dismutase, catalase and glutathione peroxidase) and non-enzymatic (methionine, glutathione, melatonin, albumin, myoglobin etc.) anti-oxidant molecules (Núñez-Sellés, 2005; Le Bras *et al.*, 2005).

An imbalance between ROS and anti-oxidant defences, associated with excessively high levels of ROS, leads to a state of oxidative stress, promoting damage to DNA, proteins and lipids.

2.1.3 The role of mitochondria in ageing

Given the damaging effects of ROS, together with the fact that mitochondria are the primary source of endogenous ROS, the free radical theory was extended to include the role of mitochondria in the ageing process, as described by D. Harman in “The biologic clock: the mitochondria?” (1972). Decades of research into the involvement of mitochondria in the ageing process ensued, and the mitochondrial free radical ageing theory is supported by several lines of evidence including:

- Mitochondrial ROS production increases with age, and is associated with a decline in mitochondrial function,
- The activity of several ROS-scavenging enzymes declines with age
- Mutations of mitochondrial DNA (mtDNA) accumulate during ageing,
- Injection of chemically uncoupled or aged mitochondria reduces cellular function in young cells,
- Reduced mtDNA damage and extended lifespans have been observed in knock-in mice with catalase overexpression localized to the mitochondria,
- Caloric restriction reduces mitochondrial ROS production, mtDNA damage and extends lifespan (Seo *et al.*, 2010; Benz & Yau, 2008; Lauri *et al.*, 2014; Bratic & Larsson, 2013)

Considerable evidence challenging this theory has also been presented, and is discussed in Chapter 4.

Numerous studies have shown that treatment with anti-oxidants such as vitamins A, C and E, and various polyphenols, are effective in improving resistance to oxidative stress and subsequently prevent or improve cellular ageing and age related diseases (Masaki, 2010; Queen & Tollefsbol, 2010; Baret *et al.*, 2013). It is therefore not surprising that anti-oxidant properties of natural products rich in anti-oxidants have attracted tremendous interest in the cosmetic and pharmaceutical industry for its potential to restore and reverse the effects of ageing.

2.2 Adipose tissue and ageing

2.2.1 Introduction

Adipose tissue is one of the largest organs in the human body, and apart from its primary energy storing function, it is also involved in immune and endocrine functions, thermoregulation, mechanical protection, and tissue regeneration (Tchkonia *et al.*, 2010). A correlation between adipose tissue and mechanisms involved in longevity, age-related diseases, inflammation, and metabolic dysfunction has been established (Tchkonia *et al.*, 2010; Sepe *et al.*, 2011). Adipose mass and tissue distribution change dramatically throughout life. In old age, adipose tissue becomes dysfunctional and is redistributed from subcutaneous to intra-abdominal visceral depots as well as other ectopic sites, including bone marrow, skeletal muscle, heart, pancreatic β cells and the liver (Sepe *et al.*, 2011; Heilbronn *et al.*, 2004).

The loss of subcutaneous adipose tissue predisposes to the development of altered cosmetic appearance (wrinkles, sunken eyes, skin folds), whereas the accumulation of visceral adipose tissue is associated with increased risk of age related diseases, including those encompassed by the metabolic syndrome such as: diabetes, hypertension, cancer, cognitive dysfunction, and atherosclerosis leading to heart attacks and strokes (Tchkonia *et al.*, 2010) Since adipose cell size and number are related to insulin sensitivity, glucose and fatty acid uptake, and cytokine release, changes in function and cellular composition of fat tissue might lead to changes in metabolic state and subsequent clinical complications (Cartwright *et al.*, 2007).

The age-related decline in adipose tissue depot size is a result of decreased adipocyte size and not a decrease in cell number, since new cells appear to be formed throughout the lifespan and fat cell number remains constant or increases in old age (Cartwright *et al.*, 2007; Kirkland *et al.*, 2002).

2.2.2 Regulation of adipogenesis

The formation of new adipocytes in adult tissues is a complex process, starting with the adipogenic commitment of mesenchymal precursor cells and ending in their terminal differentiation into metabolically active lipid laden adipocytes (Figure 2.1) (Cartwright *et al.*, 2007).

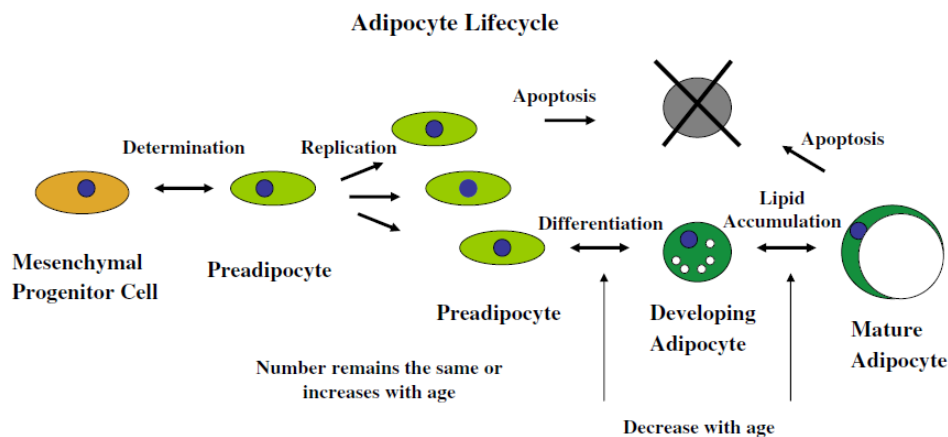


Figure 2.1: Diagram illustrating the process of adipocyte formation (Cartwright *et al.*, 2007). Preadipocyte differentiation is initiated through exposure to nutrients, hormonal effectors such as insulin, glucocorticoids and IGF-1, as well as paracrine and autocrine effectors, including free fatty acids and cyclic AMP, which activate pathways that modulate the expression and activity of a set of adipogenic transcription factors, which subsequently impacts the expression of numerous downstream differentiation dependent genes (Cartwright *et al.*, 2007)

Preadipocytes (adipocyte progenitor cells) account for 15 – 50% of all adipose tissue cells, and are capable of strongly influencing adipose tissue function (Cartwright *et al.*, 2007). The process of preadipocyte differentiation is commenced after exposure to nutrients, hormonal effectors such as insulin, glucocorticoids, paracrine and autocrine effectors, including free fatty acids and cyclic AMP (Cartwright *et al.*, 2007; Unger, 2005).

These signals subsequently activate pathways that modulate the expression and activity of adipogenic transcription factors, which ultimately affect the expression of thousands of downstream differentiation-dependent genes. It has been shown that extensive changes in preadipocyte function occur with ageing, including a decreased capacity to replicate and differentiate (Tchkonia *et al.*, 2010; Cartwright *et al.*, 2007) and that these age-dependent cell dynamic features are specific and inherent to the ageing preadipocyte. Reduced adipogenesis contributes to fat cell dysfunction, reduced fat depot size, and redistribution of fat to non-adipose tissues (Cartwright *et al.*, 2007).

Although the precise mechanism responsible for this age associated decline in preadipocyte function remains to be established, it has been suggested that factors which are likely to contribute include oxidative stress, hypoxia and mitochondrial dysfunction, and inflammation (Tchkonia *et al.*, 2010; Sepe *et al.*, 2011).

Therefore, considering the central role of mitochondria in the ageing process, as well as its involvement in preadipocyte dysfunction, the primary aim of this study was to develop an *in vitro* cell culture model, representative of mitochondrial dysfunction associated with the age related decline in preadipocyte function.

2.3 Plant phenolic compounds

Plant metabolism is divided into primary and secondary metabolism. Primary metabolism produces essential lipids, proteins, carbohydrates, and nucleic acids required for growth and development, whereas secondary metabolic pathways (shikimate, phenylpropanoid, and flavonoid pathways) produce metabolites such as alkaloids, terpenoids, and phenolic compounds, which provide unique survival or adaptive strategies according to the particular requirements of the plant (Giada, 2013; Jaganath & Crozier, 2010). An overview of the association between the primary and secondary metabolism in plants can be seen in Figure 2.2.

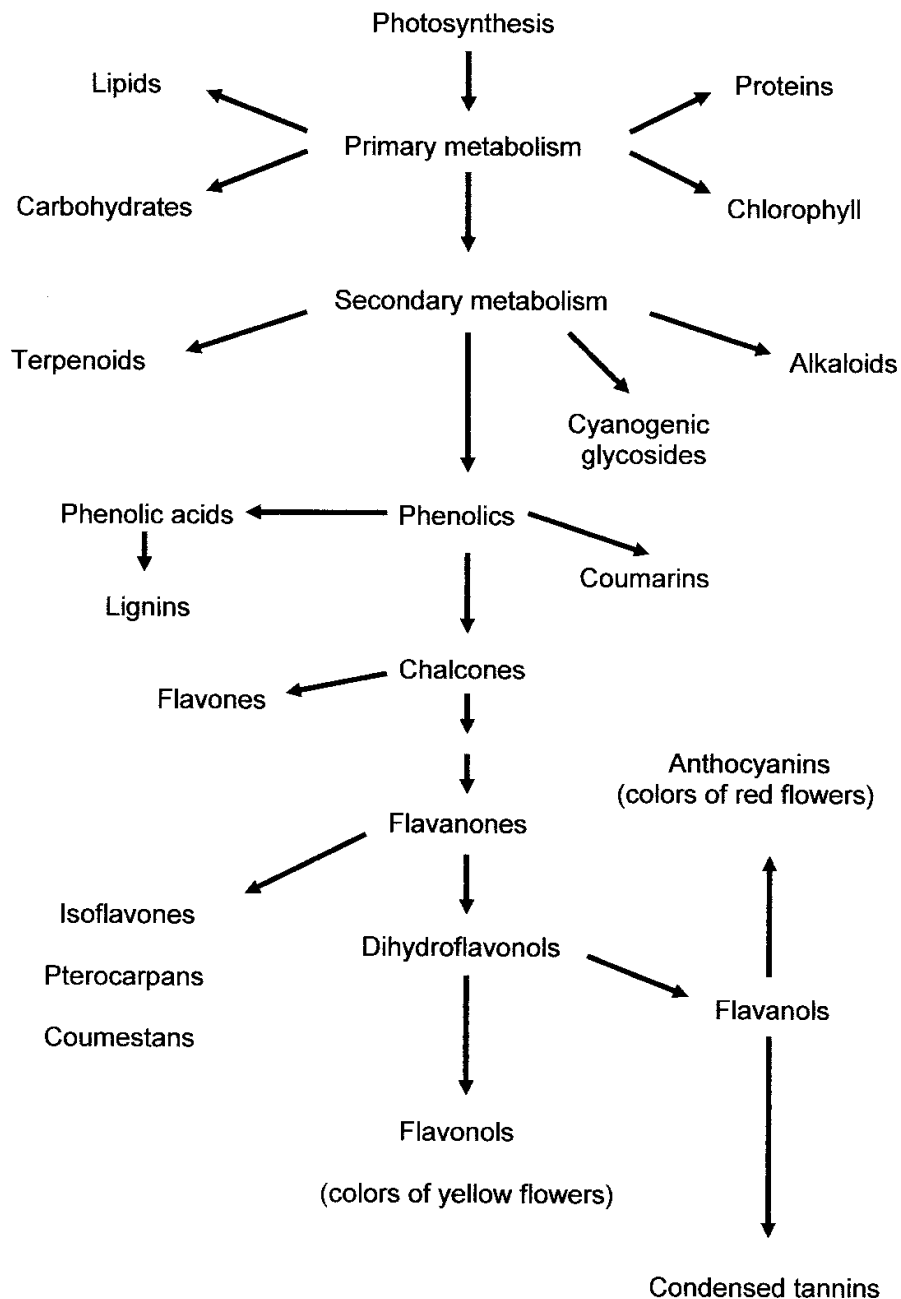


Figure 2.2: Overview of the association between primary and secondary metabolism in plants (Giada, 2013).

In plants, secondary metabolites have numerous functions including: sensorial properties including colour, aroma, taste, astringency, as well as providing structural support, stress protection, natural defence against predation, assisting the germinative processes of seeds and subsequent development and reproduction, not to mention their role as signalling molecules between plants and their environment (Han *et al.*, 2007; Jagannath & Crozier, 2010).

Apart from their functional roles in plants, secondary metabolites have gained increased commercial significance for their use as dyes, fibres, glues, oils, waxes, perfumes, flavouring agents, as well as being regarded as potential sources of new natural drugs, antibiotics, insecticides, and herbicides (Jaganath & Crozier, 2010). The important role of phytochemicals as protective dietary components has become a significant area of research, and numerous studies have shown that modest long-term intake may be beneficial in the prevention or treatment of degenerative diseases such as cardiovascular diseases, diabetes, obesity, cancer, osteoporosis, neurodegenerative diseases and ageing (Scalbert *et al.*, 2005; Jaganath & Crozier, 2010; Kim *et al.*, 2014). While extensive literature is available on the proposed health benefits of phytochemicals, evidence-based information regarding the exact molecular, cellular and physiological mechanisms, as well as possible adverse or toxic reactions are however quite limited.

Phenolic compounds constitute one of the largest and most widely distributed groups of phytochemicals, comprising more than 8000 isolated compounds, all of which are identified by a shared common structural feature, namely one or more aromatic rings bearing at least one hydroxyl group (Giada, 2013; Jaganath & Crozier, 2010). Although phenolic compounds exhibit remarkable structural diversity, they can be broadly categorized into flavonoids and non-flavonoid phenolic compounds.

2.3.1 Flavonoids

Flavonoids are widely distributed throughout nature, and are commonly located in the nucleus of mesophyll cells and within ROS generating centres of plants (Kumar & Pandey, 2013). Unsurprisingly they have been identified as some of the most potent anti-oxidants in plants, and have thus been widely studied for their associated diversity of health benefits. Flavonoids occur as aglycones, glycosides, and methylated derivatives. Esterification with glucose or other carbohydrates (glycosides) increases their solubility in water, whereas methyl and isopentyl group substitutions result in lipophilic configurations (Han *et al.*, 2007; Jaganath & Crozier, 2010). Flavonoids are structurally defined as polyphenolic compounds consisting of 15 carbons, with 2 aromatic rings connected by a 3-carbon bridge.

Based on modifications of the central C-ring, further structural classifications can be identified including: flavonols, flavones, flavan-3-ols, flavanones, isoflavones, and anthocyanidins and coumarins (Table 2.1). In an alternative arrangement, the 6-membered heterocyclic ring C is replaced by a 5-membered ring, as is observed in chalcones.

Table 2.1: Overview of flavonoid subclasses and commonly associated dietary sources.

(Adapted from Han *et al.*, 2007; Jaganath & Crozier, 2010)

| Class | Compounds | Dietary sources |
|-----------------------|---|--|
| Flavanols | Kaempferol | Apples, berries, broccoli, onions, tea, black grapes |
| | Myricetin | Apple, berries, tea, beans |
| | Quercetin | Apples, berries, grapes, olives, raisins, chilli pepper, lettuce, onions, tomatoes, coriander, tea, oregano, sage, thyme |
| Flavones | Apigenin | Olives, celery, parsley, marjoram, sage, berries |
| | Luteolin | Olives, lemon, chilli pepper, oregano, sage, thyme, celery, red pepper, apples, parsley, cereals |
| Flavanones | Hesperetin | Lemon, lime, orange, cumin, peppermint |
| | Naringenin | Grapefruit, oranges, berries |
| Flavan-3-ols | <i>Monomers</i> | Apples, apricots, berries, grapes, beans, chocolate, tea, red wine |
| | (+)-Catechins, (+)-Epicatechin | |
| | <i>Polymers and oligomers</i> Proanthocyanidins / Condensed tannins | Sour cherry, greengage plums, cherry, apricots |
| Anthocyanins | Cyanidin | Apples, berries, cocoa, asparagus, black grapes, red wine |
| | Delphinidin | Pomegranate, berries, aubergine skin |
| | Malvidin | Grape, blueberry |
| Isoflavones / flavans | Genistein | Soybeans, black beans, peas, sprouts |
| | Daidzein | Soybeans, black beans, peas, sprouts |

Dietary sources of polyphenols have received decidedly more attention over the last few years, which is expected considering the vast amount of epidemiological studies supporting the notion that a high dietary intake of fruits, vegetables and other plant products rich in polyphenols, is conducive towards a decreased risk of diseases such as cancer, neurodegenerative and cardiovascular diseases (Crozier *et al.*, 2009; Hu, 2011).

Additionally, natural compounds are often regarded as a safer alternative to conventional pharmaceutical drugs, and is generally also more accepted by the public, and more easily integrated into lifestyle changes (Kim *et al.*, 2014).

2.3.2 Non-flavonoid phenolic compounds

Of most significant dietary importance are phenolic acids and the polyphenolic stilbenes. Phenolic acids can be classified into two main groups namely hydroxybenzoic acids, containing seven carbon atoms, or hydroxycinnamic acids, containing nine carbon atoms. Phenolic acids are rarely found as free acids, possibly due to their toxic nature, and generally form part of complex structures such as lignins and hydrolyzable tannins, but can also be found linked to cellulose, proteins, flavonoids, glucose, terpenes etc. (Jaganath & Crozier, 2010; Giada, 2013). Phenolic acids are abundant in nature, and known to have high anti-oxidant activities, especially hydroxycinnamic acid, caffeic acid and chlorogenic acid (Giada, 2013).

Resveratrol is one of the most well characterised polyhydroxylated stilbenes, and is known to affect numerous biological processes. Interestingly, studies have shown that resveratrol promotes mitochondrial biogenesis during ageing (Ungvari *et al.*, 2011). Furthermore, another study combined resveratrol and the isoflavone equol, in a novel treatment strategy to investigate the combined effect of these polyphenols in the enhancement of mitochondrial biogenesis (Davinelli *et al.*, 2013). Their results indicated that co-administration of these natural products increased mitochondrial mass and mtDNA content through the upregulation of mitochondrial biogenesis enzymes in human endothelial cells (Davinelli *et al.*, 2013). Therefore supporting the role of polyphenols in the treatment of ageing and age related diseases.

2.3.3 Health benefits and mode of action

The biological activity of phenolic compounds is dependent on their chemical structure, relating to the structural class, degree of hydroxylation, substitutions and conjugations, as well as the degree of polymerization (Scalbert *et al.*, 2005).

These structural characteristics determine the redox potential of phenolic compounds, which allows them to act as reducing agents, hydrogen donors, and singlet oxygen quenchers, as well as influencing their ability to subsequently stabilize the scavenged radicals. Phenolic compounds are able to act as anti-oxidants through several ways:

- Radical scavenging through hydrogen or electron donating reactions to hydroxyl, peroxy, and peroxynitrite radicals, thereby stabilizing them and producing a relatively stable phenolic radical,
- Chelating metal ions such as copper (Cu) and iron (Fe) involved in the generation of free radicals through the Fenton reaction or related enzymatic reactions,
- Direct interaction with proteins / enzymes through the hydrophobic benzenoid rings and hydrogen-bonding potential of the phenolic hydroxyl groups, subsequently inhibiting enzymes involved in free radical generation, or interacting with receptors and enzymes involved in signal transduction ultimately modulating vital intracellular signalling cascades (Scalbert *et al.*, 2005; Pereira *et al.*, 2009; Jaganath & Crozier, 2010; Kumar & Pandey, 2013).

The biphasic effects of polyphenols have also been identified, with many polyphenols exhibiting both anti- and pro-oxidant activities *in vitro* and *in vivo* (Hu, 2011, Kim *et al.*, 2014). Small phenolic compounds such as quercetin and gallic acid are easily oxidized and exhibit significant pro-oxidant activities, whereas phenolics with higher molecular weights, such as condensed and hydrolysable tannins, have little or no pro-oxidant activity (Hu, 2011). Pro-oxidant activities are associated with increased ROS levels and/or modulation of endogenous anti-oxidant defences such as depletion of cellular GSH, resulting in enhanced oxidative damage to cellular components, and ROS-induced apoptosis (Hu, 2011). The balance between anti-oxidant/pro-oxidant activities are said to be determined, at least in part, by oxidative status within the cellular environment (Joubert *et al.*, 2005; Magcwebeba, 2013). Considering that normal cells generally have a lower basal intracellular ROS level, together with functional anti-oxidant defence mechanisms, pro-oxidant activities would have a significantly reduced impact, relative to that of stressed or diseased cells with high intracellular ROS and ineffective anti-oxidant defences (Gibellini *et al.*, 2010).

Consequently, pro-oxidant activities of phenolic compounds have attracted tremendous interest in chemoprevention, due to their ability to induce selective toxicity towards tumour cells (Scalbert *et al.*, 2005; Jaganath & Crozier, 2010; Magcwebeba, 2013).

Phenolic compounds are capable of exhibiting pleiotropic effects, which in combination provide better protection against chronic disease (Jaganath & Crozier, 2010). Synergistic effects of phenolics with other phenolics, and anti-oxidants such as vitamin C, -E, and -A have been reported, especially when anti-oxidative agents with different modes of action are combined in an effort to increase efficacy whilst minimizing toxicity (Jaganath & Crozier, 2010; Giada, 2013).

Apart from the well characterized anti-oxidant and pro-oxidant activities of phenolic compounds, numerous other biological effects and mechanisms of action have been reported in association with the extensive health benefits of phenolic compounds including, but not limited to: anti-allergic, anti-atherosclerotic, antibacterial, antidiabetic, anti-inflammatory, antimutagenic/anticarcinogenic and antiviral activity (Jaganath & Crozier, 2010; Kumar & Pandey, 2013). Additionally, effects such as cardioprotection, endothelial protection, hepatoprotection, hormone modulation, immune protection and neuroprotection have also been observed (Jaganath & Crozier, 2010; Kumar & Pandey, 2013; Giada, 2013).

In most cases, conclusive and direct experimental support is however still lacking. Nonetheless, although progress has been hindered by the complex mechanisms of action and non-specific effects due to polyphenols with pleiotropic activities, interactions with polyphenols and several biochemical pathways have been well characterised and include: modulation of the NF- κ B signalling pathway, upregulation of nuclear transcription factor erythroid 2p45 (NF-E2) related factor 2 (Nrf2), suppression of Activator protein-1 (AP-1), induction of MAPK signalling, etc. (Scalbert *et al.*, 2005; Hu, 2011; Kim *et al.*, 2014). Therefore this provides countless new opportunities to further investigate the potential of polyphenols in the treatment of disease.

CHAPTER 3: Methodology

This chapter provides a description of all the principles and other background information relating to the methods used in this study. Detailed methods and materials information are described in the relevant chapters. A comprehensive materials list can be found in Appendix I.

3.1 Culture conditions

In this study 3T3-L1 preadipocyte cells, kindly donated by the South African Medical Research Council (MRC, Cape Town, South Africa), were used. The 3T3-L1 preadipocyte cell line is a continuous substrain of Swiss albino (3T3) mouse embryonic tissue fibroblasts, originally isolated by Dr. Howard Green of Harvard Medical School (Green & Kehinde, 1975). Under appropriate conditions, 3T3-L1 preadipocytes can be differentiated into adipocytes and have therefore been fundamental in mammalian adipogenesis and metabolic disease research specifically relating to diabetes and obesity (Zen-Bio, 2010).

Adherent 3T3-L1 preadipocytes were routinely maintained in 10 cm culture dishes with Dulbecco's modified Eagle's medium (DMEM) containing 4 mM L-glutamine, 4.5 g/L glucose and sodium pyruvate, supplemented with 10% foetal bovine serum (FBS) (GE Healthcare Life Sciences, Logan, Utah, USA). Constant environmental conditions were maintained by keeping cells in a humidified 37°C incubator continuously supplied with 5% CO₂, which assists in maintaining the pH at physiological levels (pH 7.2 – 7.4). No antibiotics were added during routine maintenance, however, 1% (v/v) penicillin / streptomycin (P/S) (Sigma-Aldrich, St. Louis, MO, USA) was added to long term experiments exceeding 5 days. Throughout experimental procedures cells were seeded during log phase, at a density of 20 000 cells/mL, unless otherwise stated, in appropriate culture vessels – as indicated by the requirements for each experiment. Cells were left overnight to attach and recover before exposure to treatments. Cultures were routinely observed using an Axiovert 40C inverted microscope (Carl Zeiss, Göttingen, Germany) with phase contrast. Whenever necessary, photographs were taken using a PowerShot A640 digital camera (Canon, China).

3.2 Endotoxin analysis

Endotoxin is a lipopolysaccharide (LPS) component of the outer cell membrane of gram-negative bacteria. LPS consists of a hydrophilic polysaccharide tail, comprising a core polysaccharide and a repeating O-specific polysaccharide region (O-antigen), covalently bound to a highly conserved hydrophobic lipid group (lipid A) (Figure 3.1) (Ryan, 2008; Zu *et al.*, 2009).

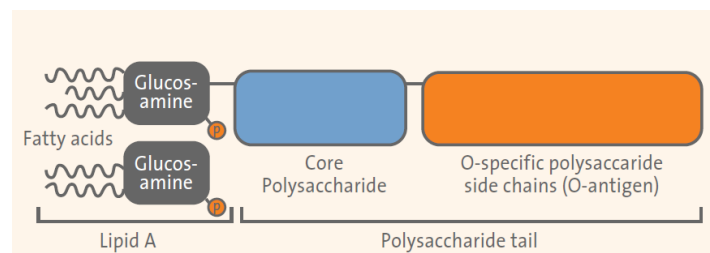


Figure 3.1: Basic structure of LPS produced by gram negative bacteria (Ryan, 2008).

The molecular weight ranges from 3000 – 40 000 Daltons according to the size of the highly variable O-specific polysaccharide side chains. Lipid A is the active moiety responsible for most of its biological effects (Dawson, 1998; Ryan, 2008).

Lipid A anchors LPS to the bacterial membrane, and is the active moiety responsible for most of its biological effects through the interactions of its fatty acid chains with lipid membranes and hydrophobic regions of proteins, as well as its phosphate groups that react with cationic proteins (Dawson, 1998; Ryan, 2008). The O-antigen elicits specific antigenic responses in humans due to its high variability between and within bacterial species, ultimately providing immunity against gram negative infections (Ryan, 2008; Zu *et al.*, 2009). These amphipathic molecules are classed as pyrogens due to their ability to induce an intense immune response, most commonly a fever, upon injection or infection of a mammalian body (Dawson, 1998; Sandle, 2012).

The effects of endotoxins on *in vitro* cell functions and growth vary greatly depending on the culture conditions, as well as the cell type and specific cell line (Ryan, 2008). Adipocytes are particularly sensitive to LPS and other factors such as tumour necrosis factor- α (TNF- α), interleukin-6 (IL-6), and interferon- γ (IFN- γ) (Chirumbolo *et al.*, 2014).

This is due to the fact that apart from its primary energy storing function, adipose tissue also forms an integral component of the innate immune response, mediated primarily through highly conserved pattern recognition receptors such as toll-like receptors (TLRs) (Schäffler & Schölmerich, 2010; Tchkonina *et al.*, 2010). Adipocytes constitutively express toll-like receptor 4 (TLR4), which can be activated by the lipid A moiety of LPS, resulting in:

- Lipolysis through the stimulation of MEK1/2-ERK1/2 signalling pathways, resulting in the up-regulation of hormone sensitive lipase and adipose triglyceride lipase expression, as well as down-regulating and phosphorylating perilipins, which coat lipid droplets in adipocytes (Zu *et al.*, 2009; Cullberg *et al.*, 2014).
- Insulin resistance and inflammation. Activation of TLR4 not only stimulates the secretion of proinflammatory adipocytokines such as monocyte chemoattractant protein-1 (MCP-1), a key regulator of macrophage recruitment, but also up-regulates toll-like receptor 2 (TLR2) expression (Lin *et al.*, 2000; Ajuwon *et al.*, 2009; Quintero-Fabián *et al.*, 2013; Cullberg *et al.*, 2014). TLR2 recognizes multiple ligands and induces a chronic inflammatory state through the expression of IL-6 and down-regulation of adiponectin receptors 1 and 2 in adipocytes (Lin *et al.*, 2000; Ajuwon *et al.*, 2009). Perhaps most importantly is the increased nuclear factor-kappa B (NF- κ B) signalling and expression of inflammatory cytokines such as TNF- α and IL-6 (Berg *et al.*, 2004; Song *et al.*, 2006; Quintero-Fabián *et al.*, 2013; Chirumbolo *et al.*, 2014). TNF- α directly impairs insulin sensitivity and stimulates lipolysis, whereas IL-6 inhibits insulin action through the inhibition of insulin receptor, insulin receptor substrate-1, and glucose transporter type 4 expression (Harkins *et al.*, 2004; Song *et al.*, 2006). Furthermore, LPS can induce increased IL-6 production through several other signalling pathways including: JNK, ERK, inhibitory G protein and PKC mediated processes (Ajuwon *et al.*, 2009; Quintero-Fabián *et al.*, 2013).

Small amounts of LPS are constantly released into the environment during bacterial cell division, and upon cell death and lysis, all of the associated LPS is liberated into the environment (Ryan, 2008; Sandle, 2012).

Additionally, when considering that endotoxins are heat stable, and unaffected by standard steam sterilization and submicron filtration (0.20 μm) techniques, the importance of endotoxin testing in the medical and pharmaceutical industry, as well as cell culture experiments, becomes clear (Ryan, 2008; Sandle, 2012).

Endotoxin concentrations were measured using the Pierce[®] *Limulus* Amebocyte Lysate (LAL) Chromogenic Endotoxin Quantitation Kit (Thermo Scientific, Logan, Utah, USA) capable of detecting endotoxin levels as low as 0.1 endotoxin unit (EU)/mL or ± 0.01 ng endotoxin/mL. The principle of this assay (Figure 3.2) is based on the activation of the proenzyme Factor C, found in circulating amebocytes of the horseshoe crab *Limulus Polyphemus* (Thermo Scientific, 2013). Upon interaction with endotoxins, the proteolytic activity of factor C is activated, allowing the subsequent proteolysis of a synthetic peptide substrate to release *p*-nitroaniline (pNA) (Thermo Scientific, 2013). The amount of endotoxin is then quantified as a function of the amount of yellow coloured pNA produced. A standard curve is constructed using an endotoxin standard of known concentration derived from *E. coli* strain O111:B4 in order to determine the exact concentration of endotoxin present in the sample.

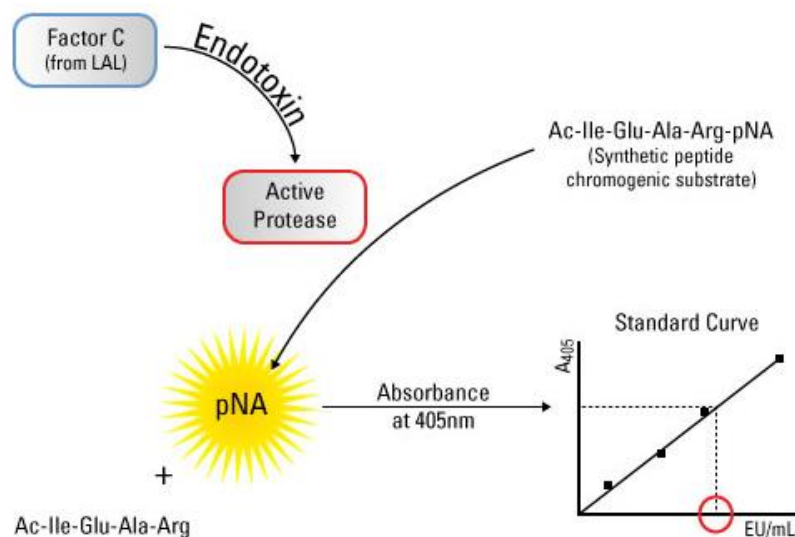


Figure 3.2: Diagrammatic illustration of the principle of the Pierce[®] LAL Chromogenic Endotoxin Quantitation Kit (Thermo Scientific, 2015). Activation of the proenzyme factor C through the interaction with endotoxins is followed by the cleavage of a synthetic peptide linked to *p*-nitroaniline (pNA). The coloured pNA product is quantified as a function of the concentration of endotoxin.

3.3 Cell counts and viability

Cell numbers and viability were routinely monitored using an automated cell counter, Luna™ (Logos Biosystems, Inc., Korea). Luna™ utilizes trypan blue exclusion to distinguish between viable and non-viable cells, as well as numerous mathematical algorithms to identify debris and cell clusters. Parameters such as cell number (total, live and dead), % viability and average cell size can therefore be determined simultaneously for each sample.

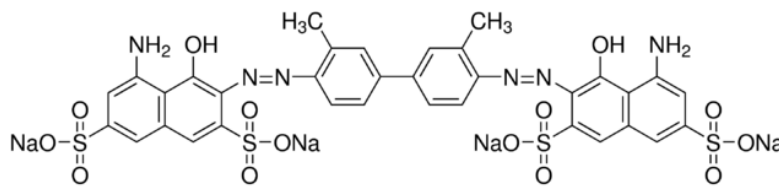


Figure 3.3: Chemical structure of trypan blue (Sigma-Aldrich, 2015c). Trypan blue is a cell membrane impermeable dye that is excluded from healthy, viable cells but can enter cells with compromised cell membranes (non-viable cells).

The trypan blue exclusion assay is a common cell culture technique used to estimate the number of viable and non-viable cells. Living cells have an intact cell membrane and can exclude the dye from the cytoplasm, whereas dead cells have a damaged cell membrane thereby allowing trypan blue (Figure 3.3) to enter the cytoplasm where it will bind to intracellular proteins and stain the cell blue (Strober, 1997). Blue stained and unstained cells are clearly discernible under a light microscope and can be used in conjunction with a haemocytometer to estimate viable and non-viable cell numbers.

3.4 Cell viability, cytotoxicity and IC₅₀ determination

The CellTiter-Blue™ cell viability assay (Promega, Madison, WI, USA) provides a sensitive fluorometric method to evaluate changes in cell viability and / or proliferation. This assay measures the metabolic activity of cells through the reduction of the blue redox indicator dye resazurin, to a highly fluorescent pink dye resorufin (Figure 3.4) (Promega, 2013).

Nonviable or growth arrested cells will rapidly lose their metabolic activity and will be unable to reduce resazurin, whereas healthy, viable cells will easily metabolize the dye. The concentration of the fluorescent resorufin end product released into the culture medium can be quantified at 540 nm (E_x) / 590 nm (E_m) and is directly proportional to amount of viable cells.

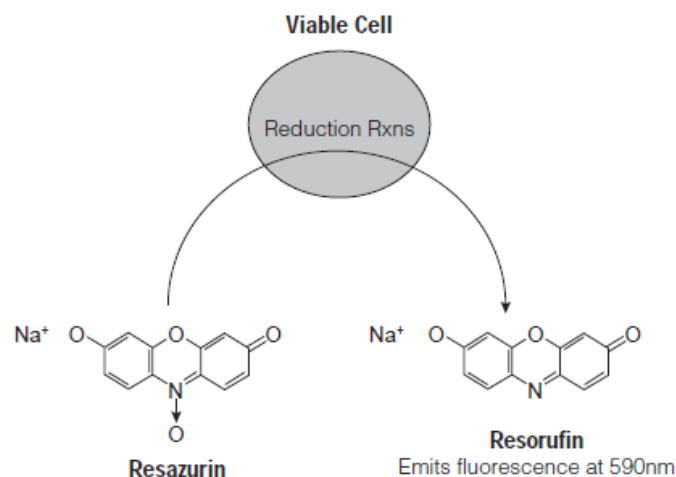


Figure 3.4: Illustration of the principle reaction in the CellTiter-Blue™ cell viability assay (Promega, 2013). In metabolically active cells, resazurin is reduced to highly fluorescent resorufin.

Cytotoxicity describes the ability of a compound to produce a change in cell viability or proliferation, in which case an IC_{50} value, which represents the compound or extract concentration required to inhibit cell viability by 50%, would be determined.

3.5 Flow cytometry

3.5.1 Introduction

Flow cytometry can be described as the process of measuring characteristics such as the relative size, internal complexity and fluorescence intensity of cells or particles in a fluid suspension, based on the way in which the cell or particle scatters incident light and emits fluorescence (BD Biosciences, 2000; Ormerod, 2000).

What sets flow cytometry apart from other traditional quantitative / semi-quantitative methods such as radioisotope assays, ELISAs, and Western Blots is the fact that instead of providing an average measurement for the entire sample population, it provides a fast and sensitive method to perform a wide variety of analyses on heterogeneous, whole cell suspensions and delivers detailed quantitative and qualitative information on each individual cell / particle in the sample (Leslie, 2006; Ormerod, 2000).

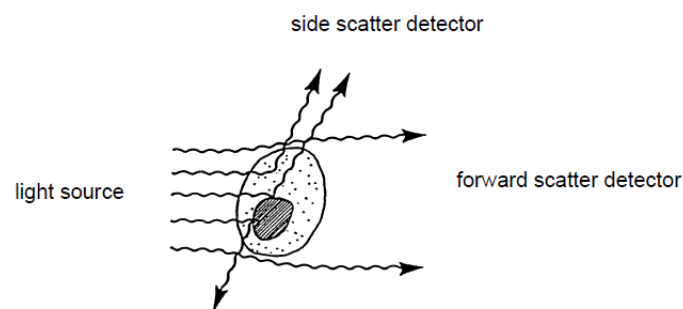


Figure 3.5: Diagram illustrating the light-scattering characteristics of a cell (BD Biosciences, 2000). Forward-scattered light is proportional to the surface area or cell size, whereas side-scattered light is proportional to granularity or internal complexity.

As illustrated in Figure 3.5, light scatter measurements are made with regards to forward-scattered (FS) light, which is proportional to the cell / particle surface area or size, as well as side-scattered (SS) light – indicating changes in refractive index along any interface within the cell / particle, which is proportional to granularity or internal complexity (BD Biosciences, 2000; Ormerod, 2000). The overall shape and surface topography also contributes to the total light scatter (BD Biosciences, 2000).

Correlated FS and SS measurements can identify different cell types within a heterogeneous cell population, such as allowing individual populations of lymphocytes, monocytes and neutrophils to be identified within a lysed whole blood sample (Leslie, 2006). Variations in FS and SS can also indicate changes in cell viability due to cell shrinkage and fragmentation, as well as cell activation and proliferation, accompanied by an increase in both FS and SS (Leslie, 2006).

In addition to FS and SS data, a wide range of fluorophores are also available and can be used to either directly estimate cellular parameters such as: nucleic acid content, enzyme activity, calcium flux, membrane potential, and pH, or it can be conjugated to ligands, polyclonal, and monoclonal antibodies to measure the density and distribution of cell-surface markers, cytoplasmic components, receptors etc. (Ormerod, 2000; Leslie, 2006). Furthermore fluorescent probes with similar excitation wavelengths but different emission wavelengths can be used simultaneously to allow concurrent detection of numerous factors (Ormerod, 2000; Brown & Wittwer, 2000).

3.5.2 Flow cytometer

Generally, a flow cytometer design involves fluidic, optic, and electronic systems. Within the fluidics system the sample is injected into a pressurised stream of liquid, known as sheath fluid, which accelerates the particles and restricts them to the centre of the stream. This keeps the sample core separate but parallel to the sheath fluid stream through a process known as hydrodynamic focussing. One by one the particles will pass through the flow cell where any particle within 0.2 – 150 µm will be detected by the optics system, which consists of lasers to illuminate and excite the particles, as well as optical filters to direct the resulting light signals to the appropriate detectors (BD Biosciences, 2000). The scattered light is collected, and through a combination of beam splitters and filters, the fluorescent light is collected at appropriate detectors. The electronics system converts the detected light signals into electronic signals which will be processed by the computer, to ultimately provide list mode (event by event) data that occurred within the sample.

In this study a Beckman Coulter Cytomics FC500 Flow Cytometer (CA, USA) was used. The FC500 is a bench top instrument equipped with a quartz-cuvette flow cell employing a vertical (upwards) flow path for better hydrodynamic focusing. An air-cooled argon-ion laser (488 nm), as well as a solid state red diode laser (635 nm) is available, together with 5 high sensitivity photomultiplier tube (PMT) detectors ranging in sensitivity from 185 – 900 nm (Beckman Coulter, 2010).

Using interchangeable optical filters, 5 different colours within specific fluorescent light (FL) channels can be detected:

- FL1: Green (525 nm)
- FL2: Yellow (572 nm)
- FL3: Orange (620 nm)
- FL4: Red (675 nm)
- FL5: Long wavelength red (755 nm)

3.5.3 Data collection and analysis

The light scatter and fluorescence parameter values measured for each event, is recorded in the exact order in which the cell / particle passed through the interrogation point (laser beam), and collected into a list mode file (BD Biosciences, 2000). This data can then be represented as single and dual parameter plots although, if required, 3 parameter plots can be developed using specialized software applications.

A single parameter plot, also known as a histogram, displays the number of events detected as a function of its intensity, and is generally used to obtain quantitative data about a particular marker (Figure 3.6, left) (Leslie, 2006). Dual parameter or dot plots on the other hand coordinate two parameters such as FS and SS, with each cell represented as a single dot, thereby allowing the identification and quantification of individual sub-populations within a heterogeneous sample (Figure 3.6, right) (Leslie, 2006).

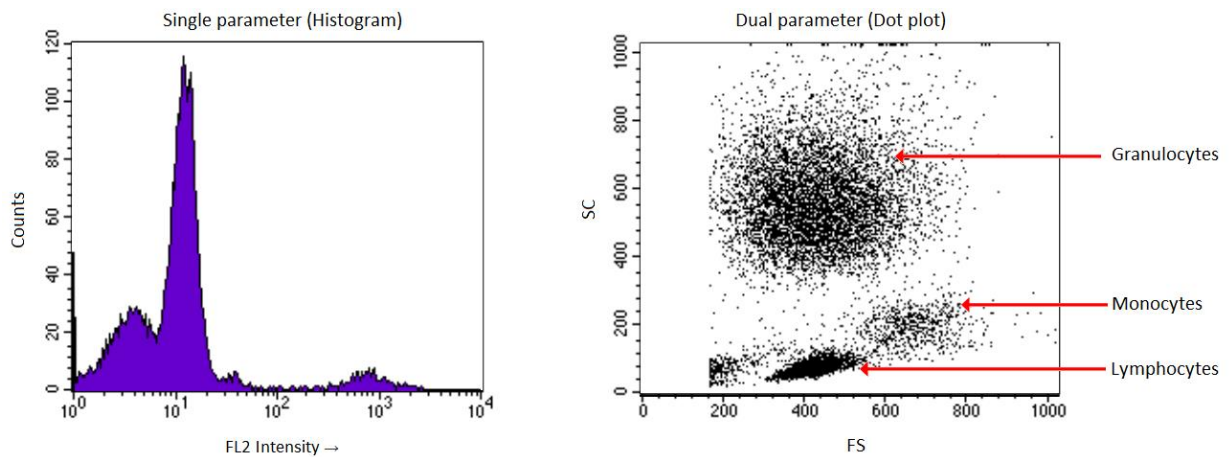


Figure 3.6: Examples of single and dual parameter plots obtained from flow cytometric analysis of blood leukocytes. A histogram illustrating the fluorescence intensity distribution of blood leukocytes stained with a B cell marker (left), accompanied by the dual parameter plot correlating the FS and SS characteristics of the leukocytes (right) (Adapted from Leslie, 2006).

Further analysis can be performed by defining and isolating specific sub populations within a sample through the application of a gate or graphical boundary, thereby excluding all other data outside the region of interest (Figure 3.7).

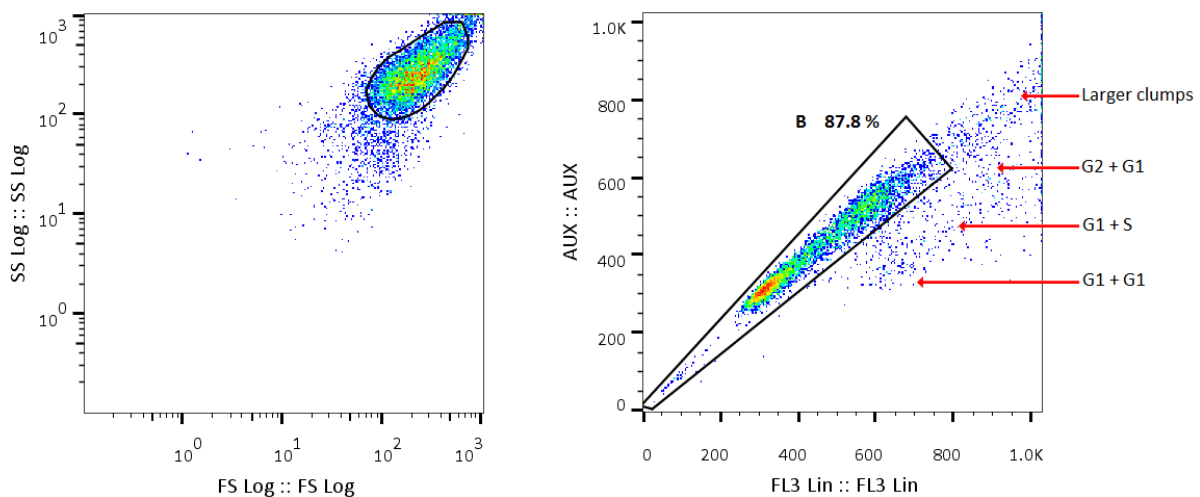


Figure 3.7: Examples of the gating selection process utilized in all flow cytometry analysis experiments in this study. FS vs SS plots (left) display populations in the sample according to their respective size and optical homogeneity, and is used to identify the actual cell population. FL3 Lin vs AUX (right) display the fluorescent signal detected in FL3 (signal area) as a function of the signal height, and used to exclude cell debris and doublets for cell cycle analysis where DNA was stained using propidium iodide. Doublet distributions are shown in accordance with their respective cell cycle phase.

The cell population is first isolated using the FS vs SS plot according to the respective size and optical homogeneity of the cells (Figure 3.7, left). Even with careful sample preparation cell doublets and debris can still be present, which is of particular importance when analysing cellular DNA content and distribution (3.6), due to the fact that two (or more) cells stuck together may register as a single event (Brotherick, 2006; Leslie, 2006; Ormerod, 2000). For example, if both cells in the doublet are diploid ($2N$), the resultant signal will record it as a single tetraploid ($4N$) cell, which can obviously be highly misleading.

The elimination of cell doublets and debris necessitates the use of a signal area vs signal height plot (FL3 Lin vs AUX) (Figure 3.7, right). When the cell passes through the laser beam, a signal is generated based on the maximum fluorescence given out by the cell (signal height), the total amount of fluorescence emitted (signal area), and the time it takes the cell to pass through the laser beam (signal width) (Brotherick, 2006). These characteristics are easily discernible for a cell that is about to divide compared to two cells stuck together, in that a doublet will produce a signal of the same total fluorescence emitted (signal area), but at a lower intensity (signal height) over a longer period (signal width) (Brotherick, 2006). This becomes even more discernible when doublets consist of cells with varying DNA content, as is illustrated in Figure 3.5, where $G1 + G1$ ($2N + 2N$), $G1 + S$ ($2N + >2N$), $G2 + G1$ ($4N + 2N$), as well as larger clump distributions are shown.

3.5.4 Applications of flow cytometry

Besides the numerous research applications, flow cytometry also has clinical and diagnostic applications including, haematology (leukaemia and lymphoma phenotyping), immunology (transplantation rejection, immunodeficiency studies) and oncology (measurement of proliferation markers and DNA content distribution) (Brown & Wittwer, 2000). In this study, flow cytometry was utilized in DNA cell cycle analysis (3.6) and mitochondrial membrane potential determination (3.7).

3.6 Cell cycle analysis

Proliferating eukaryotic cells undergo a tightly regulated, precisely ordered sequence of biochemical events to grow and divide (Nelson & Cox, 2008). This cycle of division (the cell cycle), consists of four active phases: gap 1 (G1), synthesis (S), gap2 (G2) and mitosis (M) (Figure 3.8). Fully differentiated or quiescent cells essentially leave the cell cycle and may remain in the G₀ phase permanently, where no cell division occurs. Some G₀ cells can however return to the G₁ phase through the correct mitogenic signals (growth factors, cytokines etc.) (Koolman & Roehm, 2005). Diploid cells (2N) present in the G₁/G₀ phase will start to synthesise the required RNAs and proteins to pass the G₁-S restriction point, after which cells are committed to transfer into the S phase. During the S phase, DNA is replicated, and by the beginning of the G₂ phase tetraploid cells (4N) are present, and will synthesise the remaining RNAs and proteins in preparation for M phase. Therefore the amount of DNA present in each phase varies according to its function, and quantification thereof provides important information regarding cell cycle distribution and cellular activity.

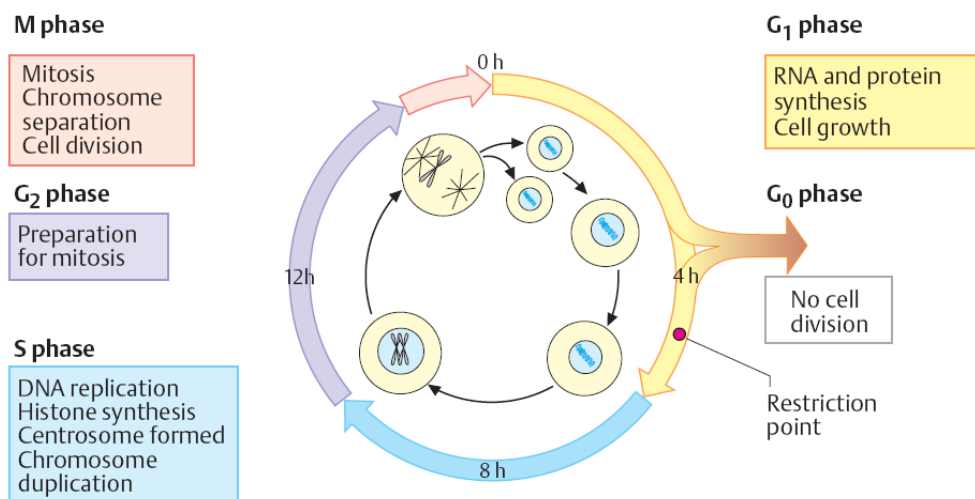


Figure 3.8: Illustration of a typical eukaryotic cell cycle (Koolman & Roehm, 2005). DNA is replicated during the S (synthesis) phase, and segregate to produce two daughter cells during the M (mitosis) phase. Separating these two phases are the G₁ and G₂ (gap) phases, during which required cellular components are synthesised.

Cell cycle analysis aims to measure the DNA content distribution for a population of cells through the utilization of propidium iodide (PI) (Figure 3.9). PI is a positively charged ionic dye and similar to trypan blue, PI is excluded from healthy, intact cells and can therefore also be used as an indicator of cell viability (Sigma-Aldrich, 2015b). For the purpose of cell cycle analysis however, cells are fixed and permeabilized to allow entry of PI into the cell. PI binds to double stranded DNA in a specific stoichiometric ratio through intercalation with the nucleic acid bases, upon which a yellow fluorescence is emitted that can be quantified using flow cytometry (Life Technologies™, 2015).

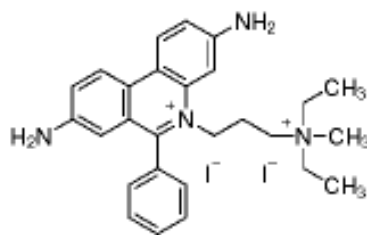


Figure 3.9: Chemical structure of propidium iodide (Sigma-Aldrich, 2015b). PI is a positively charged ionic dye that intercalates with DNA in a stoichiometric ratio of 1 PI: 4 / 5 base pairs, upon which PI emits a quantifiable yellow fluorescence.

3.7 Mitochondrial membrane potential

Metabolically active cells generate a mitochondrial membrane potential ($\Delta\Psi_m$) of \pm 150 – 180 mV through the activity of the electron transport chain during oxidative phosphorylation. Fluctuations in $\Delta\Psi_m$ impact the functioning of the mitochondria with respect to energy metabolism, intracellular ion homeostasis, and perhaps most importantly is the role of $\Delta\Psi_m$ in the cell life – death transition (Perry *et al.*, 2011). During the process of apoptosis $\Delta\Psi_m$ collapses as a result of the formation of mitochondrial permeability transition pores through the activation and assembly of pro-apoptotic Bcl-2 family proteins in the mitochondria (Zamzami, 2000). Changes in $\Delta\Psi_m$ is therefore often used as an indicator for the energetic state of the mitochondria and the cell (Rottenberg & Wu, 1998; Perry *et al.*, 2011).

The lipophilic, cationic dye JC-1 (5,5',6,6'-tetrachloro-1,1',3,3'-tetraethylbenzimidazolylcarbocyanine iodide) (Figure 3.10) is a $\Delta\Psi_m$ sensitive polychromatic probe used to detect changes in $\Delta\Psi_m$ through fluorescence detection techniques such as flow cytometry, and fluorescence microscopy (Sigma-Aldrich, 2015a; Perry *et al.*, 2011).

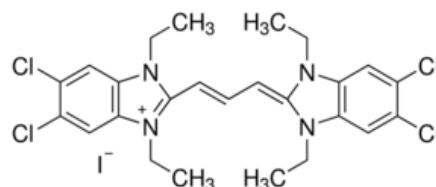


Figure 3.10: Chemical structure of JC-1 (Sigma-Aldrich, 2015a). The cell membrane permeable dye JC-1, exhibits a potential-dependent accumulation within the mitochondria. The more polarized (more negatively charged) the mitochondria, the more dye will accumulate within the mitochondria, subsequently forming red fluorescing aggregates.

JC-1 molecules generally exist in a monomeric configuration and have excitation and emission wavelengths of 485 and 535 nm, respectively (Würthner *et al.*, 2011). However, if present at a sufficiently high concentration, JC-1 monomers will undergo self-association in a process governed by strong intermolecular van der Waals-like attractive forces, resulting in the end – to – end, stacked and parallel arrangement of molecules (Würthner *et al.*, 2011). The resulting aggregate complexes are called J-aggregates after E. Jelley (1936) who first studied this phenomenon. Aggregate formation causes a bathochromic shift or change in the spectral band position, thereby shifting the absorption and emission spectrum to a longer wavelength of 520 – 570 nm and 570 – 610 nm, respectively (Würthner *et al.*, 2011). J-aggregates are also characterized by a very small Stokes shift, and therefore the resulting fluorescence exhibits a high quantum yield, ideal for analysis with fluorescence microscopy, etc. (Würthner *et al.*, 2011). The lipophilic and cationic nature of JC-1 molecules facilitates its preferential accumulation within the mitochondria, due to the negative charge established by the intact mitochondrial membrane potential.

The accumulation of JC-1 within the mitochondria is inversely proportional to the $\Delta\Psi_m$ therefore in healthy, non-apoptotic cells JC-1 will accumulate within the polarized (more negative) mitochondria and form J-aggregates which emit a red fluorescence. Depolarized mitochondria will accumulate less JC-1 and consequently more dye will diffuse into the cytoplasm, where the monomeric form will emit a green fluorescence (Wüthner *et al.*, 2011; Perry *et al.*, 2011).

3.8 Mitochondrial mass determination

Mitochondrial mass can fluctuate according to changes in mitochondrial functions during metabolism, differentiation, and cell cycle progression. Mitochondrial mass is measured using $\Delta\Psi_m$ insensitive dyes such as MitoTracker[®] Green FM (Molecular Probes[®], Life technologies, USA) (Figure 3.11).

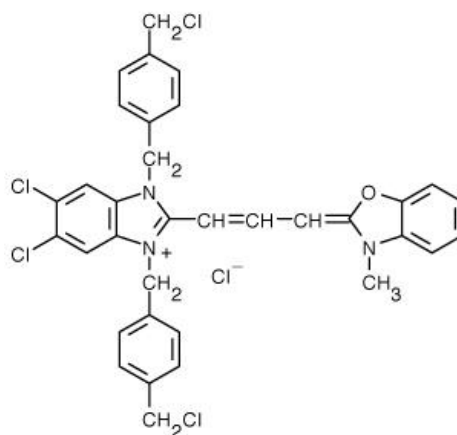


Figure 3.11: Chemical structure MitoTracker[®] Green FM (Molecular Probes[®], 2008). MitoTracker[®] Green FM is a $\Delta\Psi_m$ insensitive fluorescent probe used to determine changes in mitochondrial mass and morphology.

MitoTracker[®] Green FM is a cell permeable, mitochondrion-selective carbocyanine dye containing a mildly thiol-reactive chloromethyl moiety (Cottet-Rousselle *et al.*, 2011; Pendergrass *et al.*, 2004; Molecular Probes[®], 2008). It is essentially non-fluorescent in aqueous solution, becoming fluorescent once accumulated within the lipid rich environment of mitochondria (Cottet-Rousselle *et al.*, 2011).

The pH of the inner mitochondrial membrane contributes to the preferential accumulation of the dye within the mitochondrial membrane, where it reacts with free thiol groups of cysteine residues of mitochondrial proteins (Cottet-Rousselle *et al.*, 2011; Molecular Probes[®], 2008). Careful consideration has to be given to the fact that the amount of fluorescence observed correlates more with the inner mitochondrial membrane quantity, and may differ slightly from the full mitochondrial mass (Cottet-Rousselle *et al.*, 2011). Additionally, inner mitochondrial membrane topology may vary amongst different species and cell types, as well as different metabolic states within the same cells (Cottet-Rousselle *et al.*, 2011).

3.9 Metabolic assays

3.9.1 Glucose utilization assay

An enzymatic assay based on the method described by Trinder (1969) was used to estimate changes in cellular glucose utilization. The glucose oxidase assay is a quantitative colourimetric assay that involves a 2 step reaction process (Figure 3.12).

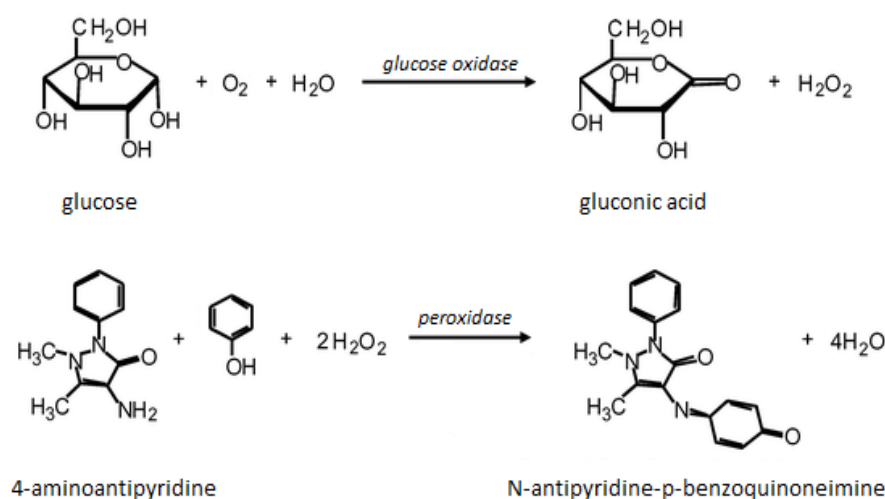


Figure 3.12: Principle of the glucose oxidase assay (Adapted from Phuoc *et al.*, 2010).

This two-step reaction process allows the quantification of glucose as a function of the concentration of *N*-antipyridine-*p*-benzoquinoneimine, which can be measured at 520 nm.

Firstly, glucose is oxidized by glucose oxidase to produce gluconic acid and hydrogen peroxide (H₂O₂), which subsequently reacts with phenol and 4-aminoantipyrine in the presence of peroxidase, to form a red-coloured quinoamine dye complex. The intensity of the coloured product is directly proportional to the concentration of glucose, and can be measured at 520 nm. The assay reagent was prepared as described in appendix II.

3.9.2 Lactate production assay

The lactate oxidase assay is a quantitative colourimetric assay based on the exact same principle as described for the glucose oxidase assay, the only difference being the first reaction step in which lactate is oxidized by lactate oxidase to produce pyruvate and hydrogen peroxide (H₂O₂) (Figure 3.13). The H₂O₂ subsequently reacts with phenol and 4-aminoantipyrine in the presence of peroxidase, to form a red-coloured quinoamine dye complex, which can be measured at 520 nm. The intensity of the coloured product is therefore directly proportional to the concentration of lactate.

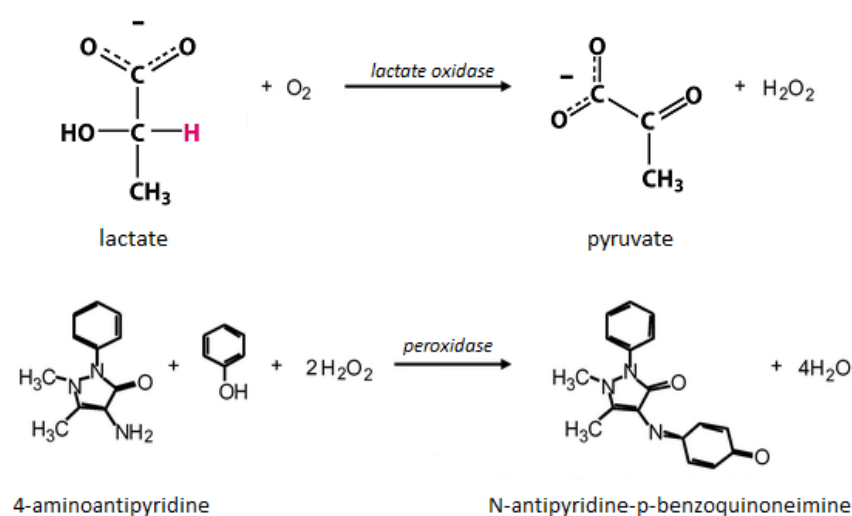


Figure 3.13: Principle of the lactate oxidase assay (Adapted from Phuoc *et al.*, 2010; Nelson & Cox, 2008). This two-step reaction process allows the quantification of lactate as a function of the concentration of *N*-antipyridine-*p*-benzoquinoneimine, which can be measured at 520 nm.

The assay reagent was prepared as described for the glucose oxidase reagent (appendix II) with the exception of glucose oxidase, which was substituted for lactate oxidase.

3.10 Data analysis and statistics

Unless otherwise stated, each experiment was performed in triplicate and repeated 3 independent times (n=3). Standard deviation (SD) of the mean of three independent experiments was calculated and expressed using error bars where appropriate. Statistical significance was determined using the two-tailed student's *t*-test where $p < 0.05$ (*) and $p < 0.005$ (**) were considered significant. For all flow cytometry assays, a minimum of 10 000 events were recorded for each sample, and data was analysed using FlowJo v10 software (Tree Star Inc., USA). Cell cycle histograms and histogram overlays are one representative of each experiment. Confocal microscopy images represent one of at least 15 images, taken during a single experiment. Post-acquisition processing of confocal microscopy images was performed using ZEN 2012 software (Carl Zeiss Microscopy GmbH, 2011).

CHAPTER 4: Mitochondrial dysfunction

4.1 Introduction

4.1.1 The mitochondria

Mitochondria, from the Greek *mitos* (thread-like) and *khondros* (grain or granule), are cellular organelles of endosymbiotic origin present in all nucleated cells (Schon *et al.*, 2012; Sagan, 1967; Wallace, 2005). The number of mitochondria present in each cell varies according to the metabolic activity of the cell, and collectively mitochondria can occupy up to 25% of the cytoplasmic volume (Khan *et al.*, 2007; Pieczenik & Neustadt, 2007). Commonly described as the cell's biochemical powerhouse, mitochondria produce about 90% of the required cellular ATP through oxidative phosphorylation. However, its cellular involvement far exceeds ATP production alone. These dynamic organelles play an essential role in the maintenance of cellular homeostasis through the regulation of numerous metabolic and signalling pathways (Alexeyev *et al.*, 2013; Bratic & Larsson, 2013; Chandel, 2014; Nunnari & Suomalainen, 2012).

Structurally mitochondria consist of two functionally distinct membranes. The smooth outer membrane is essential in the scaffolding of signalling complexes, initiation of apoptosis as well as the regulated import and export of molecules (Nunnari & Suomalainen, 2012). The folded inner membrane on the other hand, encapsulates the intermembrane space and mitochondrial matrix, respectively. Numerous energy-yielding metabolic pathways, including the tricarboxylic acid cycle, fatty acid β -oxidation, glutaminolysis, branched-chain amino acid catabolism, ketogenesis, and pyruvate oxidation occur within the mitochondrial matrix and culminate at the inner mitochondrial membrane (Nunnari & Suomalainen, 2012).

Residing within the inner mitochondrial membrane is the five respiratory chain complexes required for oxidative phosphorylation, namely complexes I – IV and ATP synthase (Complex V) (Figure 4.1).

Although frequently depicted as individual components, recent studies have shown that respiratory chain complexes I – IV form part of a larger supercomplex thought to permit easier channelling of electrons through the different complexes during oxidative phosphorylation (Nelson & Cox, 2008; Demine *et al.*, 2014; Dudkina *et al.*, 2010). The correct and stable assembly of such supercomplexes are essential to the function of the mitochondria, especially since dysfunction or absence of any one of the subunits can disturb the stability of the supercomplex (Demine *et al.*, 2014; Dudkina *et al.*, 2010).

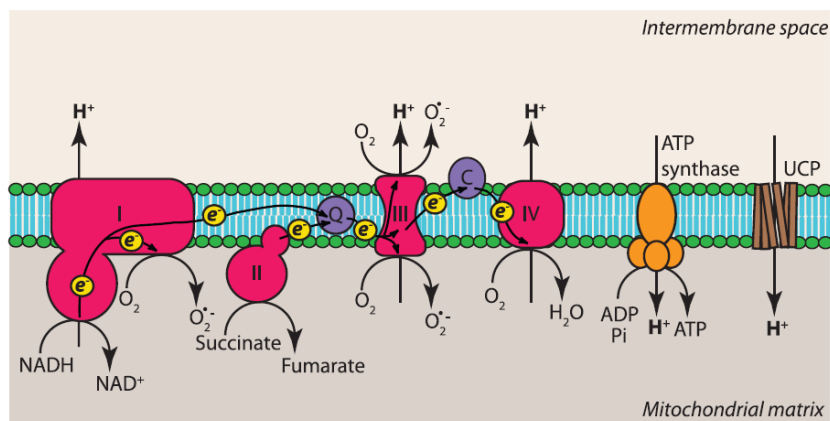
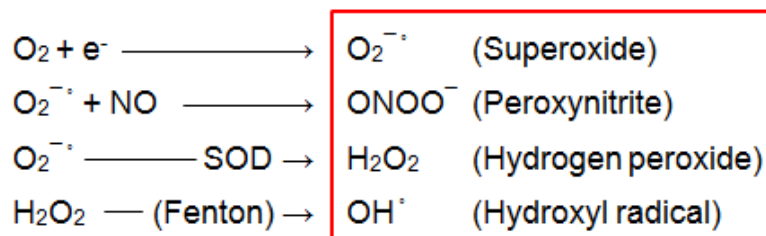


Figure 4.1: ATP production through oxidative phosphorylation. Electron carriers are oxidized by respiratory chain complexes within the inner mitochondrial membrane, prompting a series of sequential reactions to ultimately ensure the phosphorylation of ADP to ATP (Trifunovic & Larsson, 2008).

During oxidative phosphorylation, electron carriers produced during metabolic reactions in the matrix, such as NADH and FADH₂ donate electrons to complex I and II, respectively, after which electrons are sequentially transferred to complex III and IV, and finally donated to O₂ which is subsequently reduced to H₂O (Figure 4.1). Energy released during electron transfer is used to pump protons (H⁺) through complexes I, III, and IV, from the matrix into the intermembrane space, creating an electrochemical gradient across the inner mitochondrial membrane. The electrical potential of -150 to -180 mV established across the inner mitochondrial membrane is crucial for other mitochondrial functions such as protein import and responses to mitochondrial dysfunction (Nunnari & Suomalainen, 2012; Trifunovic & Larsson, 2008).

The proton gradient is released through the passive flow of H^+ back into the mitochondrial matrix, through the ATP synthase complex which drives the phosphorylation of ADP to ATP. Alternatively protons can enter the mitochondrial matrix through uncoupling proteins (UCPs), which leads to the uncoupling of oxidative phosphorylation and ATP synthesis (Bratic & Larsson, 2013).

Mitochondria also produce the majority of endogenous reactive oxygen species (ROS) as a by-product of oxidative phosphorylation. Electrons can escape the respiratory chain at several sites and react with O_2 or other electron acceptors to produce free radicals. As illustrated in Figure 4.1, complex I and III are predicted to be the key sites of superoxide production (Lagouge & Larsson, 2013).



Superoxide ($O_2^{\cdot -}$) is the most abundant ROS in the cell, and can react with nitric oxide (NO) to produce a peroxynitrite ($ONOO^-$) anion, or be converted to hydrogen peroxide (H_2O_2) by the mitochondrial and cytosolic enzymes Mn superoxide dismutase (SOD) and Cu/ZnSOD, respectively (Wallace, 2005; Lagouge & Larsson, 2013). H_2O_2 is much more stable than $O_2^{\cdot -}$ and diffuse freely throughout the cell (Wallace, 2005). H_2O_2 can be detoxified by peroxisomal catalase and glutathione peroxidase (GPx) to produce water and oxygen. Alternatively, H_2O_2 is converted to the highly reactive hydroxyl radical (OH^{\cdot}) in the presence of transition metals via the Fenton reaction. These ROS are highly reactive, especially hydroxyl radicals – which are considered to be the most damaging form of ROS.

As mentioned in Chapter 2, several enzymatic and non-enzymatic defence mechanisms exist to scavenge ROS and thereby protect the cell from oxidative damage. Consequently, an imbalance between antioxidant defences and ROS production leads to a state of oxidative stress, through which ROS damage can accumulate within cellular components including DNA with a concomitant increase in the rate of DNA mutations, commonly associated with ageing (Wallace, 2005).

Mitochondria are unique in that they contain their own genetic material, mitochondrial DNA (mtDNA), of which the inheritance is almost exclusively maternal (Nunnari & Suomalainen, 2012; Alexeyev *et al.*, 2013). MtDNA, originally referred to as ρ -nucleic acid, is highly redundant with thousands of copies present in each cell (Khan *et al.*, 2007; Alexeyev *et al.*, 2013; Schon *et al.*, 2012). Within each mitochondrion, several copies of mtDNA are packaged with key mitochondrial maintenance proteins to form protein-DNA complexes known as nucleoids that are closely associated with the inner mitochondrial membrane (Taylor & Turnbull, 2005; Spelbrink, 2010; Park & Larsson, 2011; Chen, 2013).

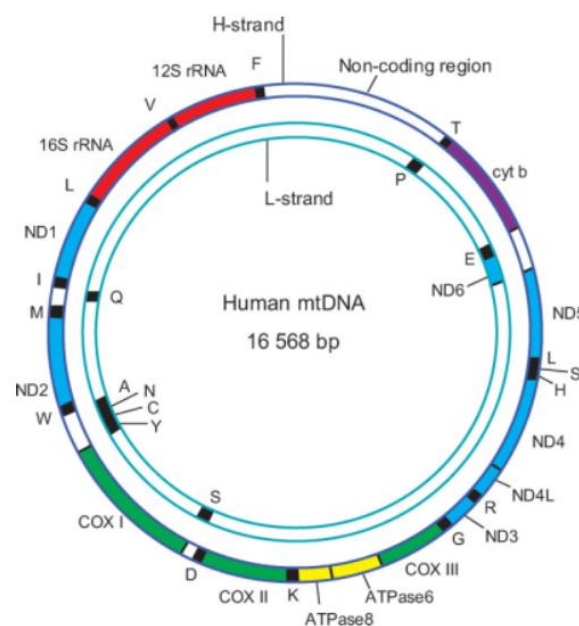


Figure 4.2: Organization of human mitochondrial DNA. The two strands represent the heavy (H) and light (L) strands. Single letters indicate the positions of the corresponding tRNA genes. ND: NADH dehydrogenase genes, cyt b: cytochrome b gene, COX: cytochrome c oxidase genes, ATPase 6/8: ATP synthase genes 6 and 8, 12S/16S: ribosomal RNA genes (Spelbrink, 2010).

Human mtDNA is a double-stranded, circular molecule of ± 16.6 kb that encodes 2 ribosomal RNAs and 22 transfer RNAs, required for mitochondrial protein synthesis, as well as 13 polypeptides. These polypeptides are subunits to 4 out of the 5 mitochondrial respiratory complexes, namely: complex I (NADH dehydrogenase), complex IV (cytochrome c oxidase), complex V (ATP synthase), as well as cytochrome b which is a subunit of complex III (Alexeyev *et al.*, 2013).

Interestingly, studies have indicated that mammalian mitochondria can contain over 1500 proteins, all of which are encoded by nuclear DNA, translated in the cytoplasm and actively imported into the mitochondria (Nunnari & Suomalainen, 2012). Therefore mitochondrial activity, including mtDNA organization, replication, repair and transmission, is completely dependent on nuclear DNA (Chen, 2013). The reasoning behind this seemingly impractical genetic distribution is unclear, but supposedly involves the hydrophobic nature of the mtDNA gene products, which would otherwise be prevented from import into the mitochondria (Park & Larsson, 2011). In an alternate hypothesis, it was suggested that mtDNA endured for a regulatory purpose and that perhaps the biogenesis of the oxidative phosphorylation system necessitates direct interactions between the mtDNA and respiratory chain subunits (Park & Larsson, 2011; Allen, 2003).

The extensive amount of resources a cell must provide in order to maintain mitochondrial function, highlights the significance and diversity of its overall cellular involvement, especially when considering the increasing number of diseases associated with mitochondrial dysfunction (Nunnari & Suomalainen, 2012).

4.1.2 Mitochondrial dysfunction

Mitochondrial dysfunction relates to the impairment and / or alteration of the mitochondria and any of its associated functions, including inhibition of oxidative phosphorylation and respiration, mitochondrial network fragmentation, membrane depolarization, mitochondrial uncoupling or proton leak, ROS production, as well as the build-up of mitochondrial protein aggregates (Demine *et al.*, 2014; Brand, & Nicholls, 2011; Pellegrino *et al.*, 2012). The consequences of mitochondrial dysfunction is as diverse as its cellular involvement, and it has not only been implicated in numerous mitochondrial diseases, but also in age-related metabolic and neurodegenerative diseases, as well as the process of ageing (Yakes & van Houten, 1997; Trifunovic & Larsson, 2008; Page *et al.*, 2010; Wallace, 2005; Park & Larsson, 2011; Bratic & Larsson, 2013; Lagouge & Larsson, 2013). The primary cause of mitochondrial dysfunction is attributed to any number of mutations in mitochondrial and / or nuclear DNA implicated in mitochondrial function (Park & Larsson, 2011; Nunnari & Suomalainen, 2012).

Apart from the substantial amount of somatic mutations such as point mutations, large-scale deletions and insertions accumulated in both the coding and control regions of mtDNA, quantitative changes in mtDNA are commonly identified in various types of solid tumours, hematologic malignancies, and age related diseases (Yu, 2011).

The mitochondrial genome is known to be more susceptible to DNA damage, with a reported 10 times greater frequency of mutagenesis compared to nDNA (Yakes & van Houten, 1997; Alexeyev *et al.*, 2013; McInnes, 2013; Kolesar *et al.*, 2014). This is primarily attributed to the close proximity of mtDNA to the large amounts of ROS produced through oxidative phosphorylation (Yakes & van Houten, 1997; Wallace, 2005). The lack of mutation-suppressing elements such as intron sequences, absence of complex chromatin organization and altered DNA repair activity has also been proposed to contribute to the greater accumulation of mutations (Yakes & van Houten, 1997; Alexeyev *et al.*, 2013; McInnes, 2013). Conversely, studies have indicated that mtDNA associated proteins and associated nucleoid organization may offer at least the same protective effect as histones in some cases (Alexeyev *et al.*, 2013). Faulty mtDNA repair mechanisms also play an important role in the accumulation of mtDNA mutations (Schapira, 2012). Despite the fact that mitochondria possess most of the DNA repair pathways available in the nucleus, damage to mtDNA is more slowly repaired compared to nDNA (Yakes & van Houten, 1997; Kolesar *et al.*, 2014).

Contrasting to the nuclear genome, the mitochondrial genome is highly redundant, with thousands of copies present in each cell. Therefore, a “repair or die” restraint is not imposed on mtDNA, and a heteroplasmic intracellular population of mutant and normal mtDNA can be present within the same cell and will be randomly distributed into daughter cells (Wallace, 2005; Alexeyev *et al.*, 2013). Conceivably, a significant amount of damaged mtDNA can persist without detrimental effects, provided that the residual mtDNA can compensate for the loss of function. As the degree of mtDNA mutations increase in association with mitochondrial dysfunction, so does the susceptibility to apoptosis, which subsequently results in the progressive loss of cells over time.

Ultimately, this contributes to a decline in tissue function, and clinical symptoms will appear when the number of functional cells declines below the threshold required to maintain normal tissue function, as is seen during the process of ageing (Taylor & Turnbull, 2005; Wallace, 2005).

4.1.3 Role of mitochondrial dysfunction in disease and ageing

As described in Chapter 2, the involvement of mitochondria in the ageing process was first proposed by Denham Harman (1972). Ever since, a wealth of correlative data has supported the role of increased ROS production and oxidative damage within the mitochondria in age related diseases (Benz & Yau, 2008; Seo *et al.*, 2010; Bratic & Larsson, 2013). However, evidence that challenge this theory in mammals has also been presented, and includes:

- Transgenic mice expressing an error-prone mtDNA polymerase show accelerated signs of ageing, and a concurrent decrease in lifespan, but are not subject to ROS overproduction or oxidative stress,
- Knockout mice heterozygous for the superoxidase dismutase 2 gene, exhibit increased oxidative damage in their nuclear DNA and mtDNA, however no signs of accelerated ageing, or a reduced lifespan is observed (Benz & Yau, 2008; Raffaello & Rizzuto, 2010; Bratic & Larsson, 2013).

The role of oxidative stress in association with mitochondrial dysfunction has therefore been subjected to considerable debate, however the fact that a functional decline in mitochondria occurs with age, together with the fact that properly functioning mitochondria are crucial for longevity and minimizing age related diseases, cannot be refuted (Seo *et al.*, 2010; Raffaello & Rizzuto, 2010; Lauri *et al.*, 2014). Changes in mitochondrial function associated with the ageing process have been well documented, and are centred around the decrease in mitochondrial quality control, as well as deteriorating respiratory chain function, increased ROS and ROS mediated damage, decreased protein disposal activity by the ubiquitin proteasomal and autophagy systems, as well as decreased mitochondrial dynamics (Khan *et al.*, 2007; Seo *et al.*, 2010).

Mitochondrial dynamics refer to the continuous cycles of fission and fusion events that occur throughout the life span of a cell. Fusion allows the exchange of solutes, metabolites, proteins and mtDNA over the entire mitochondrial network, and is therefore critical in reducing content heterogeneity, rescuing damaged units and providing resistance against mitochondrial dysfunction (Ferree & Shirihai, 2012; Lopez-Mejia & Fajas, 2015). Fission, on the other hand, is involved in numerous cell signalling pathways including mitochondrial inheritance during cellular division, mitophagy, and apoptosis (Ferree & Shirihai, 2012; Lopez-Mejia & Fajas, 2015). Apart from the role of mitochondrial dynamics in its own life cycle and within the broader concept of the cell cycle, mitochondria also modify their overall mass, sub-cellular localization, morphology and network configurations in response to cellular stress (Twig *et al.*, 2008; Margineantu *et al.*, 2002). Responsive mitochondrial dynamics and continuous network remodelling is therefore vital to maintaining mitochondrial fitness, ensuring optimal mitochondrial activity, and maintaining the integrity of the mtDNA (Ferree & Shirihai, 2012; Lopez-Mejia & Fajas, 2015). Consequently, mitochondrial dysfunction is characterised by an imbalance in the fission and fusion events, associated with a decrease in mitochondrial dynamics.

4.1.4 Cell culture models of mitochondrial dysfunction through mtDNA depletion

The most common method used to study the effects of mtDNA mutations and mitochondrial dysfunction in ageing and age related diseases, was developed as early as 1970, and is based on the intentional depletion of mtDNA from cultured cells. Such intentionally depleted cells, referred to as “ ρ -nucleic acid depleted” or “ ρ^0 ” cells, were developed using mutagens such as rhodamine 6-G, dideoxynucleoside analogues, methotrexate and, most commonly, ethidium bromide (Khan *et al.*, 2007). Ethidium bromide (3,8-diamino-5-ethyl-6-phenylphenanthridinium bromide) is a cationic phenanthridine dye that binds to, and intercalates with double stranded DNA through electrostatic interactions (Khan *et al.*, 2007; Das *et al.*, 2014). Its positive charge allows it to preferentially accumulate within the negatively charged mitochondria, where it inhibits replication and transcription of mtDNA, subsequently leading to the gradual depletion of mtDNA without significantly affecting nuclear DNA (King & Attardi, 1989; Khan *et al.*, 2007).

Accordingly, the aim of this chapter was to establish an *in vitro* cell culture model representative of mitochondrial dysfunction using 3T3-L1 preadipocytes, in order to mimic the age related decline in preadipocyte function.

Several mtDNA depleted cell lines have since been established, and are commonly used to study the process of ageing and age related diseases such as diabetes, cancer, photo-aged skin and neurodegenerative diseases such as Parkinson's (Amuthan *et al.*, 2002; Arnould *et al.*, 2002; Lim *et al.*, 2006; Park & Lee, 2007; Schroeder *et al.*, 2008).

4.2. Methods and materials

4.2.1 Establishment of an mtDNA depleted 3T3-L1 preadipocyte cell line

Cells were routinely maintained as described in section 3.1. Briefly, 3T3-L1 preadipocytes (wildtype) were routinely maintained in 10 cm culture dishes with DMEM medium containing 4 mM L-glutamine, 4.5 g/L glucose and sodium pyruvate, supplemented with 10% FBS (GE Healthcare Life Sciences, Logan, Utah, USA). It is generally recommended that newborn calf serum (NCS) be used in the complete growth medium for 3T3-L1 cells, however due to changes in legislation and import criteria at the time, NCS could not be obtained initially and FBS was used instead. To minimise additional variables, FBS was subsequently used throughout this study. The use of FBS is deemed acceptable if the intent is to maintain cells as preadipocytes.

In order to generate a mtDNA depleted 3T3-L1 preadipocyte cell line (ρ^0 mutants) wildtype preadipocytes were exposed to 50 ng/mL EtBr (Sigma-Aldrich, St. Louis, MO, USA) every day for a minimum of 30 days, in complete medium (DMEM: 10% FBS) supplemented with 50 μ g/mL uridine (Sigma-Aldrich, St. Louis, MO, USA). Due to the short half-life of EtBr in culture medium, the culture medium was replaced daily. During routine maintenance, a small sample of the ρ^0 mutant cell population was frequently sub-cultured in pyruvate free DMEM culture medium, without uridine and EtBr in order to evaluate the mtDNA status of the ρ^0 mutants. ρ^0 cells are characteristically auxotrophic for pyruvate and pyrimidines (uridine) and were therefore unable to survive in their absence. Both cell lines were used from passage number 8 to 24, and confluency never exceeded 80%. No antibiotics were added during routine maintenance, however, 1% (v/v) penicillin / streptomycin (P/S) (Sigma-Aldrich, St. Louis, MO, USA) was added to long term experiments exceeding 5 days.

Throughout this study, ρ^0 mutants were used in experimental procedures after exactly 30 days of exposure to EtBr, and never more than 40 days. This not only limited the depletion of specific cell phenotypes that occur as a result of excessive passaging, but also reduced the possibility of unintended nDNA depletion due to continuous EtBr exposure.

4.2.2 Characterization of ρ^0 3T3-L1 preadipocytes

Throughout experimental procedures wildtype and ρ^0 mutant cells were seeded during log phase, at a density of 20 000 cells/mL, unless otherwise stated, in appropriate culture vessels – as indicated by the requirements for each experiment. Cells were left overnight to attach and recover. Negative controls (untreated cells) and appropriate positive controls were used wherever possible. Unless otherwise stated, each treatment was performed in triplicate and the experiment was repeated 3 times (n=3).

4.2.2.1 Cell growth characteristics

Cell growth characteristics relating to viability and proliferation were continuously evaluated using an automated cell counter, Luna™ (Logos Biosystems, Korea) (3.3). Wildtype and ρ^0 mutant cells were seeded at a density of 10 000 cells/mL in 10 mL aliquots in 10 cm culture dishes. After 24 hours of incubation, cells were collected from culture plates by first washing with 500 μ L of Dulbecco's phosphate buffered saline (DPBS, without Ca^{2+} and Mg^{2+}) (Lonza, Walkersville, MD, USA), followed by trypsinization (trypsin: EDTA) for 10 minutes at 37°C, and resuspension in 1 mL of complete medium. A 10 μ L aliquot of the cell suspension was removed and added to 10 μ L of 0.4% trypan blue, followed by analysis using the automated cell counter. The remaining cells were seeded back into the original culture dish, and the process repeated every 24 hours for a total of 6 consecutive days as described by Yu *et al.* (2007).

4.2.2.2 Cell cycle analysis

Cell cycle analysis was performed on synchronized wildtype and ρ^0 mutant cells using the Coulter® DNA Prep™ kit (Beckman Coulter, CA, USA) which utilizes propidium iodide (PI) to stain DNA and determine cell cycle distribution (3.6). Wildtype and ρ^0 mutant cells were seeded in 1.5 mL aliquots at 20 000 cells/mL in 6 well culture dishes and left overnight to attach and recover. Cells were synchronised through serum deprivation overnight, after which the serum free medium was replaced with complete culture medium containing 10% FBS, to permit re-entry into the cell cycle.

DNA cell cycle analysis was performed using the Coulter[®] DNA Prep[™] kit, as per manufacturer's instructions. Cells were collected 24, 48, and 72 hours after adding the 10% FBS (in the absence of EtBr) by washing with 500 μ L of DPBS (without Ca²⁺ and Mg²⁺) (Lonza, Walkersville, MD, USA), followed by trypsinization for 10 minutes at 37°C, and resuspension in 500 μ L of DPBS (with Ca²⁺ and Mg²⁺) (Lonza, Walkersville, MD, USA). Cell suspensions were transferred into suitable polypropylene tubes, and the cells collected by centrifugation at 500 x g for 5 minutes at room temperature. A 100 μ L aliquot of lysis reagent (< 0.1% sodium azide, non-ionic detergents, saline, and stabilizers) was added to each sample, vortexed and incubated for 5 minutes at room temperature. A 500 μ L aliquot of PI (50 μ g/mL) was then added to the samples and incubated in the dark for 15 minutes at 37°C, after which samples were analysed using a Beckman Coulter Cytomics FC500 Flow Cytometer (CA, USA) (3.5) and data was recorded in FL3. Results were analysed on FlowJo v10 software (Tree Star Inc., USA).

4.2.2.3 Mitochondrial membrane potential

The effect of EtBr treatment and mtDNA depletion on the mitochondrial membrane was evaluated using the cytofluorimetric, lipophilic cationic dye JC-1 (Sigma-Aldrich, St. Louis, MO, USA) (3.7). Wildtype and ρ^0 mutant cells were seeded in 1.5 mL aliquots at 20 000 cells/mL in 6 well culture dishes and left overnight to attach and recover. Cells were collected after 24, 48, and 72 hours (in the absence of EtBr) into polypropylene tubes, and JC-1 (1 mg/mL) was added to a final concentration of 2 μ g/mL in pre-warmed, complete medium. Samples were allowed to incubate for 10 minutes in the dark at room temperature, after which three wash steps were performed using 500 μ L of DPBS (Lonza, Walkersville, MD, USA) and centrifugation at 500 x g for 5 minutes. Red (FL3) and green (FL1) fluorescence was recorded using a Beckman Coulter Cytomics FC500 Flow Cytometer (CA, USA) (3.5). Results were analysed on FlowJo v10 software (Tree Star Inc., USA). Valinomycin (Sigma-Aldrich, St. Louis, MO, USA), a K⁺ ionophore, was used as a positive control due to its ability to dissipate the mitochondrial membrane potential (Felber & Brand, 1982). Positive control wildtype and ρ^0 mutant cells were incubated with 400 nM Valinomycin for 30 minutes prior to JC-1 staining and flow cytometric analysis.

4.2.2.4 Metabolic parameters: glucose utilization and lactate production

Depletion of mtDNA results in defective mitochondrial respiration and oxidative phosphorylation, therefore alternative energy yielding pathways are used in order to produce cellular ATP. Changes in glucose utilization and lactate production were considered markers for mitochondrial dysfunction and analysed using the glucose oxidase (3.9.1) and lactate oxidase (3.9.2) assay, respectively.

4.2.2.4.1 Glucose utilization assay

Wildtype and ρ^0 mutant cells were seeded at a density of 20 000 cells/mL in 200 μ L aliquots in a 96 well plate, and allowed to attach and recover overnight. After 24, 48 and 72 hours of incubation, 5 μ L of the culture medium was removed and added to 200 μ L of the glucose oxidase assay reagent (prepared as described in Appendix II), incubated for 10 minutes at 37°C and the absorbance was read at 520 nm using a BioTek® PowerWave XS spectrophotometer (Winooski, VT, USA). The resultant absorbance values indicated the amount of glucose remaining in the culture medium, and glucose utilization was subsequently calculated as a percentage of the control (wildtype cells).

4.2.2.4.2 Lactate production assay

Similar to the glucose oxidase assay, wildtype and ρ^0 mutant cells were seeded at a density of 20 000 cells/mL in 200 μ L aliquots in a 96 well plate, and allowed to attach and recover overnight. After 24, 48 and 72 hours of incubation, 5 μ L of the culture medium was removed and added to 200 μ L of the lactate oxidase assay reagent (prepared as described in Appendix II), incubated for 10 minutes at 37°C and the absorbance was read at 520 nm using a BioTek® PowerWave XS spectrophotometer (Winooski, VT, USA). The resultant absorbance values indicated the amount of lactate remaining in the culture medium, and lactate production was subsequently calculated as a percentage of the control (wildtype cells).

4.2.2.5 Confocal microscopy

To characterise mitochondrial function in wildtype and ρ^0 mutants, cells were stained with JC-1 (3.7) and MitoTracker[®] Green FM (3.8). Confocal microscopy was subsequently used to observe the mitochondrial membrane potential, as well as the mitochondrial mass and distribution, respectively.

Confocal microscopy imaging was performed at the Confocal and Light Microscope Imaging Facility at the University of Cape Town, under the supervision of Professor Dirk Lang and Mrs. Susan Cooper. A Zeiss Axiovert LSM 510 META confocal microscope, equipped with a Zeiss AxioCam camera for fluorescent imaging, was used. The confocal microscope stage was also equipped with a specialized pre-heated (37°C) humidified chamber supplied with 5% CO₂, thus enabling live cell imaging. This was required due to the fact that MitoTracker[®] Green FM and JC-1 dyes are not well retained after fixation, and enabled real time observation of mitochondrial movement and cellular activities.

Cells were maintained as described in section 3.1 and 4.2.1. Wildtype and ρ^0 mutant cells were seeded in 500 μ L aliquots at a density of 2 000 cells/mL in specialized 35 mm glass bottom culture dishes to enable the use of higher objective imaging, and left overnight to attach and recover. JC-1 (Sigma-Aldrich, St. Louis, MO, USA) and MitoTracker[®] Green FM (Molecular Probes[®], Life technologies, USA) staining was performed according to manufacturer's instructions. Briefly, cells were incubated with pre-warmed complete culture medium containing either JC-1 (2 μ g/mL) or MitoTracker[®] Green FM (20 nM) for 20 minutes, in the dark at 37°C. The staining solutions were removed and cells were carefully washed using DPBS (Lonza, Walkersville, MD, USA). Fresh complete culture medium was added to the culture dishes, which were then allowed to equilibrate in the chamber for \pm 10 minutes.

A 488 nm laser line was used for excitation, along with appropriate band pass filters (CH2: BP 500-550 IR; CH3: BP 575-630 IR) to enable detection of green (CH2) and red (CH3) fluorescence emissions. High resolution static images, time lapse images, as well as optical slice (Z-stack) images taken at 1 μ m intervals along the z axis, were acquired using a Plan-Apochromat 63x oil immersion objective (NA=1.4).

The laser light intensity and detector gains were set such that fluorescence intensities of both dyes were below saturation levels. Similarly, the pinhole size was kept constant throughout acquisition at 192 μm (CH2) and 220 μm (CH3) to avoid oversampling. Post-acquisition processing was performed using ZEN 2012 software (Carl Zeiss Microscopy GmbH, 2011).

4.3 Results and discussion

The aim of this chapter was to establish and characterize an *in vitro* cell culture model mimicking mitochondrial dysfunction observed during the ageing process. This was achieved by continuous, long term exposure of 3T3-L1 preadipocytes to low levels of EtBr, which has been shown to specifically deplete mtDNA without affecting the nuclear DNA of cultured cells, due to its preferential accumulation within the mitochondria (Armand *et al.*, 2004; King & Attardi, 1989; Leibowitz, 1971). No literature pertaining to mtDNA depletion using EtBr with 3T3-L1 preadipocytes could be found, but studies on other cell lines reported using EtBr concentrations of 50 – 500 ng/mL, and exposure times varying between 20 to 40 days (Biswas *et al.*, 1999; Arnould *et al.*, 2002; Armand *et al.*, 2004; Lim *et al.*, 2006; Park & Lee, 2007; Yu *et al.*, 2007; Magda *et al.*, 2008; Schroeder *et al.*, 2008). After numerous attempts conducted on a trial-and-error basis, using cell growth parameters and mitochondrial membrane potential to monitor the effects of EtBr treatment, it was determined that a 50 ng/mL treatment every day over a period of 30 days was sufficient to decrease mitochondrial function corresponding to expectations for mtDNA depleted cells (Results not shown).

The resultant ρ^0 mutant cells were then further characterised by examining biochemical indicators of mitochondrial dysfunction including changes in: cell proliferation, population doubling time, cell cycle distribution, mitochondrial membrane potential, lactate production and glucose utilization. Together these characteristics confirmed that 3T3-L1 preadipocytes treated with EtBr produced a model representative of mitochondrial dysfunction.

4.3.1 Characterization of ρ^0 3T3-L1 preadipocytes

4.3.1.1 Cell growth characteristics

Compared to wildtype cells, ρ^0 mutants displayed noticeable morphological and biochemical differences in culture. During routine observation of cultures with phase contrast microscopy, the most apparent difference was the clearly reduced rate of proliferation exhibited by ρ^0 mutants (Figure 4.3). Phase contrast photographs were taken of untreated wildtype and ρ^0 mutants after 6 days in culture, providing a representation of the significantly altered growth kinetics as a result of EtBr treatment.

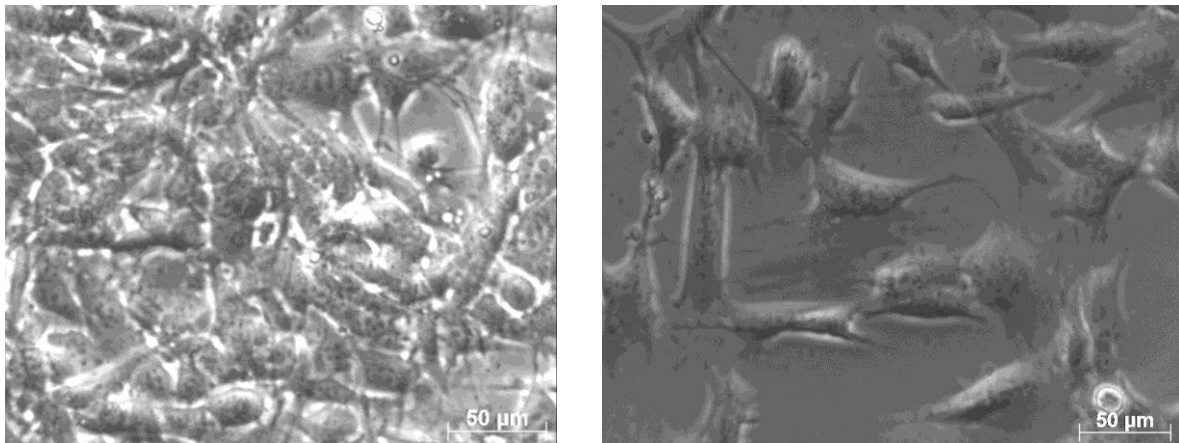


Figure 4.3: Phase contrast images illustrating the contrasting growth kinetics between untreated wildtype (left) and EtBr treated (ρ^0) 3T3-L1 preadipocytes (right). Both cell lines were seeded at 100 000 cells/10mL in 10 cm culture dishes, photographs were taken after about 8 days in culture. Scale bar: 50 μm .

Figure 4.3 simply provides an illustration of the contrasting growth kinetics between wildtype and EtBr treated 3T3-L1 preadipocytes. It is important that 3T3-L1 preadipocytes never reach confluency during routine cell maintenance, due to the fact that contact-inhibited preadipocytes enter a unique temporary quiescent state, arresting at the G0/G1 cell cycle boundary, in preparation for mitotic clonal expansion and subsequent differentiation into adipocytes (Patel & Lane, 2000).

Using an automated cell counter, wildtype and ρ^0 mutant cell numbers (total, live and dead) and % viability were evaluated every day for 6 consecutive days in order to establish growth curves (Figure 4.4) from which population doubling times could be calculated.

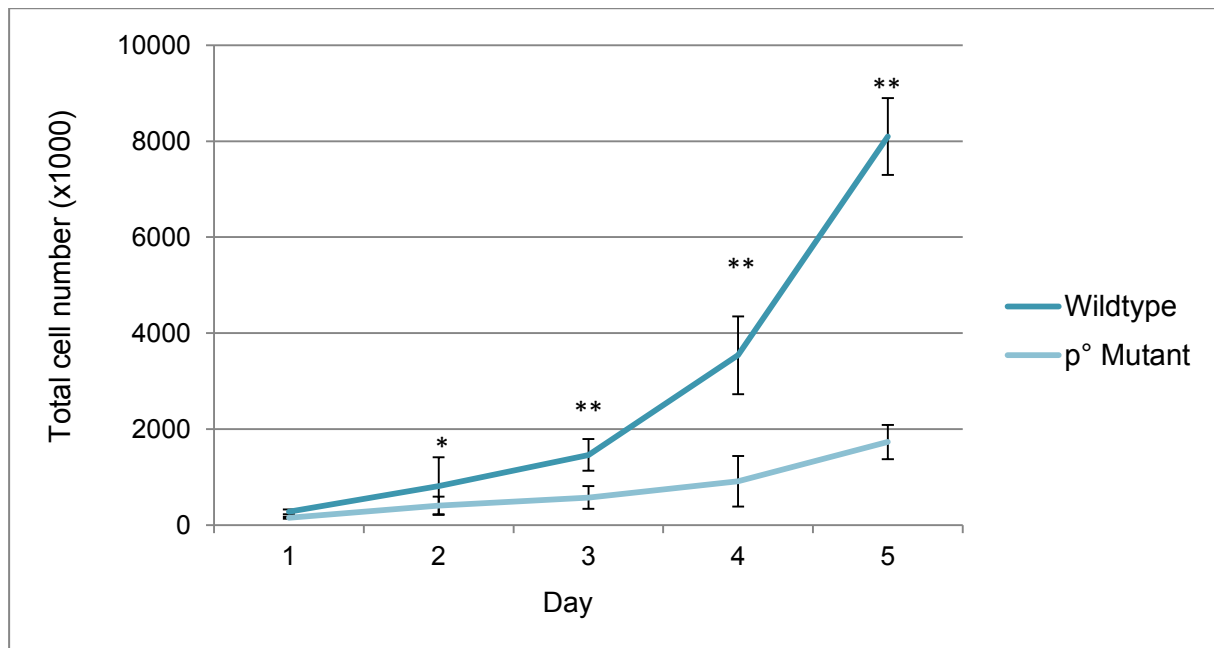


Figure 4.4: Comparison of the growth rate of wildtype and EtBr treated (ρ^0) 3T3-L1 preadipocytes. Total cell number indicates the viable cell density determined using trypan blue staining. Error bars represent SD of nine replicate values ($n=3$). Statistical significance was determined using the two-tailed Student t -test and is indicated for $p < 0.05$ (*) and $p < 0.005$ (**) relative to ρ^0 mutant cells.

A statistically significant difference between the total number of viable wildtype and EtBr treated ρ^0 cells is already evident after just 2 days in culture (Figure 4.4). Using these results population doubling times were calculated during the most linear growth phases (48 – 120 hours) using the formula:

$$DT = \frac{t \ln(2)}{\ln \frac{X_e}{X_b}} \quad \begin{array}{l} X_e = \text{Cell number at time point (t).} \\ X_b = \text{Cell number at } t = 0 \end{array}$$

Wildtype cells had a mean population doubling time of 18.8 ± 2.1 hours, compared to 30.2 ± 4.2 hours for ρ^0 mutants, which is in accordance with findings by other studies (Yu *et al.*, 2007; Magda *et al.*, 2008).

In addition to the analysis of total cell numbers displayed in Figure 4.4, total live and dead cell numbers were recorded by the automatic cell counter, and subsequently used to display the % cell viability for each analysed sample during the experiment (Figure 4.5). These results were confirmed using standard cell counting techniques involving a haemocytometer and trypan blue exclusion.

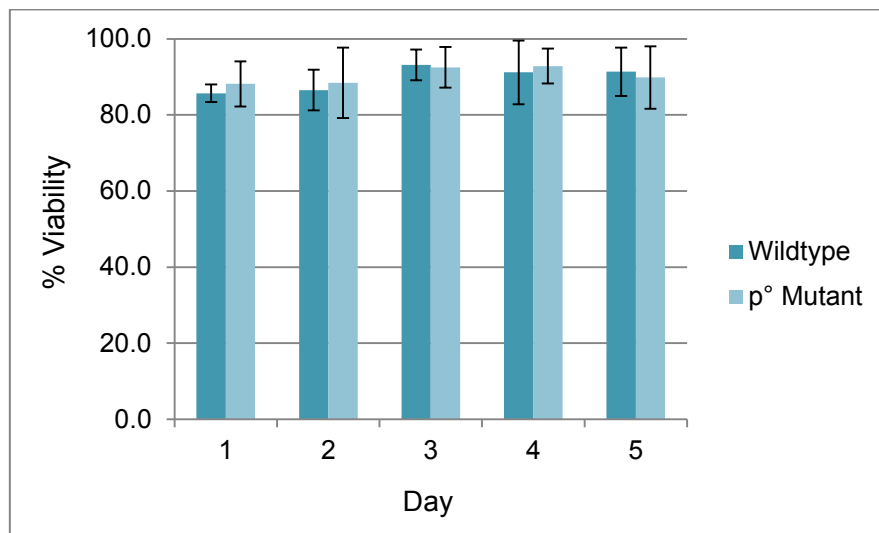


Figure 4.5: Percentage (%) cell viability of ρ^0 mutant and wildtype cells observed over 5 days in the presence of EtBr. Data represents total % viable cells determined using trypan blue staining. Error bars represent SD of nine replicate values ($n=3$). No statistically significant difference between wildtype and ρ^0 mutant cells could be determined using the two-tailed Student *t*-test.

Continuous treatment with EtBr had no detectable effect on cell viability relative to wildtype cells (Figure 4.5). However, ρ^0 mutants are characteristically auxotrophic for pyruvate and pyrimidines (uridine) and were therefore unable to grow in media devoid of pyruvate and uridine. Culture medium was routinely replaced with a pyruvate free substitute without additional uridine supplementation in order to evaluate the mtDNA status of ρ^0 mutants. After \pm 3 days cell viability progressively decreased until \pm day 7 (Results not shown). The reliance on external supplementation of pyruvate and uridine can be attributed to dysfunctional mitochondrial respiration and oxidative phosphorylation (Armand *et al.*, 2004; Yu *et al.*, 2007; Magda *et al.*, 2008).

Uridine dependence is attributed to inactive dihydroorotate dehydrogenase, an enzyme that relies on the activity of the electron transport chain to catalyse the conversion of dihydroorotic acid to orotic acid and following downstream processes to produce uridine (Khan *et al.*, 2007). Similarly, pyruvate auxotrophy is a result of a compensatory overreliance on glycolysis to produce cellular energy, thereby leading to increased accumulation of cytosolic NADH (Armand *et al.*, 2004; Khan *et al.*, 2007; Yu *et al.*, 2007). Excess pyruvate can therefore assist in the regeneration of NAD⁺ through the conversion of pyruvate to lactate via lactate dehydrogenase (Armand *et al.*, 2004; Khan *et al.*, 2007; Yu *et al.*, 2007).

Collectively all of the above results, defining the growth characteristics of ρ^0 mutants, illustrate that mitochondrial dysfunction induced through mtDNA depletion using EtBr treatment severely decreased the proliferation rate and population doubling time of treated cells without affecting cell viability. This is in accordance with findings by Lim *et al.* (2006) using C2C12 myotubes, and Yu *et al.* (2007) using T47D human breast cancer cells. However, whilst decreased proliferation is observed in some ρ^0 cell lines, others have illustrated normal and even two times faster proliferation rates compared to wildtype cells (Armand *et al.*, 2004; Haque *et al.*, 2006; Magda *et al.*, 2008, Yu *et al.*, 2007). Therefore, various cell types respond differently to intracellular changes induced by mtDNA depletion, and the isolation and characterisation of a ρ^0 3T3-L1 preadipocyte cell line presents a novel finding in mitochondrial research relating to preadipocyte dysfunction and ageing.

4.3.1.2 Cell cycle analysis

The profoundly delayed growth rate observed for ρ^0 cells prompted the investigation of cell cycle distribution. Cell cycle analysis was performed on synchronised wildtype and ρ^0 mutant cells after 24, 48 and 72 hours. A summary of the percentage cells present in each cell cycle phase is presented in Table 4.1, and representative histograms in Figure 4.6.

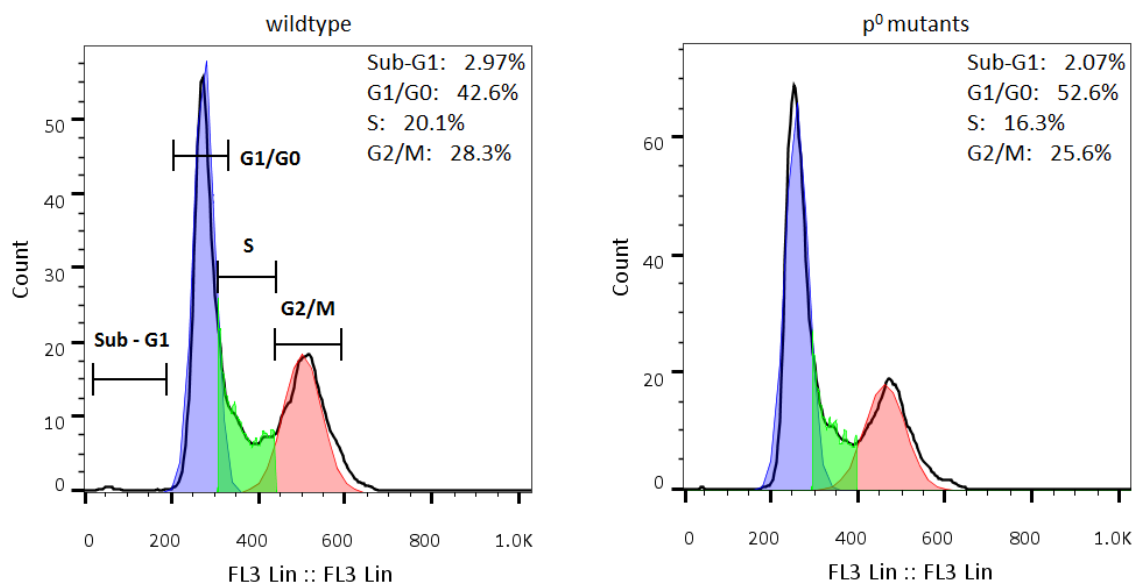


Figure 4.6: Representative cell cycle histograms illustrating DNA distribution for wildtype and ρ^0 mutants. Cells were synchronised through serum deprivation overnight, after which re-entry into the cell cycle was initiated by the addition of 10% FBS to the culture medium. Cell cycle analysis was performed after 24 hours using PI staining. Ten thousand events were recorded for each sample on a Beckman Coulter Cytomics FC500 flow cytometer, and results were analysed using FlowJo v10 software. Percentage (%) values indicate the amount of cells present in each phase. Note difference in y axis for wildtype (left) and ρ^0 mutant (right) histograms. One representative of 3 experiments performed in triplicate.

Table 4.1: Summary of cell cycle analysis results obtained for wildtype and ρ^0 mutants.

Cell cycle analysis was performed using PI staining 24, 48, and 72 hours after re-entry into the cell cycle following synchronization through serum deprivation.

| | | wildtype | ρ^0 mutants |
|----------|--------|-----------------|--------------------|
| 24 hours | Sub-G1 | 3.13 \pm 0.38 | 2.43 \pm 1.53 |
| | G1/G0 | 44.6 \pm 1.38 | 48.8 \pm 3.34 * |
| | S | 20.2 \pm 1.26 | 18.8 \pm 3.02 |
| | G2/M | 26.5 \pm 1.04 | 23.2 \pm 2.68 * |
| 48 hours | Sub-G1 | 2.93 \pm 0.55 | 2.02 \pm 0.46 * |
| | G1/G0 | 42.2 \pm 2.78 | 49.0 \pm 2.70 ** |
| | S | 18.5 \pm 4.66 | 13.3 \pm 3.47 * |
| | G2/M | 30.0 \pm 3.17 | 31.7 \pm 2.15 |
| 72 hours | Sub-G1 | 3.70 \pm 0.54 | 2.99 \pm 0.95 |
| | G1/G0 | 43.0 \pm 1.51 | 47.7 \pm 2.22 ** |
| | S | 15.2 \pm 2.65 | 11.6 \pm 1.68 * |
| | G2/M | 31.7 \pm 1.76 | 32.2 \pm 1.05 |

Experiments were conducted in triplicate and performed 3 independent times. Values indicate mean % \pm SD of all experimental data. Statistical significance was determined using the two-tailed Student *t*-test and is indicated for $p < 0.05$ (*) and $p < 0.005$ (**) relative to untreated control.

ρ^0 mutants progressed through the cell cycle much slower than wildtype cells, as indicated by the significantly increased number of cells remaining in the G1/G0 phase, as well as the reciprocal reduction in the number of cells present in the S phase after 24, 48, and 72 hours. It has been hypothesised that the persistent delay or arrest in G1/G0 phase could be a result of the activation of the mitochondrial damage check point or mitochekpoint, which is activated by mitochondrial damage and mtDNA depletion (Singh, 2004; Yu *et al.*, 2007). This will permit cells to arrest in the cell cycle, and repair some mitochondrial function in order to avoid apoptosis, but if the damage is too severe, cells will become senescent and ultimately undergo programmed cell death (Singh, 2004; Yu *et al.*, 2007). The lack of a significant sub-G1 cell population (Table 4.1) supports this theory, especially when considering that no change in cell viability was evident for ρ^0 mutants relative to wildtype cells as discussed previously (Figure 4.5).

The presence of cell populations in the sub-G1 region generally indicates the presence of apoptotic cells, this is however not a conclusive test for apoptosis and other assays are generally used to confirm apoptosis.

It has also been shown that cell cycle progression is influenced by mitochondrial dynamics and bioenergetics (Mitra *et al.*, 2009; Lopez-Mejia & Fajas, 2015). In conjunction with an increased mitochondrial membrane potential, mitochondria coalesce into a large hyperfused tubular network prior to the transition from G1 to S phase (Mitra *et al.*, 2009; Boland *et al.*, 2013; Lopez-Mejia & Fajas, 2015). This allows the expression and accumulation of cyclin E, a cell cycle regulator protein required to form the active cyclin-CDK2 (cyclin dependent kinase) complex that regulates numerous cellular processes and perhaps most importantly G1 to S phase progression (Siu *et al.*, 2012). Consequently, mitochondrial dysfunction has been linked to a delay in S phase entry (Boland *et al.*, 2013; Mitra *et al.*, 2009). The effects of EtBr treatment on mitochondrial function and membrane polarization is discussed further throughout this study.

4.3.1.3 Mitochondrial membrane potential

The mitochondrial membrane potential ($\Delta\Psi_m$), established through the activity of oxidative phosphorylation (4.1), is an important indicator of mitochondrial function and the overall health-status of a cell. Complex I, III, and IV pump H^+ from the mitochondrial matrix into the intermembrane space, thereby creating an electrochemical gradient across the inner mitochondrial membrane with an associated electrical potential of about $\pm 150 - 180$ mV. Complex I, III, and IV subunits are encoded by the mitochondrial genome, therefore depletion of mitochondrial DNA will result in dysfunctional oxidative phosphorylation and possible depolarization of the mitochondrial membrane, resulting in the attenuation of mitochondrial functions.

Changes in $\Delta\Psi_m$ can be detected through the use of the lipophilic cationic dye JC-1, which exhibits a potential-dependent accumulation in the mitochondria (3.7).

JC-1 will either be retained in the mitochondria due to the negative charge established by the intact $\Delta\Psi_m$ and form J-aggregate complexes emitting a red fluorescence (polarised mitochondria) or, will diffuse into the cytoplasm due to a collapse in $\Delta\Psi_m$, where the monomeric form will exhibit a green fluorescence (depolarised mitochondria). The results shown in Figure 4.6 illustrate the changes in the mean green fluorescence intensity (FL1) of cells stained with JC-1 observed after 24 hours, and results shown in Table 4.2 illustrate the ratio of red (FL3) to green (FL1) fluorescence observed after 24 hours.

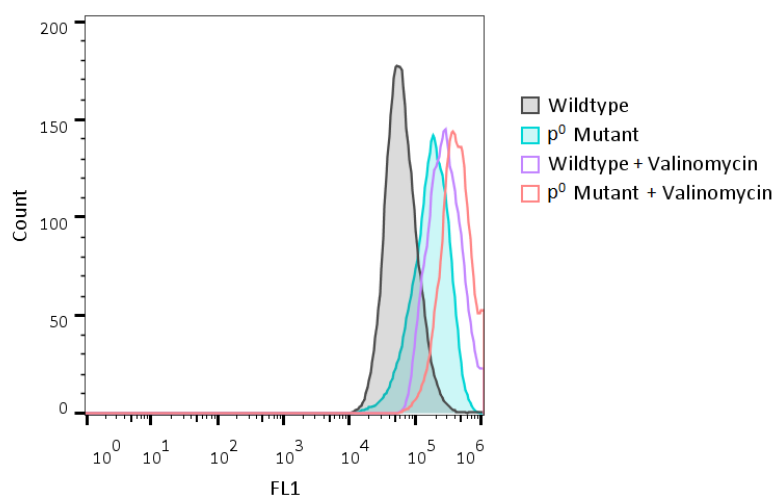


Figure 4.7: Histogram overlay representing the decreased mitochondrial membrane potential in p^0 mutants compared to wildtype cells as well as valinomycin treated wildtype and p^0 mutant cells. Cells were stained with the polychromatic, $\Delta\Psi_m$ sensitive probe JC-1. An increase in the mean fluorescence intensity of FL1 (green) is indicative of a decrease in mitochondrial membrane potential. Ten thousand events were recorded for each sample on a Beckman Coulter Cytomics FC500 flow cytometer, and results were analysed using FlowJo v10 software. One representative of 3 experiments performed in triplicate.

A significant increase in green fluorescence intensity was evident for p^0 mutant cells (Figure 4.7), and indicates that EtBr treatment causes depolarization of the mitochondrial membrane, resulting in a decreased $\Delta\Psi_m$. Valinomycin (400 nM) was used as a positive control due to its ability to completely dissipate the $\Delta\Psi_m$. Treatment of wildtype cells with valinomycin induced an intense depolarization of the mitochondrial membrane as illustrated by the rightward shift in the green fluorescence intensity peak relative to untreated wildtype cells. Similarly, treatment of p^0 mutant cells with valinomycin produced an even more intense depolarization of the mitochondrial membrane.

Interpretation of JC-1 fluorescence intensity results requires special consideration when looking at single-component fluorescent signals compared to a ratio of red (FL3) to green (FL1) fluorescence intensities. Single-component fluorescent signals merely indicate changes in either the relative amount of JC-1 monomers (green fluorescence) or aggregate complexes (red fluorescence), and can be influenced by factors such as mitochondrial size, shape and density. Considering the impact of valinomycin treatment on the green fluorescence intensities observed for wildtype and ρ^0 mutant cells (Figure 4.7), along with the fact that the valinomycin treatment time of 30 minutes is too short to induce changes in the mitochondrial content, it would suggest that changes in single-component fluorescent signals can still provide an additional view point when analysing changes in $\Delta\Psi_m$.

Table 4.2: Summary of results obtained for analysis of mitochondrial membrane potential for wildtype and ρ^0 mutants. Representing the mitochondrial membrane potential is the ratio of the mean fluorescence intensity of FL3 (red) to FL1 (green).

| | Ratio (FL3/FL1) |
|---|------------------------|
| wildtype | 1.503 \pm 0.69 |
| wildtype + Valinomycin | 0.564 \pm 0.08 * |
| ρ^0 mutant | 1.020 \pm 0.50 * |
| ρ^0 mutant + Valinomycin | 0.316 \pm 0.05 ** |

Experiments were conducted in triplicate and performed 3 independent times. Values indicate the mean fluorescence intensity ratio \pm SD of all experimental data. Statistical significance was determined using the two-tailed Student *t*-test and is indicated for $p < 0.05$ (*) and $p < 0.005$ (**) relative to wildtype cells, and relevant untreated control cell populations.

Mitochondrial depolarization is indicated by a decrease in the red / green fluorescence intensity ratio (Table 4.2) independent of changes in mitochondrial size, shape or density. An approximately 2.5 fold decrease in $\Delta\Psi_m$ is observed for ρ^0 mutants relative to wildtype cells. Valinomycin treatment resulted in a respective \pm 3.2 and 2.7 fold decrease in $\Delta\Psi_m$ for wildtype and ρ^0 mutants, relative to the untreated controls. Therefore, the results obtained clearly indicate that EtBr treatment results in a significantly decreased mitochondrial membrane potential.

4.3.1.4 Metabolic parameters: glucose utilization and lactate production

Mitochondria play a fundamental role in several metabolic pathways and produce about 90% of the required cellular ATP through oxidative phosphorylation conducted by respiratory chain on complexes located within the inner mitochondrial membrane. Out of the 5 respiratory chain complexes, 4 are encoded by the mitochondrial genome. Therefore, depletion of mtDNA results in defective mitochondrial respiration and oxidative phosphorylation, and subsequently alternative energy yielding pathways have to be used. Changes in glucose utilization and lactate production into the culture medium were examined in untreated wildtype and ρ^0 mutant cells using glucose oxidase and lactate oxidase assays, respectively. Considering the variation in cell growth characteristics (4.3.1.1), results were normalised to the respective cell densities.

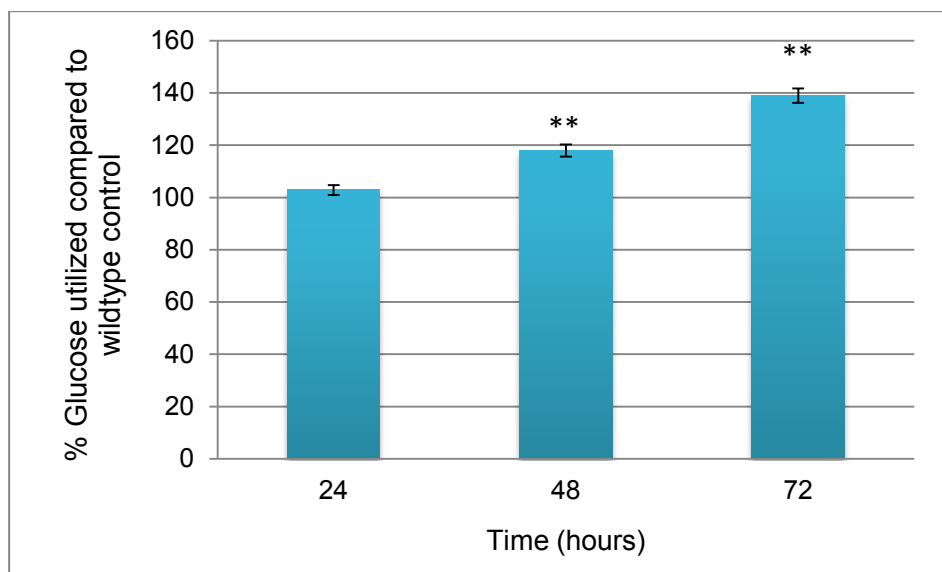


Figure 4.8: Glucose utilization by ρ^0 mutants after 24, 48 and 72 hours, represented as a percentage of the wildtype control (100%). Error bars represent SD of nine replicate values (n=3). Statistical significance was determined using the two-tailed Student *t*-test and is indicated for $p < 0.005$ (**) relative to untreated control.

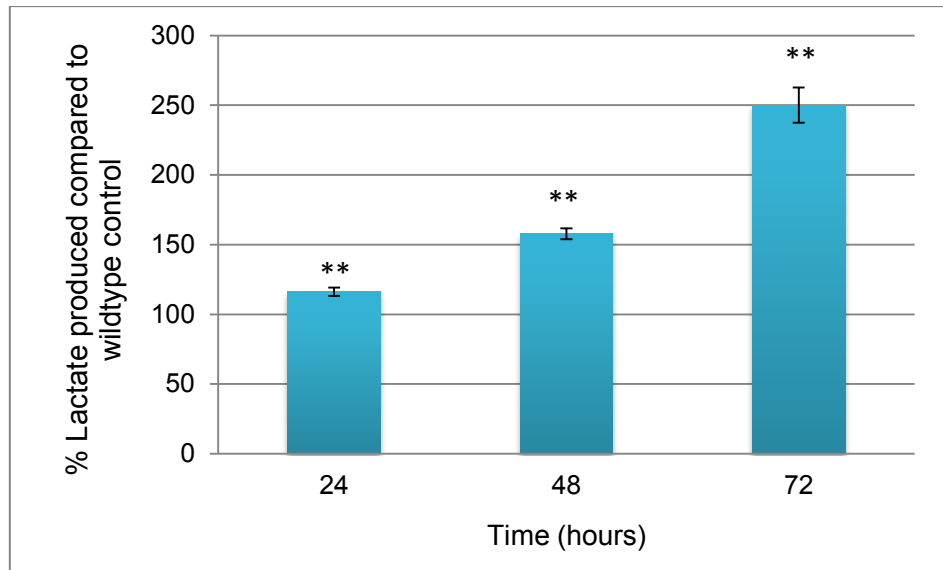


Figure 4.9: Lactate production by ρ^0 mutants after 24, 48 and 72 hours, represented as a percentage of the wildtype control (100%). Error bars represent SD of nine replicate values (n=3). Statistical significance was determined using the two-tailed Student *t*-test and is indicated for $p < 0.005$ (**) relative to untreated control.

From the above results it is evident that, compared to untreated wildtype cells, ρ^0 mutants had utilized 2.83 ± 1.86 %, 18.0 ± 2.32 %, and 39.0 ± 2.74 % more glucose after 24, 48 and 72 hours respectively (Indicated as % increase in glucose utilization relative to wildtype cells \pm SD). Correspondingly, an increase in lactate production of 16.2 ± 2.98 %, 57.8 ± 3.93 %, and 150 ± 12.7 % is seen after 24, 48, and 72 hours respectively (Indicated as % increase in lactate production relative to wildtype cells \pm SD).

Glucose is a primary source of energy in mammalian cells, and is catabolized through glycolysis to form NADH and pyruvate. Generally, pyruvate is converted to acetyl-Co-A by pyruvate dehydrogenase and enters the TCA cycle to produce electron carrying intermediates for oxidative phosphorylation. Mitochondrial respiration and oxidative phosphorylation is however impaired in ρ^0 mutants, therefore a big compensatory increase in glycolysis is necessary in order to produce the required cellular ATP (Qian & van Houten, 2010). Only 2 ATP molecules are produced per glucose molecule during glycolysis alone, compared to a total of 36 produced through the complete mitochondrial respiration process. Therefore an increase in glucose utilization is expected to compensate for this energy deficit.

The overreliance on glycolysis leads to an accumulation of NADH which has to be regenerated to NAD⁺ through the conversion of pyruvate to lactate via lactate dehydrogenase. This accounts for the fact that ρ^0 cells are dependent on externally supplied pyruvate discussed previously (4.3.1.1) for survival, as well as the observed increase in lactate production. It is also important to consider that the culture medium contains pyruvate and glutamine, which are also involved in bioenergetic processes associated with the mitochondria and could therefore underestimate the effects observed.

4.3.1.5 Confocal microscopy

JC-1 staining was used to confirm and visualise the mitochondrial membrane potential ($\Delta\Psi_m$) changes observed using flow cytometry (4.3.1.3), whereas mitochondrial mass was measured through accumulation of the $\Delta\Psi_m$ insensitive fluorescent probe, MitoTracker[®] Green FM.

Using the confocal microscopy images obtained for JC-1 stained mitochondria, individual wildtype and ρ^0 mutant cells were isolated and analysed using Zen software post-acquisition processing. A ratio of red / green fluorescence intensity, indicating mitochondrial membrane potential, was determined for 10 randomly selected cells from both the wildtype and ρ^0 mutant cell populations. A ratio of 1.550 ± 0.39 was determined for wildtype cells, compared to 1.093 ± 0.20 * for ρ^0 mutants, therefore indicating that EtBr treatment decreased the mitochondrial membrane potential. (Ratio = red / green \pm SD, statistical significance determined using the two-tailed Student *t*-test and is indicated for $p < 0.05$ (*)). This is in agreement with results obtained for JC-1 staining and analysis using flow cytometry (4.3.1.3). Representative images are presented in Figure 4.10.

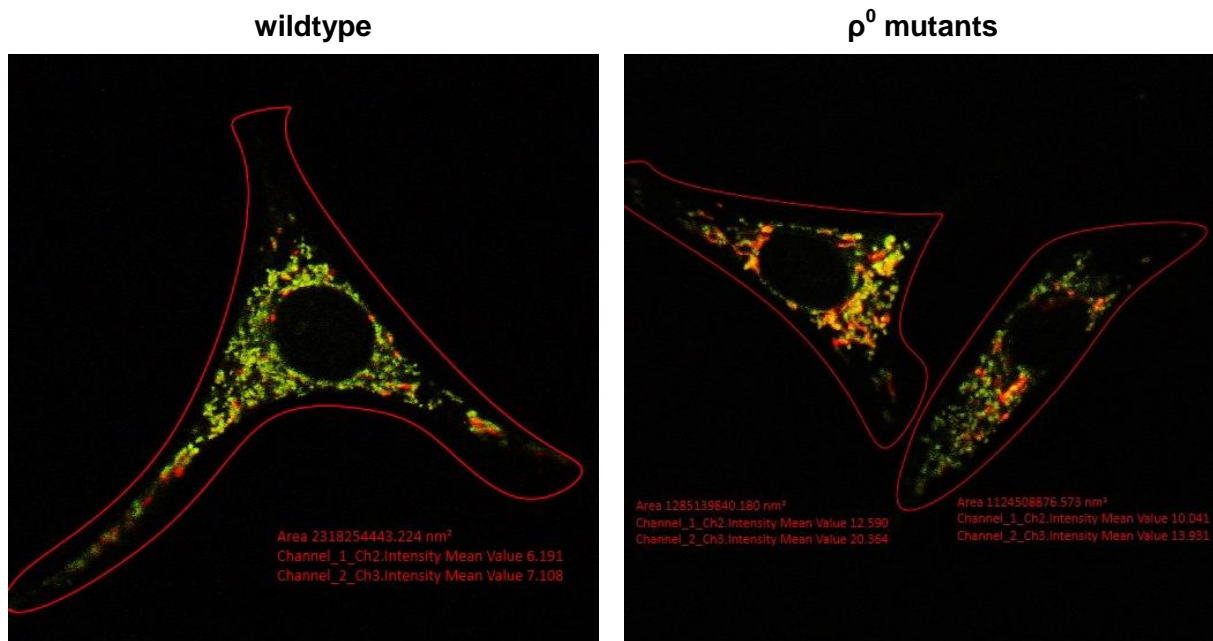


Figure 4.10: Representative confocal microscopy images of JC-1 stained mitochondria in individually characterised wildtype and ρ^0 mutant cells. Live cell imaging was performed using confocal microscopy (63x oil immersion magnification). JC-1 is a polychromatic $\Delta\Psi_m$ sensitive fluorescent probe, exhibiting membrane potential dependent accumulation and aggregate formation within the mitochondria. Polarized (red) and depolarized (green) mitochondria are indicated with yellow colouration representing overlap. One representative of 15 images taken for each respective cell population, during a single experiment.

MitoTracker[®] Green FM accumulates in the mitochondria irrespective of $\Delta\Psi_m$ and is commonly used to determine and observe mitochondrial mass, morphology and distribution (Cottet-Rousselle *et al.*, 2011; Pendergrass *et al.*, 2004; Stankov *et al.*, 2010). However, some studies have reported varying sensitivities to $\Delta\Psi_m$ in some cell lines (Cottet-Rousselle *et al.*, 2011; Mitra & Lippincott-Schwartz, 2010; Pendergrass *et al.*, 2004). Although the use of MitoTracker[®] Green FM as a $\Delta\Psi_m$ insensitive probe has previously been established in 3T3-L1 preadipocytes (Stankov *et al.*, 2010; Wilson-Fritch *et al.*, 2003), the potential sensitivity of MitoTracker[®] Green FM to changes in $\Delta\Psi_m$ was evaluated for both the wildtype and ρ^0 mutant cells using valinomycin (400nM). No discrepancies were found, confirming the independence on mitochondrial membrane potential (Results not shown). Using the confocal microscopy images obtained for MitoTracker[®] Green FM stained mitochondria, individual wildtype and ρ^0 mutant cells were isolated and analysed using Zen software post-acquisition processing (Figure 4.11).

Fluorescence intensities, indicating the accumulation of MitoTracker[®] Green FM within the mitochondria, was determined for 10 randomly selected cells from both the wildtype and ρ^0 mutant cell populations. The mean green fluorescence intensity \pm SD obtained for ρ^0 mutants 42.19 ± 5.97 was similar to that obtained for the wildtype cells 42.72 ± 7.01 . This is in accordance with findings by Armand *et al.* (2004), Holmuamedov *et al.* (2003), Gilkerson *et al.* (2000) and Kukat *et al.* (2008), indicating that mtDNA depletion does not affect the number or biogenesis of mitochondria. These findings are however somewhat subjective, seeing as results in this study only represent the mean fluorescence intensity measured for a few individual cells within the respective wildtype and ρ^0 mutant cell populations. It should also be considered that mitochondrial mass changes during cell cycle progression (Figure 4.12), therefore even though no significant changes in mitochondrial mass was observed for ρ^0 mutant cells in this study, further analysis should be performed to confirm.

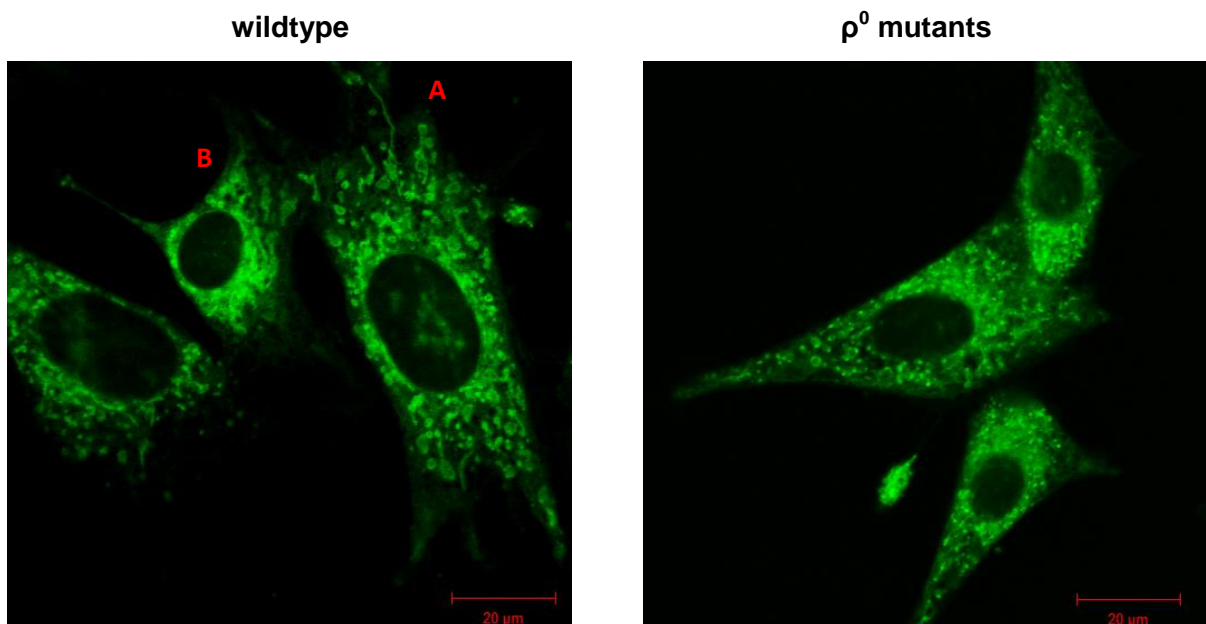
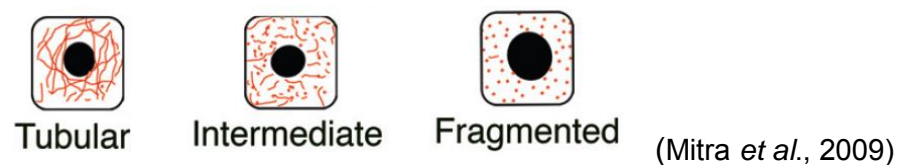


Figure 4.11: Confocal microscopy images of MitoTracker[®] Green FM stained mitochondria in wildtype and ρ^0 mutant cells. Live cell imaging was performed using confocal microscopy (63x oil immersion magnification). MitoTracker[®] Green FM accumulates in the mitochondria irrespective of the mitochondrial membrane potential ($\Delta\Psi_m$ insensitive) and is used to determine mitochondrial mass and distribution. Refer to text for explanations of “A” and “B”. One representative of 10 images taken during a single experiment. Scale bar: 20 μm .

Mitochondria are dynamic organelles that exist in networks continually remodelled through fusion and fission. The balance of mitochondrial fission and fusion adapts to the metabolic demands of the cell to ensure the bioenergetic efficiency of the mitochondrial population within a cell, and is also involved in cellular stress responses (Ferree & Shirihai, 2012; Twig *et al.*, 2008). During the progression of the cell cycle, mitochondria undergo changes in morphology, size, distribution and abundance (Ferree & Shirihai, 2012; Arakaki *et al.*, 2006). This morphological spectrum has been characterised according to the cell cycle progression into tubular, intermediate and fragmented conformations (Mitra *et al.* 2009; Margineantu *et al.*, 2002).



This provides valuable insight into the mitochondrial networks observed in Figure 4.11. As expected, wildtype cells (left) exhibited a more intermediate distribution typical of proliferating cells. The swollen donut shaped mitochondria visible in wildtype cell denoted A, is typical of apoptotic cells, whereas the localization of condensed filamentous mitochondria around the nuclear region in the cell denoted B is indicative of late G2 / early M phase. A primarily fragmented mitochondrial distribution was observed in ρ^0 mutant cells (right), indicating G1 arrested or G0 phase cells, which is consistent with the results obtained for cellular growth characteristics (4.3.1.1) and cell cycle analysis (4.3.1.2). This is in accordance with findings by Margineantu *et al.* (2002), Minamikawa *et al.* (1999) and Arduíno *et al.* (2012) indicating similar trends in mitochondrial morphology and distribution for mtDNA depleted 143B osteosarcoma cells NT2 teratocarcinoma cells.

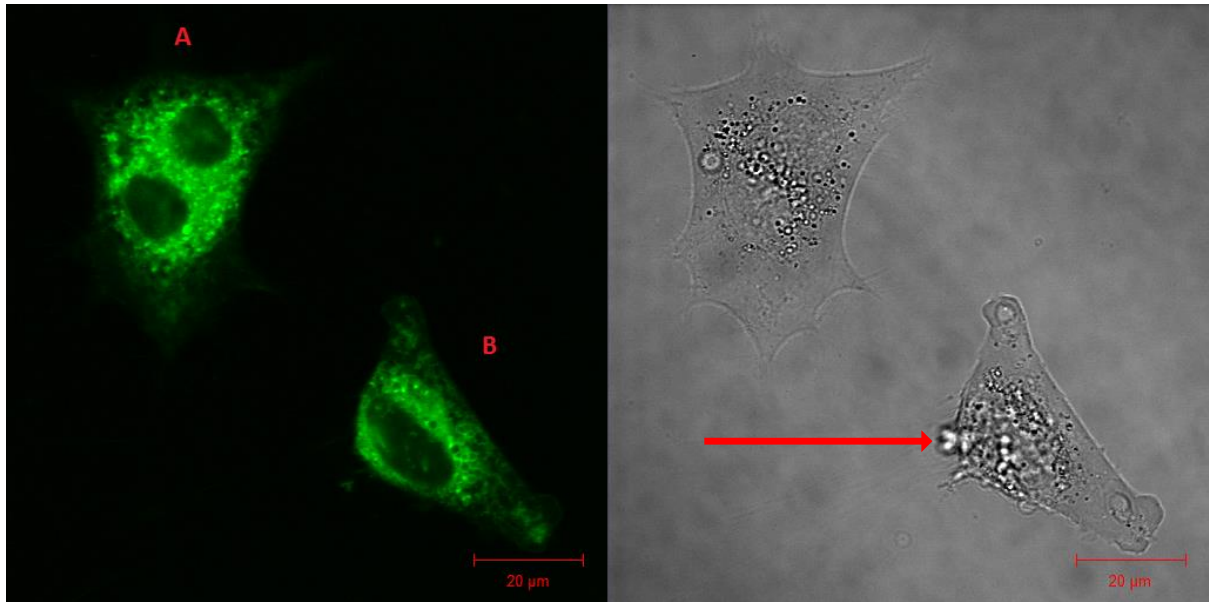


Figure 4.12: Confocal microscopy image of MitoTracker[®] Green FM stained mitochondria in ρ^0 mutant cells (left) accompanied by the corresponding bright field image (right). Live cell imaging was performed using confocal microscopy (63x oil immersion magnification). One representative of 10 images taken during a single experiment. Scale bar: 20 μm .

Figure 4.12 illustrates the different cellular dynamics within a given ρ^0 mutant cell population. Within the same image, one cell can be observed during the final stage of mitosis (A), compared to the other cell undergoing apoptosis (B) (indicated by the swollen donut shaped mitochondria, as well as the membrane blebbing indicated with the red arrow, observed in the bright field image (right)). The mitotic cell also has visibly more green fluorescing mitochondria (Mean fluorescence intensity = 65.526) compared to the apoptotic cell (Mean fluorescence intensity = 43.605), supporting the argument made with regards to the subjective nature of the mitochondrial mass estimation.

It should also be mentioned that ρ^0 mutant cells were much more sensitive to the process of confocal microscopy image acquisition, and would easily start to exhibit membrane blebbing and undergo apoptosis long before the onset of photobleaching effects. Interestingly, this effect was much more prominent for MitoTracker[®] Green FM stained cells compared to those stained with JC-1.

This could be attributed to photosensitisation, which occurs when chromophores induce chemical damage to cells through the excessive generation of ROS in response to photoirradiation during processes such as confocal microscopy, resulting in cell death (Minamikawa *et al.*, 1999). However no literature could be found pertaining to photosensitisation effects of MitoTracker[®] Green FM.

Although the inclusion of a nuclear stain such as DAPI or Hoechst would have provided more definitive images and assisted in the interpretation thereof, these dyes were unavailable at the time of experiment.

Mitochondrial depolarization as a result of EtBr treatment was therefore confirmed using flow cytometry and confocal microscopy. Additionally, results indicated that EtBr treatment did not appear to affect the number or biogenesis of mitochondria.

4.4 Conclusion

The induction of mitochondrial dysfunction through long term exposure to sub lethal concentrations of EtBr have been used to study many age related diseases such as diabetes, cancer, photo-aged skin and neurodegenerative diseases such as Parkinson's (Amuthan *et al.*, 2002; Arnould *et al.*, 2002; Lim *et al.*, 2006; Park & Lee, 2007; Schroeder *et al.*, 2008). The depletion of mtDNA has previously been studied in adipocytes using nucleoside reverse transcriptase inhibitors (NRTI) (Stankov *et al.*, 2010). This is due to the fact that NRTI therapy results in mitochondrial dysfunction as a consequence of mtDNA depletion, which has been suggested as a possible pathogenic mechanism involved in lipodystrophy or the progressive subcutaneous fat wasting observed in HIV-infected patients (Stankov *et al.*, 2010). However, the establishment and characterisation of a ρ^0 3T3-L1 preadipocyte cell line in this study, presents a novel pathway in mitochondrial research relating to preadipocyte dysfunction and ageing.

Summarising the results obtained throughout this study, the following observations can be made. In comparison to wildtype cells, ρ^0 mutant cells exhibited:

Reduced cell growth kinetics:

ρ^0 mutant cells exhibited a significantly reduced growth rate, as illustrated by the substantially increased population doubling time of 30.2 ± 4.2 hours, compared to 18.8 ± 2.1 hours for wildtype cells, as well as the delayed cell cycle progression indicated by an average increase of $\pm 12\%$ in the number of cells remaining in the G1/G0 phase, with a reciprocal reduction of $\pm 19\%$ in the number of cells in the S phase. These results may be attributed to the activation of mitochekpoint, which will permit cells to arrest in the cell cycle and repair some mitochondrial function in order to avoid apoptosis (Singh, 2004; Yu *et al.*, 2007). Additionally, reduced mitochondrial dynamics and bioenergetics associated with mitochondrial dysfunction could also be a contributing factor due to the fact that mitochondria are required to coalesce into a large hyperpolarised, hyperfused tubular network prior to the transition from G1 to S phase (Finkel & Hwang, 2009; Mitra *et al.*, 2009).

This is in turn associated with the mitochondrial membrane potential alterations observed in ρ^0 cells, discussed below.

Metabolic alterations:

Cell viability remained unaffected throughout EtBr treatment, however metabolic alterations became visibly apparent as a progressive increase in acidification (as indicated by the colour changes of the pH indicator phenol red) of the cell culture medium was observed during routine maintenance of ρ^0 mutant cells. This was attributed to an increase in lactate production, which was confirmed by the $\pm 150\%$ increase in lactate production relative to wildtype cells after 72 hours. An increased rate of lactate production can be attributed to a number of factors relating to mitochondrial dysfunction. The decline in ATP production in dysfunctional mitochondria, leads to a compensatory increase in the glycolytic flux with a concomitant increase in pyruvate, the substrate for lactate dehydrogenase (LDH). In addition, ρ^0 mutant cells are dependent on pyruvate and uridine supplementation for cell growth and survival, as removal of pyruvate and uridine from the cell culture medium resulted in a progressive decline in cell number over a period of ± 7 days.

Auxotrophic reliance of EtBr treated cells on pyruvate and uridine is commonly associated with ρ^0 cells, and is considered a useful indicator of the cellular respiratory status and therefore mtDNA content (King & Attardi, 1996; Yu *et al.*, 2007). Depletion of mtDNA, encoding complex I, III, and IV of the respiratory chain, results in dysfunctional mitochondrial respiration and oxidative phosphorylation, thereby constraining the cell to use alternative energy generation pathways namely glycolysis. The overreliance on this more inefficient ATP generating process results in a significantly increased demand for glucose, which was evident in the $\pm 33\%$ increase in glucose utilization after 72 hours relative to wildtype cells. It should however be considered that although these results were normalised to compensate for the differences in cell growth kinetics, glucose utilization and lactate production is indicated as a percentage of the control (wildtype cells). This is of importance when comparing the $\pm 33\%$ increase in glucose utilization to the $\pm 150\%$ increase in lactate production by ρ^0 mutants relative to wildtype cells.

Although during glycolysis the breakdown of 1 glucose molecule ultimately results in the production of 2 lactate molecules, the discrepancy is also due to the fact that under normal conditions, wildtype cells do not produce significant amounts of lactate. Additionally the culture medium also contains other bioenergetic intermediates such as glutamine which is mitochondrially metabolised and can ultimately increase the production of NADPH or be converted to metabolic intermediates such as pyruvate, and may therefore underestimate the results obtained.

It is also important to consider that glucose is not exclusively used as an energy source, and that it is also the main carbon source in many other biochemical pathways and cellular components required for cell growth. Therefore, the different growth characteristics would also impact the ratio of glucose utilization to lactate production. Considering the reduced growth rate of ρ^0 mutants relative to wildtype cells, it would indicate that more glucose carbon would end up as lactate compared to wildtype cells.

Decreased mitochondrial membrane potential ($\Delta\Psi_m$):

Relative to wildtype cells, a small but significant decrease in $\Delta\Psi_m$ was observed. Considering that no changes in cell viability or sub-G1 phase cell populations were observed for ρ^0 mutants relative to wildtype cells, it shows that the decrease in $\Delta\Psi_m$ was insufficient to induce cell death. This can be related to the results obtained during cell cycle analysis and confocal microscopy, seeing as in order to progress from the G1 to S phase, mitochondria need to coalesce into a continuous, hyperpolarised network, to ensure the expression and accumulation of cyclin E. This is required to form the active cyclin-CDK2 complex that regulates numerous cellular processes and ensures the progression from G1 to S phase. Thus it can be said that the reduced $\Delta\Psi_m$, associated with mitochondrial dysfunction, impedes the formation of the hyperpolarised, hyperfused mitochondrial network required for progression from the G1 to S phase, as illustrated by the reduced cell growth characteristics, increase in G1/G0 cell populations and reduced S phase population. This is supported by the fragmented mitochondrial distribution, indicative of G1/G0 arrested cells, observed in ρ^0 mutant cells.

Bearing in mind that the $\Delta\Psi_m$ is established by the activity of oxidative phosphorylation, it begs the question of how these ρ^0 cells are able to maintain this moderately low $\Delta\Psi_m$, considering that ATP production primarily proceeds via glycolysis. The observation that nuclear DNA encoded mitochondrial proteins were still imported into the mitochondria of ρ^0 cells despite the reduction in $\Delta\Psi_m$, prompted Buchet & Godinot (1998) to investigate the F1/F0-ATPase assembly in mtDNA depleted HeLa S3 and 143B cells. Surprisingly, their results indicated that despite the absence of the mtDNA encoded F0 subunits, the F1-ATPase α and β subunits were present, and involved in the maintenance of the $\Delta\Psi_m$ and ρ^0 cell growth. The identification of a functional adenine nucleotide translocater of mitochondria in ρ^0 T47D and other ρ^0 cells could also be of significance, however in both cases, the precise mechanisms involved still need to be elucidated (Buchet & Godinot, 1998; Yu *et al.*, 2007).

Together these characteristics confirmed that 3T3-L1 preadipocytes treated with EtBr produced an *in vitro* cell culture model representative of mitochondrial dysfunction as a consequence of the proposed effect of EtBr treatment on mtDNA. Furthermore, the growth characteristics of these mitochondrial dysfunctional cells reflect that of ageing adipose tissue preadipocytes and therefore provide a suitable model to investigate potential anti-ageing therapeutics.

CHAPTER 5: Anti-ageing properties of Rooibos: Effects on mitochondrial dysfunction

Preadipocytes lose their ability to replicate and differentiate during ageing, and although the precise mechanisms involved remains to be established, it has been suggested that factors which are likely to contribute include mitochondrial dysfunction (Cartwright *et al.*, 2007; Tchkonja *et al.*, 2010; Sepe *et al.*, 2011). Treatment with natural products rich in antioxidants has attracted remarkable interest in the cosmetic and pharmaceutical industry to combat oxidative stress and reverse the effects of ageing. Rooibos (*Aspalathus linearis*) is a South African fynbos plant, well-known for its strong antioxidant capacity and use in many cosmetic products, however little published research exists on its potential as an anti-ageing treatment. The anti-ageing properties of fermented and unfermented rooibos extracts were investigated using an *in vitro* cell culture model designed to evaluate the involvement of mitochondrial dysfunction.

5.1 Introduction

5.1.1 Rooibos (*Aspalathus linearis*)

The leaves and stems of the *Aspalathus linearis* plant, commonly referred to as rooibos or red bush, have been used for hundreds of years to make a uniquely aromatic and soothing herbal tea that is well known for its health-promoting properties (Joubert & de Beer, 2011). It is caffeine free, rich in minerals and polyphenols, and lower in tannins compared to traditional *Camellia sinensis* tea, thereby minimising the risk of reduced iron absorption observed in tea drinkers, due to iron-tannin complexation (Erickson, 2003; Joubert & de Beer, 2011). Apart from its reputation as an enjoyable, healthy herbal tea, countless anecdotal reports supporting its therapeutic value has encouraged the use of rooibos in numerous other products, however it is clear that its phytopharmaceutical potential is only just being realised.

5.1.1.1 Geographical distribution, classification and identification

Rooibos (*Aspalathus linearis* (Burm.f.), R. Dahlgren) is a robust fynbos plant endemic to the Cederberg Mountain region in the Western Cape of South Africa (Figure 5.1) (Morton, 1983; Joubert & de Beer, 2011). It is the only commercially important species within the genus *Aspalathus* (Family Fabaceae; Tribe Crotalarieae) which contains a total of \pm 278 species native to South Africa, most of which are endemic to the Cape Floristic Region with a few others spreading to southern KwaZulu-Natal (van Heerden *et al.*, 2003; Joubert & de Beer, 2011)



Figure 5.1: Geographical distribution of Rooibos in South Africa (Adapted from Rooibos Ltd, 2015). Rooibos is naturally distributed around the Cederberg Mountain region, encompassing the western and south-east areas of the Western Cape Province, as well as limited areas within the south-west of the Northern Cape Province (Joubert & de Beer, 2011).

Rooibos is highly polymorphic and numerous wild types varying in geographical distribution patterns, morphology, ecology, and chemical composition have been described (Morton, 1983; van Heerden *et al.*, 2003). Out of all the naturally occurring *Aspalathus* species and ecotypes originally used to produce rooibos tea, only the red type or Rocklands type is cultivated for commercial use today (Morton, 1983; Joubert & de Beer, 2011).

The Rocklands type is categorised into the wild-growing Cederberg type, and the improved, cultivated Nortier type named after Dr. P. le Fras Nortier who initiated the selection and cultivation of rooibos in plantations (Morton, 1983; Joubert & de Beer, 2011). In recent years the growing demand for rooibos has also reignited support for the development of small scale organisations that harvest and export several wild types of rooibos to niche markets under organic and fair-trade certification (Joubert & de Beer, 2011; van Heerden *et al.*, 2003).

Even though morphological characteristics such as size, density of branching, leaf size and colour, etc. vary considerably within the species, this shrub-like bush can typically grow up to 2 m high in its natural state, compared to 0.5 – 1.5 m for cultivated plants, depending on its age, environmental conditions, and geographical distribution (Rooibos Ltd., 2015; Joubert & de Beer, 2011). As shown in Figure 5.2, the needle-like leaves are bright green, long (15 – 60 mm) and thin (± 1 mm), however coarser and broader leaves are generally observed in wild type plants (Morton, 1983; Joubert & de Beer, 2011). During spring or early summer, small yellow sweet pea-like flowers appear at the tips of the straight, slender branches which are often red-brown in colour, and the fruit is a small lance-shaped legume usually containing one or two hard yellow seeds (Morton, 1983; South African National Biodiversity Institute, 2007).



Figure 5.2: The rooibos (*Aspalathus linearis*) plant (Beltrán-Debón *et al.*, 2011). This highly polymorphic plant species is generally identifiable by its thin needle-like green leaves and woody red stem.

5.1.1.2 History and commercial importance

Rooibos was first discovered hundreds of years ago by the indigenous Khoi tribe of the Cederberg and Elephants river valley region of the Western Cape (Joubert *et al.*, 2008; Morton, 1983). They used the leaves and stems to make an herbal tea infusion traditionally used for its calming effects on the nervous and digestive system, as well as alleviating insomnia (van Niekerk & Viljoen, 2008). This practice was documented in 1772 by European botanist Carl Humberg, during his travels through Africa (Morton, 1983). Commercialization and marketing was initiated in 1904 by Russian immigrant Benjamin Ginsberg, a merchant of Clanwilliam, and by 1930 commercial crops were being grown with the assistance of Dr. le Fras Nortier (Joubert *et al.*, 2008; Morton, 1983). Rooibos was listed as a South African medicinal plant in 1932 by Watt and Breyer-Brandwijk, although exploitation of its extensive therapeutic value (5.1.1.4) only started in 1968 when Annetjie Theron discovered that rooibos tea alleviated colic in her baby – ultimately establishing an extensive brand of skin-care and wellness products containing rooibos extracts (Joubert *et al.*, 2008). Rooibos extracts are now used as value-added products in anything from bread to yoghurt, jams, sauces, hot and cold beverages, liqueur, craft beer, skin, hair and pet care products. In accordance with its increased popularity, production of rooibos in South Arica has grown to an average of about 12 000 tons per annum, most of which is exported to countries such as Germany, Netherlands, United Kingdom, Japan and The United States of America (SARC, 2013; Joubert & de Beer, 2011).

5.1.1.3 Processing of plant material

Rooibos is traditionally consumed as a “fermented” product of the plant leaves and stems. The production process begins when plants are harvested during summer and early autumn (December to April) (Joubert & Schulz, 2006; Joubert *et al.*, 2008). The leaves and stems are shredded, bruised and placed in a fermentation heap. The subsequent addition of water and additional bruising of the plant material accelerates the fermentation process initiated during shredding by encouraging the release and subsequent enzymatic oxidation of polyphenols, leading to rapid browning and producing the characteristic red-brown coloured product (Joubert *et al.*, 2008).

Throughout the fermentation process, the heap is turned over several times to aerate the plant material, thereby ensuring sufficient oxidation to produce a high quality end product (Joubert, 1994; Joubert, 1998). Depending on the age of the plant material, climatic conditions etc., the fermentation process is generally complete within 12 – 14 hours, or when the sweet, honey-like aroma and red-brown colour have fully developed (Joubert, 1994; Joubert & Schulz, 2006). The heap is then spread out into a thin 15 – 20 mm layer, and allowed to dry in the sun before sieving, steam pasteurisation and packaging (Joubert & Schulz, 2006).

Numerous studies have shown that the fermentation process significantly reduces the polyphenolic content of rooibos products (Bramati *et al.*, 2003; Joubert *et al.*, 2008; Marnewick *et al.*, 2000; Standley *et al.*, 2001). As the antioxidant properties of polyphenols, and the perceived health benefits thereof became more apparent, demand for natural products rich in antioxidants, such as an unfermented or “green” rooibos product, increased exponentially.

The production of green rooibos requires minimal oxidative changes, and generally involves simply spreading the shredded plant material in a thin layer, and leaving it to dry naturally in the sun (Joubert & Schulz, 2006). This can however be challenging due to some loss in aspalathin content, especially if the plant material was not properly dried, resulting in uncontrolled fermentation processes. Alternative methods are however available (Joubert & de Beer, 2011).

5.1.1.4 Anecdotal and biological properties

Rooibos is not only enjoyed as a soothing herbal tea with a pleasing and unique aroma. Anecdotal reports have included its use in the alleviation of numerous ailments, including:

- Stomach and digestive problems: colic, indigestion, heartburn, nausea, vomiting, diarrhoea, stomach cramps, constipation;
- Allergies: asthma and hay fever;
- Dermatological problems: eczema, psoriasis, dermatitis, acne and nappy rash;
- Improve hair growth, reduce hair loss;

- Improve appetite and hydration;
- Reduce nervous tension, depression, insomnia, tension and headaches, and promote sound sleep (Morton, 1983; Joubert *et al.*, 2008; Petrova, 2009; South African National Biodiversity Institute, 2007).

Even though in some cases there is still limited scientific proof to support these anecdotal reports, extensive *in vitro*, *ex vivo* and *in vivo* studies have been conducted to evaluate the potential health-promoting effects of rooibos, and have been comprehensively reviewed by Joubert *et al.* (2008) and Joubert & de Beer (2011).

Despite the increasing popularity and the well-known antioxidant capacity of Rooibos (see above mentioned reviews), there exists little published research on its precise molecular and cellular involvement against ageing. It is currently believed that ageing is caused, at least in part, by an imbalance between antioxidant defences and oxidative stress, further associated with mitochondrial dysfunction. Even though numerous *in vitro* studies have investigated the antioxidant capacity of rooibos, subsequent investigations into the ageing process have been limited, and only a few *in vivo* studies have investigated the link between oxidative stress and ageing. In one of the earliest studies Inanami *et al.* (1995) investigated the effects of rooibos treatment on the accumulation of age related lipid peroxidation in 5 week and 24 month old rats. The high degree of lipid peroxidation observed in aged rat brain tissue is reportedly the result of increased spontaneous free radical generation accompanied by an age-related reduction in antioxidant defence mechanisms. Rooibos extracts, fed after weaning throughout a 24 month period, was shown to significantly decrease the accumulation of lipid peroxides in several regions of the brain, presumably due to the superoxide and hydroxyl radical scavenging properties of flavonoids (Joubert *et al.*, 2008).

Juráni *et al.* (2008) investigated the effects of rooibos on the postnatal development and egg production in aged Japanese quail (*Coturnix coturnix japonica*) hens. Birds can be used as a model for ageing in biomedical research due to the fact that most species have a relatively slow ageing rate in relation to their high metabolic rates, lifetime energy expenditure, body temperature and high blood glucose levels (Juráni *et al.*, 2008).

Substitution of drinking water with rooibos tea, or supplementation of food with rooibos tea extract positively affected body weight and egg production in hens, and prolonged the productive period of aged hens. The effects observed were attributed to either the antioxidant activity or the phyto-oestrogenic activity of rooibos (Juráni *et al.*, 2008; Joubert *et al.*, 2008). Using *Caenorhabditis elegans*, Chen *et al.* (2013) investigated the protective effect of rooibos extracts against oxidative stress induced by the pro-oxidant juglone or a high glucose environment. Their results indicated that treatments with aspalathin (one of the main polyphenols in rooibos) can extend the life span of *C. elegans* during stressed conditions via the insulin/IGF signalling pathway, in addition to enhancing resistance to oxidative stress through the up-regulation and expression of stress-response related genes (Chen *et al.*, 2013).

5.1.1.5 Chemical composition

Rooibos has an interesting and unique chemical profile. An extensive range of compounds have been identified in the volatile fraction of fermented rooibos, including: ketones, aldehydes, alcohols, esters, ethers, phenols and acids, and are reported to contribute to the unique aroma of rooibos (Habu *et al.*, 1985; Kawakami *et al.*, 1993). Several non-phenolic metabolites, and minerals such as sodium, calcium, copper, iron, potassium, magnesium, manganese, nickel, phosphorous and zinc, have also been identified to a limited extent in rooibos plant material (Joubert *et al.*, 2008; Malik *et al.*, 2008). Most importantly however is the phenolic composition of rooibos. Extensive characterisation of rooibos plant material has revealed a diverse mixture of secondary phenolic metabolites including single ring phenolic acids, and monomeric flavonoids from the subclasses: dihydrochalcones, flavanones, flavones and flavonols (Beelders *et al.*, 2012).

Dihydrochalcones are biogenetic precursors of flavonoids in higher plants and have demonstrated an extensive variety of pharmacological effects (Forejtníková *et al.*, 2005). Of particular interest are the two rare dihydrochalcone C-glycosides, aspalathin and nothofagin, which have been identified in rooibos. Rooibos is currently the only known natural source of aspalathin (2',3,4,4',6'-pentahydroxy-3'-C- β -D-glucopyranosyldihydrochalcone), as well as its cyclised form aspalinin (Snijman *et al.*, 2009; Joubert & de Beer, 2011).

Nothofagin, the 3-deoxy analogue of aspalathin, has previously only been identified in the heartwood of *Nothofagus fusca* and the bark of a Chinese medicinal plant *Schoepfia chinensis*, and is present in much lower quantities (Snijman *et al.*, 2009; Joubert & de Beer, 2011). Other phenolic compounds of interest that have been identified include:

- **Flavanones:** Dihydro-orientin, dihydro-isoorientin, hemiphlorin,
- **Flavones:** Orientin, iso-orientin, vitexin and iso-vitexin, luteolin, luteolin-7-O-glucoside, chrysoeriol,
- **Flavonols:** Quercetin, isoquercitrin, hyperoside, rutin, quercetin-3-O-robinobioside,
- **Phenolic acids:** Caffeic acid, ferulic acid, *p*-coumaric acid, vanillic acid, protocatechuic acid, chlorogenic acid, salicylic acid, gallic acid, syringic acid,
- **Flavan-3-ols:** (+)-catechin, procyanidin B3
- Lignans, a phenylpyruvic acid glycoside (PPAG), as well as coumarins esculetin and esculin (von Gadow *et al.*, 1997; Mckay & Blumberg, 2007; Joubert *et al.*, 2008; Beelders *et al.*, 2012)

In addition to the compounds listed above, many others can be identified due to the fact that they can be present as free aglycones, or undergo extensive hydroxylation, methylation and glycosylation with carbohydrates and glycosides (Jaganath & Crozier, 2010). This not only contributes to their structural complexity, but also the vast number of individual compounds which have been isolated and identified.

5.1.1.5.1 Factors affecting the phenolic composition of rooibos

The phenolic composition of plant material is remarkably variable. Apart from the expected variation in phenolic composition between different populations and ecotypes of wild rooibos plants, unpublished data reported by Joubert & de Beer (2011) demonstrated large variations in aspalathin and its flavone analogue orientin within individual plants from the same plantation. Numerous factors including: the genetic variation of the seedling, geographical location, seasonal variation, cultivation methods, and harvest date have been reported to affect polyphenol compositions (van Heerden *et al.*, 2003; Joubert & Schulz, 2006; Joubert & de Beer, 2011).

Most importantly however, are the effects of plant processing and manufacturing processes (5.1.1.3). Numerous studies have shown that the fermentation process significantly reduces the total polyphenolic content of rooibos products (Bramati *et al.*, 2003; Joubert *et al.*, 2008; Marnewick *et al.*, 2000; Standley *et al.*, 2001).

Dihydrochalcones are particularly susceptible to oxidative changes. This is illustrated by the extensive degradation of aspalathin and, to a lesser extent, nothofagin during fermentation (Bramati *et al.*, 2003; Schulz *et al.*, 2003). According to the reaction mechanism described by Krafczyk & Glomb (2008), aspalathin is photochemically and enzymatically converted to its flavone analogues orientin and iso-orientin through the flavanone intermediate dihydro-iso-orientin. A similar reaction mechanism was suggested for the oxidation of nothofagin to iso-vitexin and vitexin, but lacks experimental support (Hillis & Inoue, 1967; Joubert & de Beer, 2011). Additionally, Krafczyk *et al.* (2009) demonstrated the formation of high molecular weight aspalathin and nothofagin dimers during oxidation. These high molecular weight dimers were subsequently identified as key chromophores contributing to the characteristic red-brown colour development during the fermentation of rooibos (Joubert & de Beer, 2011; Krafczyk *et al.*, 2009). These chromophores are ultimately degraded into tannin-like structures, which could therefore provide a possible explanation for the significant difference in the amount of complex tannin-like structures in fermented and green rooibos (Joubert *et al.*, 2008).

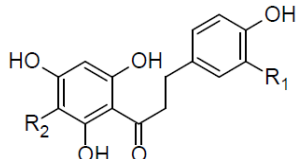
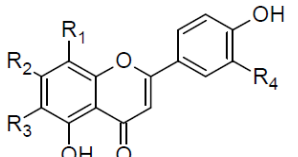
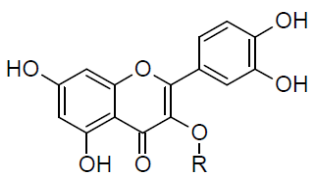
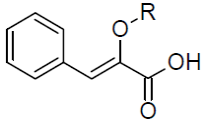
Therefore, when considering the numerous factors that influence the already complex chemical composition of plants, it becomes clear that quantitative data and comprehensive characterisation is required not only for quality control purposes, but also to assist in the complete understanding of the potential biological activity.

5.1.1.5.2 Preparation and characterization of rooibos extracts

The fermented and green rooibos extracts used in this study were a kind donation from Prof Elizabeth Joubert from the Agricultural Research Council (ARC, Infruitec-Nietvoorbij, Stellenbosch, South Africa). Characterisation of the major secondary metabolites can be seen in Table 5.1. Further information regarding the phenolic composition of the rooibos extracts will be discussed throughout this chapter.

Methods used for the preparation and characterisation of these extracts are described in section 5.2.1.

Table 5.1: Characterisation of secondary metabolites in green and fermented rooibos extracts used in this study. Phenolic content (g/100g extract) provided by Prof Elizabeth Joubert. (Muller *et al.*, 2012; Mazibuko *et al.*, 2013). (General structure and substituents adapted from Joubert *et al.*, 2008).

| Structure | Compounds | Green | Fermented |
|---|---|--------------|--------------|
|  | <i>Dihydrochalcones</i> | | |
| | Aspalathin R1 = OH, R2 = C-β-D-glucosyl | 18.44 | 0.364 |
| | Nothofagin R1 = H, R2 = C-β-D-glucosyl | 1.292 | 0.070 |
|  | <i>Flavones</i> | | |
| | Orientin R1 = C-β-D-glucosyl, R2 = R4 = OH, R3 = H | 1.050 | 0.721 |
| | Iso-orientin R1 = H, R2 = R4 = OH, R3 = C-β-D-glucosyl | 2.054 | 0.924 |
| | Luteolin-7-O-glucoside R1 = R3 = H, R2 = O-β-D-glucosyl, R4 = OH | ND | 0.069 |
| | Vitexin R1 = C-β-D-glucosyl, R2 = OH, R3 = R4 = H | 0.270 | 0.152 |
| | Iso-vitexin R1 = R4 = H, R2 = OH, R3 = C-β-D-glucosyl | 0.389 | 0.140 |
|  | <i>Flavonols</i> | | |
| | Rutin R = O-β-D-rutinosyl | 0.536 | 0.185 |
| | Quercetin-3-O-robinobioside R = O-robinosyl | 1.053 | 0.446 |
| | Hyperoside R = O-β-D-galactosyl | 0.266 | 0.087 |
| | Isoquercitrin R = O-β-D-glucosyl | 0.377 | 0.063 |
|  | <i>Phenylpyruvic acid derivative</i> | | |
| | PPAG R = O-glucosyl | 0.491 | 0.713 |
| | Total | 26.22 | 3.931 |

PPAG, 3-phenyl-2-glucopyranosyloxypropenoic acid; ND, not detected.

5.2. Methods and materials

5.2.1 Extract preparation and characterisation

Please note that the extract preparation and characterisation described below (5.2.1) was not done by the author, and that the information supplied is only intended to provide a comprehensive overview on the methods that had been used in the preparation of the extracts used in this study.

Fermented and green rooibos extracts were prepared and characterised, and then received as a kind donation from Prof Elizabeth Joubert from the Agricultural Research Council (ARC, Infruitec-Nietvoorbij, Stellenbosch, South Africa). The fermented rooibos extract was prepared on industrial scale (600 kg) as described by Mazibuko *et al.* (2013). Briefly, a hot water (>90°C) extraction was performed using a percolator type extraction vessel on a 1:10 solid: solvent mixture (m/m) for 30 minutes. This was followed by centrifugation, concentration, high-temperature short-time sterilisation and vacuum-drying. The green rooibos extract was prepared according to a patented process involving an organic solvent extraction process (80% ethanol–water mixture, at room temperature) to produce an aspalathin-enriched green rooibos extract (Grüner-Richter *et al.*, 2008). The extract was filtered, vacuum dried and finally the powder was extracted with ethylacetate to reduce the chlorophyll content.

Both extracts were characterised in terms of phenolic composition (Table 5.1) using high performance liquid chromatography with diode – array detection (HPLC-DAD) analysis as described by Beelders *et al.* (2012) and Muller *et al.* (2012). Briefly, the water-based fermented extract was dissolved in water and the solvent-based green extract was dissolved in 10% DMSO, to a concentration of 2 mg/mL. Ascorbic acid was added to a final concentration of 10 mg/ml, and filtered using a 0.22 µm pore-size Millex-GV syringe filter devices (Millipore) prior to HPLC analysis. Finally, aspalathin, nothofagin and PPAG were quantified at 288 nm, whereas orientin, iso-orientin, vitexin, iso-vitexin, hyperoside, isoquercetin, rutin and quercetin-3-O-robinobioside (as rutin equivalents) were quantified at 350 nm using 5-point calibration curves (Muller *et al.*, 2012).

Peaks were identified by comparing retention times and UV–Vis spectra with those of authentic standards, as well as through comparison to relative retention times reported by Beelders *et al.* (2012) (Muller *et al.*, 2012).

5.2.2 Endotoxin analysis

To detect the presence of bacterial endotoxins in the fermented and green rooibos extracts, the Pierce[®] LAL Chromogenic Endotoxin Quantitation Kit (Thermo Scientific, Logan, Utah, USA) was used as per manufacturer's instructions (3.2). The 96 well microplate was equilibrated at 37°C for 15 minutes. A 50 µL aliquot of the rooibos extracts (500 µg/mL) dissolved in endotoxin free water was added to the plate, covered and allowed to equilibrate at 37°C. After 5 minutes, 50 µL LAL was carefully added to each well, and the covered plate was placed on a plate shaker and left to gently shake for 10 seconds. After incubating the plate at 37°C for exactly 10 minutes, a 100 µL aliquot of the substrate solution was carefully added to each well. The plate was again placed on the plate shaker for 10 seconds, followed by incubation at 37°C for 6 minutes. A 50 µL aliquot of the Stop Reagent (25% acetic acid) was added, followed by another 10 seconds on the plate shaker. Finally the absorbance was read at 405 nm using a BioTek[®] PowerWave XS spectrophotometer (Winooski, VT, USA), and the endotoxin concentration of the rooibos extracts was then determined from a standard curve prepared as per manufacturer's instructions.

5.2.3 Cell line maintenance

Cell lines were routinely maintained as described in section 3.1. Briefly, the 3T3-L1 preadipocyte cell line (wildtype) was routinely maintained in 10 cm culture dishes with DMEM medium containing 4 mM L-glutamine, 4.5 g/L glucose and sodium pyruvate, supplemented with 10% FBS (GE Healthcare Life Sciences, Logan, Utah, USA). The mtDNA depleted 3T3-L1 preadipocyte cell line (p^0 mutants), established and characterised in Chapter 4, was routinely maintained in 10 cm culture dishes with complete medium (DMEM and 10% FBS) supplemented with 50 µg/mL uridine and 50 ng/mL EtBr (Sigma-Aldrich, St. Louis, MO, USA). Due to the short half-life of EtBr in culture medium, the culture medium was replaced daily.

During routine maintenance, a small sample of the ρ^0 mutant cell population was frequently sub-cultured in pyruvate free DMEM culture medium, without uridine and EtBr in order to evaluate the mtDNA status of the ρ^0 mutants. ρ^0 cells are characteristically auxotrophic for pyruvate and pyrimidines (uridine) and were therefore unable to survive in their absence. Both cell lines were used from passage number 8 to 24, and confluency never exceeded 80%. No antibiotics were added during routine maintenance, however, 1% (v/v) penicillin / streptomycin (P/S) (Sigma-Aldrich, St. Louis, MO, USA) was added to long term experiments exceeding 5 days.

5.2.4 Experimental design

Throughout experimental procedures wildtype and ρ^0 mutant cells were seeded during log phase, at a density of 20 000 cells/mL, unless otherwise stated, in appropriate culture vessels – as indicated by the requirements for each experiment. Cells were left overnight to attach and recover before exposure to treatments. Stock solutions of fermented and green rooibos extracts were freshly prepared in dimethyl sulfoxide (DMSO) and diluted with complete medium (DMEM and 10% FBS) to the concentration(s) required for each experiment, and therefore the final concentration of DMSO in the cultures never exceeded 0.25% (v/v). Based on preliminary findings in our laboratory a treatment concentration of 100 $\mu\text{g/mL}$ was selected for both fermented and green rooibos extracts. Included in each experiment was an untreated control, a vehicle control (0.25% DMSO in complete medium) when relevant, as well as appropriate positive controls when available. Unless otherwise stated, each treatment was performed in triplicate and the experiment was repeated 3 times (n=3).

5.2.5 Cell viability and IC₅₀ determination

In order to determine possible cytotoxic effects of rooibos extracts on wildtype and ρ^0 mutant cells, the CellTiter-Blue™ cell viability assay (Promega, Madison, WI, USA) was used (3.4). Wildtype and ρ^0 mutant cells were seeded at a density of 20 000 cells/mL in 200 μL aliquots in a 96 well plate, and allowed to attach and recover overnight.

Green and fermented rooibos extract concentration ranges of 5 – 500 µg/mL were tested in quadruplicate. Exposure times of 24, 48 and 72 hours were allowed, after which the culture medium was removed and replaced with fresh complete medium containing 200 µL/mL CellTiter-Blue™ reagent. After 3 hours of incubation at 37°C, fluorescence was measured at 540 nm (E_x) / 590 nm (E_m) using a Fluoroskan Ascent FL fluorometer (Thermo Labsystems, Finland).

5.2.6 Cell growth characteristics

Cell growth characteristics relating to viability and proliferation were continuously evaluated using an automated cell counter, Luna™ (Logos Biosystems, Korea) (3.3). Wildtype and ρ^0 mutant cells were seeded at a density of 10 000 cells/mL in 10 mL aliquots in 10 cm culture dishes. After 24 hours of incubation and exposure to treatments, cells were collected from culture plates by first washing with 500 µL of Dulbecco's phosphate buffered saline (DPBS, without Ca^{2+} and Mg^{2+}) (Lonza, Walkersville, MD, USA), followed by trypsinization (trypsin: EDTA) for 10 minutes at 37°C, and resuspension in 1 mL complete medium. A 10 µL aliquot of the cell suspension was removed and added to 10 µL of 0.4% trypan blue, followed by analysis using the automated cell counter. The remaining cells were seeded back into the original culture dish, and the process was repeated on the same plate every 24 hours for a total of 6 consecutive days as described by Yu *et al.*, 2007.

5.2.7 Cell cycle analysis

Cell cycle analysis was performed on synchronized wildtype and ρ^0 mutant cells using the Coulter® DNA Prep™ kit (Beckman Coulter, CA, USA) which utilizes propidium iodide (PI) to stain DNA and determine cell cycle distribution (3.6). Wildtype and ρ^0 mutant cells were seeded in 1.5 mL aliquots at 20 000 cells/mL in 6 well culture dishes and left overnight to attach and recover. Cells were synchronised through serum deprivation overnight, after which the serum free medium was replaced with complete culture medium containing 10% FBS, to permit re-entry into the cell cycle. DNA cell cycle analysis was performed using the Coulter® DNA Prep™ kit, as per manufacturer's instructions.

Cells were collected 24, 48, and 72 hours after adding the 10% FBS (in the absence of EtBr) and exposure to treatments, by washing with 500 μ L of DPBS (without Ca^{2+} and Mg^{2+}) (Lonza, Walkersville, MD, USA), followed by trypsinization for 10 minutes at 37°C, and resuspension in 500 μ L DPBS (with Ca^{2+} and Mg^{2+}) (Lonza, Walkersville, MD, USA). Cell suspensions were transferred into suitable polypropylene tubes, and the cells collected by centrifugation at 500 x g for 5 minutes at room temperature. A 100 μ L aliquot of lysis reagent (< 0.1% sodium azide, non-ionic detergents, saline, and stabilizers) was added to each sample, vortexed and incubated for 5 minutes at room temperature. A 500 μ L aliquot of PI (50 μ g/mL) was then added to the samples and incubated in the dark for 15 minutes at 37°C, after which samples were analysed using a Beckman Coulter Cytomics FC500 Flow Cytometer (CA, USA) (3.5) and data was recorded in FL3. Results were analysed on FlowJo v10 software (Tree Star Inc., USA).

5.2.8 Mitochondrial membrane potential

The effect of rooibos extracts on the mitochondrial membrane potential of wildtype and ρ^0 mutant cells was evaluated using the cytofluorimetric, lipophilic cationic dye JC-1 (Sigma-Aldrich, St. Louis, MO, USA) (3.7). Wildtype and ρ^0 mutant cells were seeded in 1.5 mL aliquots at 20 000 cells/mL in 6 well culture dishes and left overnight to attach and recover. Cells were collected after 24, 48, and 72 hours of exposure to treatments (in the absence of EtBr) into polypropylene tubes. JC-1 (1 mg/mL) was added to a final concentration of 2 μ g/mL in pre-warmed complete medium. Samples were allowed to incubate for 10 minutes in the dark at room temperature, after which three wash steps were performed using 500 μ L of DPBS (Lonza, Walkersville, MD, USA) and centrifugation at 500 x g for 5 minutes. Red (FL3) and green (FL1) fluorescence was recorded using a Beckman Coulter Cytomics FC500 Flow Cytometer (CA, USA) (3.5). Results were analysed on FlowJo v10 software (Tree Star Inc., USA). Valinomycin (Sigma-Aldrich, St. Louis, MO, USA), a K^+ ionophore, was used as a positive control due to its ability to dissipate the mitochondrial membrane potential (Felber & Brand, 1982). Positive control wildtype and ρ^0 mutant cells were incubated with 400 nM Valinomycin for 30 minutes prior to JC-1 staining and flow cytometric analysis.

5.2.9 Metabolic parameters: glucose utilization and lactate production.

To determine the effect of rooibos extracts on glucose utilization and lactate production of wildtype and ρ^0 mutant cells, the glucose oxidase (3.9.1) and lactate oxidase (3.9.2) assays were used.

5.2.9.1 Glucose utilization assay

Wildtype and ρ^0 mutant cells were seeded at a density of 20 000 cells/mL in 200 μ L aliquots in a 96 well plate, and allowed to attach and recover overnight. After 24, 48 and 72 hours of exposure to treatments, 5 μ L of the culture medium was removed and added to 200 μ L of the glucose oxidase assay reagent (prepared as described in Appendix II) incubated for 10 minutes at 37°C and the absorbance was read at 520 nm using a BioTek[®] PowerWave XS spectrophotometer (Winooski, VT, USA). The resultant absorbance values indicated the amount of glucose remaining in the culture medium, and glucose utilization was subsequently calculated as a percentage of the control (untreated cells).

5.2.9.2 Lactate production assay

Similar to the glucose oxidase assay, wildtype and ρ^0 mutant cells were seeded at a density of 20 000 cells/mL in 200 μ L aliquots in a 96 well plate, and allowed to attach and recover overnight. After 24, 48 and 72 hours of exposure to treatments, 5 μ L of the culture medium was removed and added to 200 μ L of the lactate oxidase assay reagent (prepared as described in Appendix II), incubated for 10 minutes at 37°C and the absorbance was read at 520 nm using a BioTek[®] PowerWave XS spectrophotometer (Winooski, VT, USA). The resultant absorbance values indicated the amount of lactate present in the culture medium, and lactate production was subsequently calculated as a percentage of the control (untreated cells).

5.2.10 Confocal microscopy

To characterise mitochondrial function in rooibos treated wildtype and ρ^0 mutant cells, JC-1 staining (3.7) was used in conjunction with confocal microscopy to observe changes in the mitochondrial membrane potential.

Confocal microscopy imaging was performed at the Confocal and Light Microscope Imaging Facility at the University of Cape Town, under the supervision of Professor Dirk Lang and Mrs. Susan Cooper. A Zeiss Axiovert LSM 510 META confocal microscope, equipped with a Zeiss AxioCam camera for fluorescent imaging, was used. The confocal microscope stage was also equipped with a specialized pre-heated (37°C) humidified chamber supplied with 5% CO₂, thus enabling live cell imaging. This was required due to the fact that JC-1 is not well retained after fixation, and enabled real time observation of mitochondrial movement and cellular activities. Cells were maintained as described in section 5.2.3. Wildtype and ρ^0 mutant cells were seeded in 500 μ L aliquots at a density of 2 000 cells/mL in specialized 35 mm glass bottom culture dishes to enable the use of higher objective imaging, and left overnight to attach and recover. After 48 hours of exposure to treatments, JC-1 (Sigma-Aldrich, St. Louis, MO, USA) staining was performed according to manufacturer's instructions. Briefly, cells were incubated with pre-warmed complete culture medium containing JC-1 (2 μ g/mL), for 20 minutes in the dark at 37°C. The staining solution was removed and cells were carefully washed using DPBS (Lonza, Walkersville, MD, USA). Fresh complete culture medium was added to the culture dishes, which were then allowed to equilibrate in the chamber for \pm 10 minutes. A 488 nm laser line was used for excitation, along with appropriate band pass filters (CH2: BP 500-550 IR; CH3: BP 575-630 IR) to enable detection of green (CH2) and red (CH3) fluorescence emissions. High resolution static images, time lapse images, as well as optical slice (Z-stack) images taken at 1 μ m intervals along the z axis, were acquired using a Plan-Apochromat 63x oil immersion objective (NA=1.4). The laser light intensity and detector gains were set such that fluorescence intensities of both dyes were below saturation levels. Similarly, the pinhole size was kept constant throughout acquisition at 192 μ m (CH2) and 220 μ m (CH3) to avoid oversampling. Post-acquisition processing was performed using ZEN 2012 software (Carl Zeiss Microscopy GmbH, 2011).

5.3 Results and discussion

The aim of this study was to investigate the potential anti-ageing properties of green and fermented rooibos extracts using the *in vitro* cell culture model representative of mitochondrial dysfunction associated with the age related decline in preadipocyte function, established and characterised in chapter 4. The effects of rooibos on cell growth and proliferation, mitochondrial membrane potential, and metabolic parameters such as glucose utilization and lactate production, was therefore evaluated using 3T3-L1 preadipocytes (wildtype) as well as ρ^0 3T3-L1 preadipocytes (ρ^0 mutants).

Please note that throughout this chapter, experimental results are presented for wildtype and ρ^0 mutant cell populations in purple and red, respectively.

Based on previous work done in our laboratory with regards to the positive effect of rooibos extracts as well as the lack of cytotoxicity, a treatment concentration of 100 $\mu\text{g}/\text{mL}$ was selected for both fermented and green rooibos extracts, and was used throughout this study. Wisman *et al.* (2008) showed that polyphenolic compounds strongly interfere with the redox chemistry of metabolic assays such as the MTT assay. Therefore, the results obtained from the initial cell viability assays, including those described in section 5.2.5 were re-evaluated using the trypan blue exclusion assay (as described for cell growth characteristics in section 5.2.6), which revealed significantly different results. It was however confirmed that the concentration of 100 $\mu\text{g}/\text{mL}$ used throughout this study was not cytotoxic, and no IC_{50} value could be established for both the green and fermented rooibos extracts in the wildtype and ρ^0 mutant cell lines in the range tested.

5.3.1 Endotoxin analysis

Adipocytes (including preadipocytes) are particularly sensitive to endotoxins (LPS) and other factors such as tumour necrosis factor- α (TNF- α), interleukin-6 (IL-6), and interferon- γ (IFN- γ) due to the fact that, apart from its primary energy storing function, adipose tissue also forms an integral component of the innate immune response, mediated primarily through highly conserved pattern recognition receptors such as toll-like receptors (TLRs) (Chirumbolo *et al.*, 2013; Schäffler & Schölmerich, 2010; Tchkonja *et al.*, 2010).

Preadipocytes constitutively express toll-like receptor 4 (TLR4), which can be activated by the lipid A moiety of LPS, resulting in lipolysis, insulin resistance and inflammation (3.2). Pharmacopoeias describe acceptance criteria and limits of endotoxin levels in *in vitro* biological test systems, which should be below 1 ng/mL (Ryan, 2008). Using the Pierce LAL Chromogenic Endotoxin Quantitation Kit (Thermo Scientific, Logan, Utah, USA), capable of detecting endotoxin levels as low as 0.1 endotoxin unit (EU)/mL or ± 0.01 ng endotoxin/mL, it was established that both the fermented and green rooibos extracts were free of detectable endotoxins (Results not shown).

5.3.2 Cell growth characteristics

Using an automated cell counter, cell numbers (total, live and dead) and % viability were evaluated every day for 6 consecutive days in order to establish growth curves (Figure 5.3 and 5.5) from which population doubling times could be calculated as described in section 4.3.1.1.

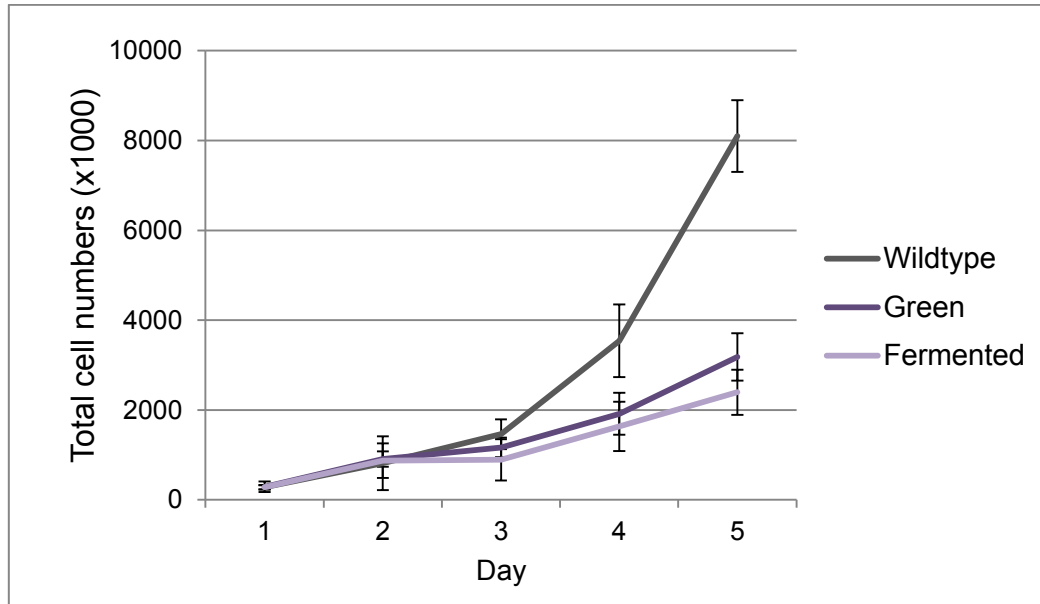


Figure 5.3: Comparison of the growth rate of untreated and rooibos treated (100 $\mu\text{g}/\text{mL}$) wildtype cells. Total cell number indicates the viable cell density determined using trypan blue staining. Error bars represent SD of nine replicate values ($n=3$).

Comparing the growth curve of the untreated cell population with the green and fermented rooibos treated cell populations (Figure 5.3) a considerably decreased growth rate can be observed. This was confirmed by the increased population doubling times observed for green (19.3 ± 3.8) hours) and fermented (20.6 ± 4.6) hours) rooibos treated cell populations, relative to that of untreated cells (18.8 ± 2.1) hours). It should however be considered that the population doubling times were calculated during the most linear growth phases (48 – 120 hours), thereby excluding and underestimating the positive effects seen within 24 (day 1) and 48 hours (day 2) of treatment. Although the growth curves provide an interesting perspective on the effect of extensive rooibos treatment (5 days) on cell proliferation, the observable effects within the first two days of treatment are unclear, therefore an alternative representation of these results can be seen in Figure 5.4, in which the cell density of rooibos treated cells was calculated as a percentage relative to untreated wildtype cells.

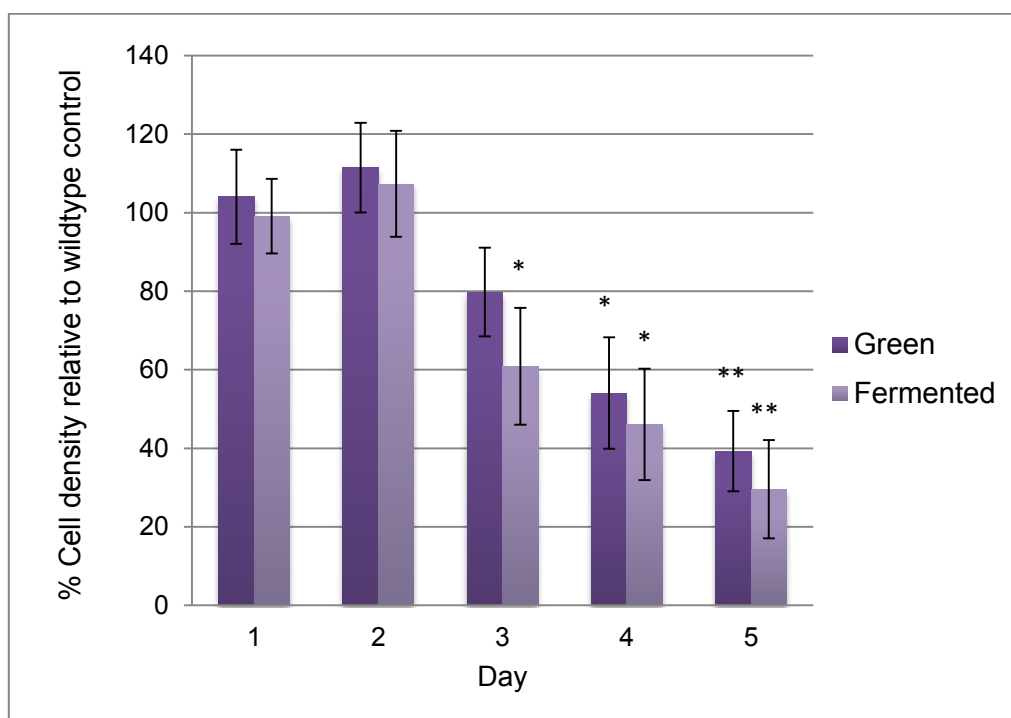


Figure 5.4: Cell density of rooibos treated (100 µg/mL) wildtype cells represented as a percentage of the untreated wildtype control (100%). Total viable cell number determined using trypan blue staining, represented as a % value relative to the untreated control. Error bars represent SD of nine replicate values (n=3). Statistical significance was determined using the two-tailed Student *t*-test and is indicated for $p < 0.05$ (*) and $p < 0.005$ (**) relative to untreated control.

From the results presented in Figure 5.4, it can be seen that although not statistically significant, after 48 hours (day 2) of treatment with green and fermented rooibos, the respective cell densities had increased by 11% and 7%, relative to the untreated control. However, after 72 hours (day 3) of treatment with rooibos, the cell densities were significantly reduced compared to the untreated control.

As established in section 4.3.1.1, ρ^0 mutants have a significantly decreased growth rate compared to wildtype cells. Figure 5.5 and 5.6 illustrate the effect of green and fermented rooibos on the growth rate of ρ^0 mutants.

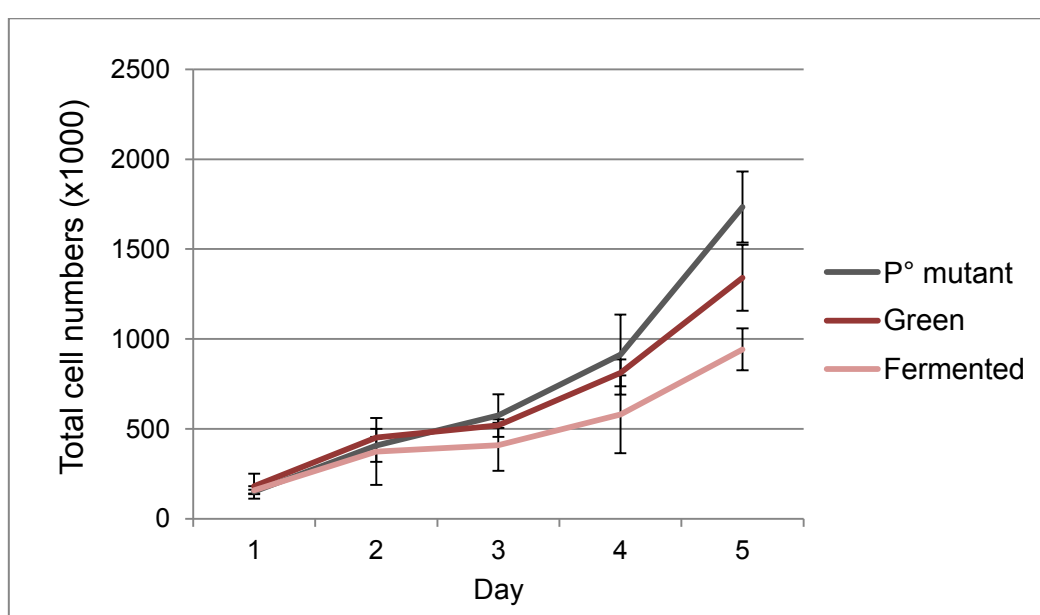


Figure 5.5: Comparison of the growth rate of untreated and rooibos treated (100 $\mu\text{g/mL}$) ρ^0 mutant cells. Total cell number indicates the viable cell density determined using trypan blue staining. Error bars represent SD of nine replicate values ($n=3$).

Using the above results (Figure 5.5) population doubling times of 29.8 ± 3.8 and 32.4 ± 3.8 hours were determined for green and fermented rooibos treated ρ^0 mutant cell populations, compared to 30.2 ± 4.2 hours established for untreated ρ^0 mutant cells (4.3.1.1). Again it should be considered that population doubling times were calculated during the most linear growth phases (48 – 120 hours), thereby excluding and underestimating the positive effects seen within the 24 and 48 hours of treatment. Consequently, an alternative representation of these results can be seen in Figure 5.6.

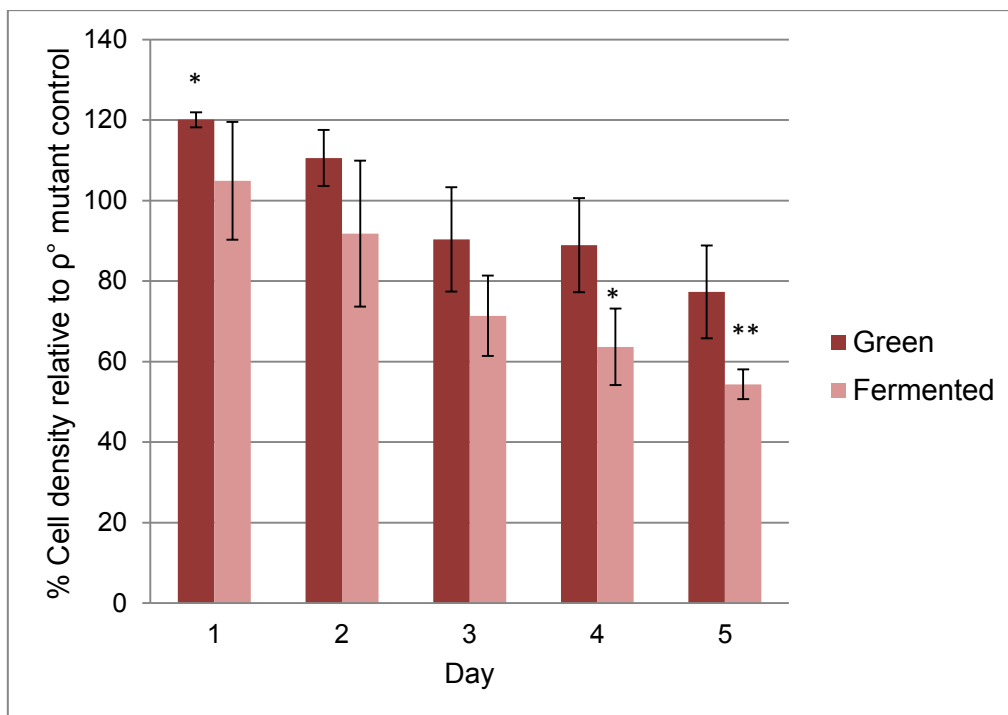


Figure 5.6: Cell density of rooibos treated (100 $\mu\text{g/mL}$) ρ^0 mutants represented as a percentage of the untreated ρ^0 mutant control (100%). Total viable cell number determined using trypan blue staining, represented as a % value relative to the untreated control. Error bars represent SD of eight replicate values. Statistical significance was determined using the two-tailed Student *t*-test and is indicated for $p < 0.05$ (*) and $p < 0.005$ (**) relative to untreated ρ^0 mutant control.

Relative to untreated ρ^0 mutant cells, treatment with green rooibos resulted in a 20% increase in the cell density after 24 hours (day 1), an effect which was somewhat diminished after 48 hours (day 2) of treatment when only a 10% increase in cell density was observed. Treatment with fermented rooibos on the other hand, only resulted in a slight, insignificant 5% increase in cell density after 24 hours (day 1), after which a progressive decrease in cell density can be observed.

The results obtained indicate that although an increase in cell density was initially observed for wildtype and ρ^0 mutant cell populations after 24 and 48 hours of treatment with green rooibos, prolonged treatment (day 3 – day 5) resulted in a progressive decrease in cell density. This effect was even more notable for fermented rooibos treated wildtype and ρ^0 mutant cell populations, thereby implicating the different phenolic compositions of the rooibos extracts, as defined in Table 5.2, which will be discussed at the end of this results and discussion section.

Of particular interest, is the observation that ρ^0 mutant cells responded much more favourably to the rooibos treatments compared to wildtype cells, as can be seen when comparing the cell densities throughout the 5 days of treatment. Cell viability as determined by trypan blue exclusion was unaffected throughout the 5 days of treatment with green and fermented rooibos in both the wildtype and ρ^0 mutant cell populations, thereby indicating that the decrease in cell density is attributed to altered cell growth kinetics, possibly involving a delay in the cell cycle progression at certain checkpoints.

5.3.3 Cell cycle analysis

The effect of rooibos treatment on the cell growth characteristics prompted the investigation of the cell cycle distribution. Cell cycle analysis was performed on synchronised rooibos treated and untreated wildtype and ρ^0 mutant cells after 24, 48 and 72 hours. A summary of the percentage cells present in each cell cycle phase is presented in Table 5.2 and 5.3, and representative histograms in Figure 5.7 and 5.8.

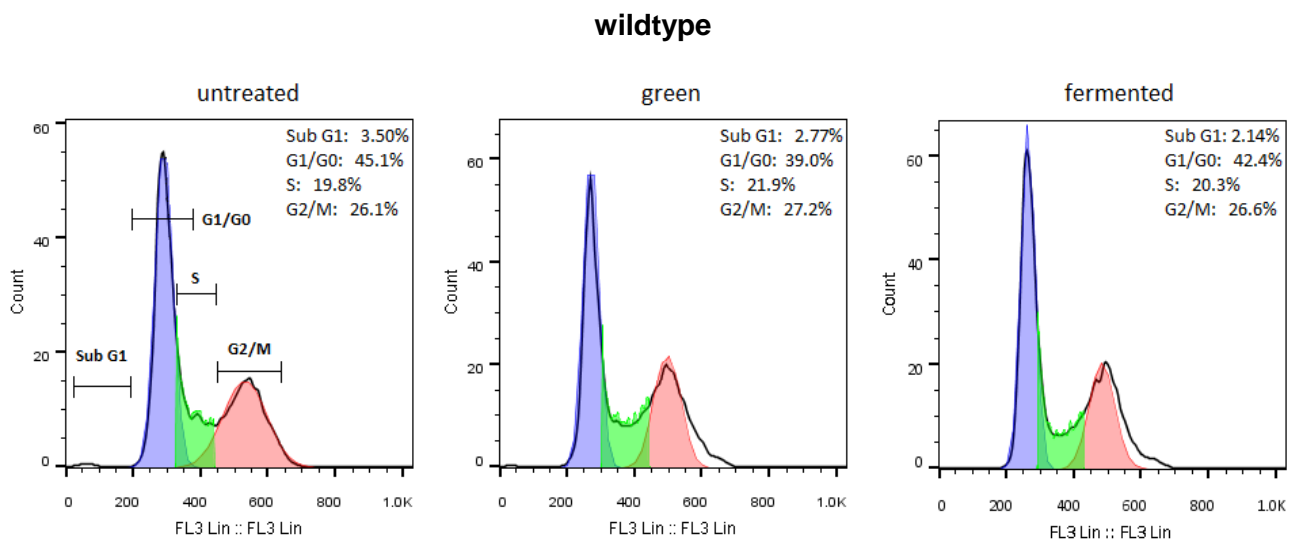


Figure 5.7: Representative cell cycle histograms illustrating DNA distribution for untreated and rooibos treated (100 $\mu\text{g}/\text{mL}$) wildtype cells. Cells were synchronised through serum deprivation overnight, after which re-entry into the cell cycle was initiated by the addition of 10% FBS to the culture medium. Cell cycle analysis was performed after 48 hours using PI staining. Ten thousand events were recorded for each sample on a Beckman Coulter Cytomics FC500 flow cytometer, and results were analysed using FlowJo v10 software. Percentage (%) values indicate the amount of cells present in each phase. One representative of 3 experiments performed in triplicate.

Table 5.2: Summary of cell cycle analysis results obtained for untreated and rooibos treated (100 µg/mL) wildtype cells. Cell cycle analysis was performed using PI staining 24, 48, and 72 hours after re-entry into the cell cycle following synchronization through serum deprivation.

| | | wildtype | green | fermented |
|-----------------|---------------|-------------|---------------|---------------|
| 24 hours | Sub-G1 | 3.13 ± 0.38 | 4.14 ± 1.48 | 3.67 ± 0.88 |
| | G1/G0 | 44.6 ± 1.38 | 36.5 ± 5.80 * | 41.7 ± 7.32 |
| | S | 20.2 ± 1.26 | 29.5 ± 10.9 * | 24.1 ± 6.52 |
| | G2/M | 26.5 ± 1.04 | 26.0 ± 6.81 | 26.9 ± 6.72 |
| 48 hours | Sub-G1 | 2.93 ± 0.55 | 3.59 ± 1.20 | 3.35 ± 0.38 |
| | G1/G0 | 42.2 ± 2.78 | 42.3 ± 3.52 | 48.0 ± 4.84 * |
| | S | 18.5 ± 4.66 | 14.6 ± 5.20 | 15.2 ± 5.68 |
| | G2/M | 30.0 ± 3.17 | 34.2 ± 5.77 * | 28.7 ± 4.19 |
| 72 hours | Sub-G1 | 3.70 ± 0.54 | 3.74 ± 1.18 | 3.09 ± 0.89 |
| | G1/G0 | 43.0 ± 1.51 | 45.3 ± 8.75 | 45.7 ± 9.66 |
| | S | 15.2 ± 2.65 | 19.6 ± 7.80 | 14.8 ± 4.21 |
| | G2/M | 31.7 ± 1.76 | 26.8 ± 2.15 * | 31.2 ± 6.53 |

Experiments were conducted in triplicate and performed 3 independent times. Values indicate mean % ± SD of all experimental data. Statistical significance was determined using the two-tailed Student *t*-test and is indicated for $p < 0.05$ (*) and $p < 0.005$ (**) relative to untreated control.

As expected, the most significant changes in the cell cycle distribution of rooibos treated wildtype cell populations were observed after 24 and 48 hours of treatment. Most notably, after 24 hours of treatment with green rooibos an 8.1% decrease in the amount of cells present in the G1/G0 phase is observed, corresponding to a 9.3% increase in the amount of cells present in the S phase. This is followed by a concurrent 3.9% increase in the amount of cells present in the G2/M phase after 48 hours of treatment. A more moderate response was observed for the fermented rooibos treated cells which, after 24 hours of treatment, exhibited a much smaller increase in the amount of cells present in the G1/G0 phase (2.9%) corresponding to a small increase in the amount of cells present in S phase (4.1%).

However, after 48 hours a significant increase (5.8%) in the amount of cells present in the G1/G0 phase was observed. Therefore the cell cycle analysis results were consistent with the observed growth rates. The progression of ρ^0 mutants through the cell cycle occurred much slower compared to wildtype cells, as indicated by the significant increase (5.3%) in the amount of cells remaining in the G1/G0 phase associated with the decreased (2.4%) amount of cells present in the S phase.

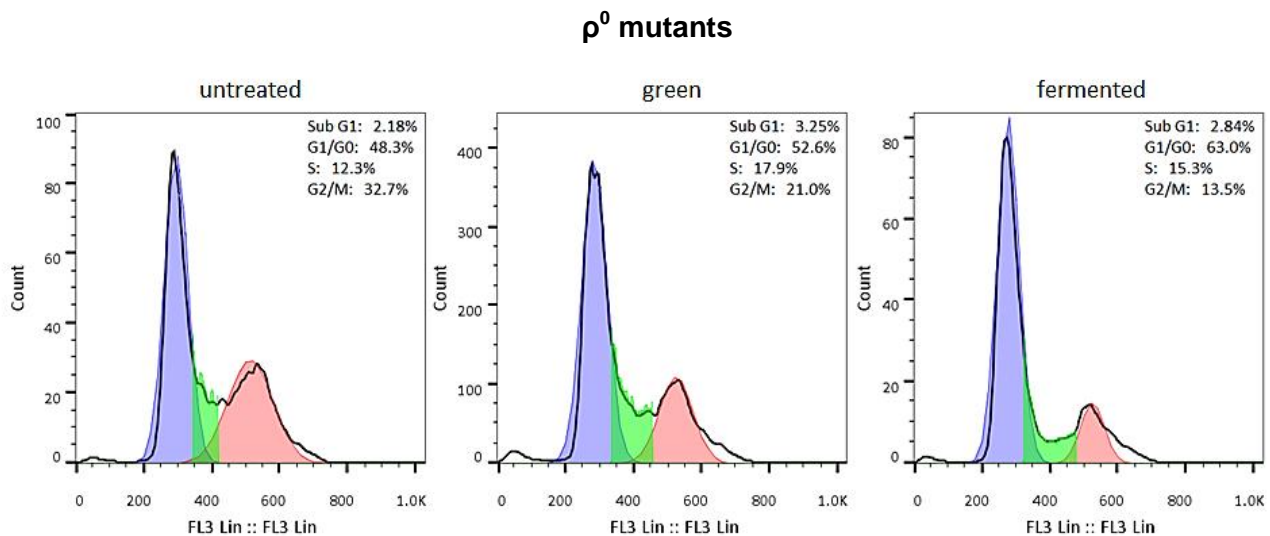


Figure 5.8: Representative cell cycle histograms illustrating DNA distribution for untreated and rooibos treated (100 $\mu\text{g}/\text{mL}$) ρ^0 mutants. Cells were synchronised through serum deprivation overnight, after which re-entry into the cell cycle was initiated by the addition of 10% FBS to the culture medium. Cell cycle analysis was performed after 48 hours using PI staining. Ten thousand events were recorded for each sample on a Beckman Coulter Cytomics FC500 flow cytometer, and results were analysed using FlowJo v10 software. Percentage (%) values indicate the amount of cells present in each phase. One representative of 3 experiments performed in triplicate.

Comparing the DNA distribution throughout the cell cycle histogram of the green and fermented treated ρ^0 mutants, relative to the untreated ρ^0 mutant cells, a decrease in the size of the G2/M peak area is apparent, together with a small but significant increase in the S phase area. These results are congruent with the growth rates observed for ρ^0 mutants.

Ideally these results would have been confirmed using a proliferation assay to determine new DNA synthesis, thereby providing more information on the S phase population. However due to technical difficulties, and subsequent inconsistent results, this experiment was excluded from this document and would have to be repeated.

Table 5.3: Summary of cell cycle analysis results obtained for untreated and rooibos treated (100 µg/mL) ρ^0 mutants. Cell cycle analysis was performed using PI staining 24, 48, and 72 hours after re-entry into the cell cycle following synchronization through serum deprivation.

| | | ρ^0 mutant | green | fermented |
|-----------------|---------------|-----------------|----------------|-----------------|
| 24 hours | Sub-G1 | 2.43 ± 1.53 | 1.68 ± 0.35 | 2.56 ± 0.66 |
| | G1/G0 | 48.8 ± 3.34 | 42.0 ± 0.83 ** | 47.1 ± 2.17 |
| | S | 18.8 ± 3.02 | 18.3 ± 1.45 | 17.1 ± 1.87 |
| | G2/M | 23.2 ± 2.68 | 32.0 ± 2.63 ** | 28.1 ± 1.77 * |
| 48 hours | Sub-G1 | 2.02 ± 0.46 | 2.61 ± 0.43 | 2.68 ± 1.11 |
| | G1/G0 | 49.0 ± 2.70 | 52.4 ± 5.60 | 59.8 ± 4.92 ** |
| | S | 13.3 ± 3.47 | 16.8 ± 3.91 | 15.0 ± 4.80 |
| | G2/M | 31.7 ± 2.15 | 24.3 ± 2.95 ** | 18.9 ± 3.36 ** |
| 72 hours | Sub-G1 | 3.59 ± 0.95 | 3.86 ± 1.41 | 2.96 ± 1.65 |
| | G1/G0 | 48.7 ± 2.22 | 55.4 ± 9.21 | 63.7 ± 8.87 ** |
| | S | 14.6 ± 1.68 | 18.9 ± 4.76 * | 17.8 ± 7.34 |
| | G2/M | 33.2 ± 1.05 | 20.9 ± 5.08 ** | 19.94 ± 4.37 ** |

Experiments were conducted in triplicate and performed 3 independent times. Values indicate mean % ± SD of all experimental data. Statistical significance was determined using the two-tailed Student *t*-test and is indicated for $p < 0.05$ (*) and $p < 0.005$ (**) relative to untreated ρ^0 mutant control.

Considering that ρ^0 mutants generally exhibit a delay in G1-S phase transition, as indicated by a significant increase in the amount of cells present in the G1 phase relative to wildtype cells, the significant decrease (6.8%) in the amount of cells in the G1/G0 phase after 24 hours of treatment with green rooibos, along with a concurrent increase (8.8%) in the amount of cells present in the G2/M phase, indicates that the rooibos treatment stimulated cell cycle progression.

This is in accordance with the increased proliferation and cell density observed after 24 hours of treatment with green rooibos, as indicated previously (Figure 5.5 and 5.6).

However, after 48 hours of treatment with green and fermented rooibos, a complete change in the cell cycle distribution is seen due to the increase in the amount of cells present in the G1/G0 phase, as well as the S phase compared to a significant decrease in the amount of cells present in the G2M phase. Interestingly, after 72 hours of exposure to rooibos, the most notable change observed is the increased number of cells present in the G1/G0 phase for both green and fermented rooibos, along with a slight increase in the number of cells present in the S phase, and a large decrease in the number of cells present in the G2/M phase. This is therefore in accordance with the decreased proliferation rate, as well as the subsequent decrease in cell density, as previously indicated (Figure 5.5 and 5.6).

It is difficult to compare results of other rooibos studies to that of this study, due to the fact that different rooibos extracts were used, at different concentrations, for different cell lines, at different exposure times. Lamosová *et al.* (1997) showed that treatment with 2, 10 and 100% of rooibos tea extract significantly inhibited proliferation of chick embryonic skeletal muscle cells. It was proposed that apart from the harmful effect of ROS on cellular constituents, it is also involved in cell division and mitosis among other physiological functions. Therefore, the strong antioxidant properties of the rooibos extracts could inhibit mitosis and cell division by removing reactive oxygen species needed for mitogenic stimulation of cells (Lamosová *et al.*, 1997). Low physiologic levels of ROS have been shown to stimulate cell proliferation in multiple cell types, similarly the reduction of intracellular ROS in response to the addition of antioxidants such as vitamins (E, C and A), or N-acetyl-L-cysteine, has been shown to decrease cellular proliferation (Havens *et al.*, 2006). Although this could be relevant to the results obtained in the present study, comparing the phenolic composition of the green and fermented rooibos extracts (Table 5.1) showed that the green rooibos extract had a total phenolic content of 26.22 g/100g compared to the fermented extract, 3.931 g/100g. Bearing in mind that antioxidant properties of rooibos are related to its total phenolic content, this does not provide an adequate explanation for the results obtained.

The synergistic / antagonistic effects between any of these phenolic compounds are obviously of critical importance, however very little is known about the exact reaction mechanisms involved. Considering that a positive effect on the cell density, and therefore the rate of proliferation was seen within the shorter treatment times of 24 and 48 hours, and that the inhibitory effects were only seen after 72 hours of treatment, it could indicate that oxidative changes in the phenolic compounds could have taken place, due to their instability in the culture medium, which could have induced a pro-oxidant effect (Joubert *et al.*, 2005; Magcwebeba, 2011). The pro-oxidant effects of flavonoids are associated with an increase in ROS and/or variation in endogenous antioxidant molecules such as GSH. Semiquinone or phenoxyl radicals and ROS can be generated from flavonoid compounds through processes such as auto-oxidation involving redox active polyphenol-metal complexes, radical scavenging, as well as the Fenton type reaction (Magcwebeba, 2011; Procházková *et al.*, 2011).

The effects of these pro-oxidant properties have been investigated *in vitro* (Joubert *et al.*, 2005; Marnewick *et al.*, 2009). In this regard, testing lower concentrations of rooibos, within a range that does not negatively influence proliferation may provide an opportunity to distinguish the apparent biphasic effect of rooibos on preadipocyte function. Nonetheless it is clear that the health benefits of rooibos may be context dependent and thus require careful experimental design and data interpretation to ensure accurate conclusions.

5.3.4 Mitochondrial membrane potential

The effect of rooibos treatment on the mitochondrial membrane potential ($\Delta\Psi_m$) was determined using the lipophilic cationic dye JC-1, which exhibits a potential-dependent accumulation in the mitochondria (3.7). JC-1 will either be retained in the mitochondria due to the negative charge established by the intact $\Delta\Psi_m$ and form J-aggregate complexes emitting a red fluorescence (polarised mitochondria) or, will diffuse into the cytoplasm due to a collapse in $\Delta\Psi_m$, where the monomeric form will exhibit a green fluorescence (depolarised mitochondria).

The results shown in Figures 5.9 and 5.10 illustrate the effects of rooibos treatment on the mitochondrial membrane potential of wildtype and ρ^0 mutant cells, respectively, observed after 24, 48 and 72 hours. Representing the $\Delta\Psi_m$ is the ratio of the mean fluorescence intensity of FL3 (red) to FL1 (green).

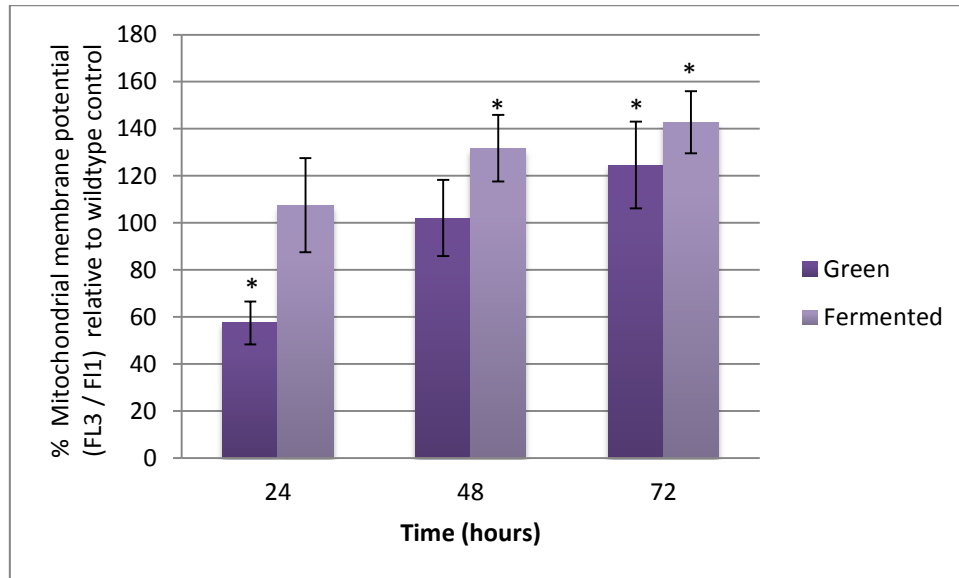


Figure 5.9: Mitochondrial membrane potential of rooibos treated (100 $\mu\text{g}/\text{mL}$) wildtype cells after 24, 48 and 72 hours, represented as a percentage of the untreated wildtype control (100%). Cells were stained with the polychromatic, $\Delta\Psi_m$ sensitive probe JC-1. The mitochondrial membrane potential is represented as the ratio of the mean fluorescence intensity of FL3 (red) to FL1 (green). Error bars represent SD of nine replicate values ($n=3$). Statistical significance was determined using the two-tailed Student t -test and is indicated for $p < 0.05$ (*) and $p < 0.005$ (**) relative to untreated control.

Compared to untreated wildtype cells, the above results show that after 24 hours of treatment with green rooibos, a significant reduction (45%) in $\Delta\Psi_m$ was observed, followed by a significant increase (25%) in $\Delta\Psi_m$ after 72 hours. Treatment with fermented rooibos resulted in a significant increase in $\Delta\Psi_m$ after 48 (32%) and 72 (43%) hours.

P^0 mutants have a significantly lowered $\Delta\Psi_m$ compared to wildtype cells (4.3.1.3). The $\Delta\Psi_m$ is established through the activity of oxidative phosphorylation, conducted by respiratory chain complexes located within the inner mitochondrial membrane.

Out of the 5 respiratory chain complexes, 4 are encoded by the mitochondrial genome, consequently depletion of mtDNA results in defective mitochondrial respiration and oxidative phosphorylation, subsequently dissipating the $\Delta\Psi_m$.

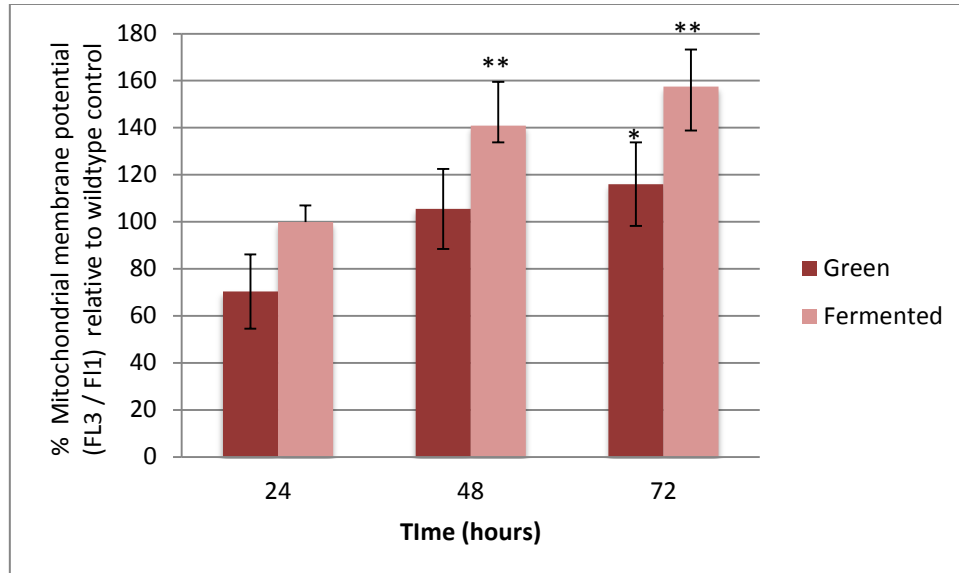


Figure 5.10: Mitochondrial membrane potential of rooibos treated (100 $\mu\text{g/mL}$) ρ^0 mutants after 24, 48 and 72 hours, represented as a percentage of the untreated ρ^0 mutant control (100%). Cells were stained with the polychromatic, $\Delta\Psi_m$ sensitive probe JC-1. The mitochondrial membrane potential is represented as the ratio of the mean fluorescence intensity of FL3 (red) to FL1 (green). Error bars represent SD of nine replicate values ($n=3$). Statistical significance was determined using the two-tailed Student t -test and is indicated for $p < 0.05$ (*) and $p < 0.005$ (**). Error bars represent SD of nine replicate values ($n=3$). Statistical significance was determined using the two-tailed Student t -test and is indicated for $p < 0.05$ (*) and $p < 0.005$ (**). Error bars represent SD of nine replicate values ($n=3$). Statistical significance was determined using the two-tailed Student t -test and is indicated for $p < 0.05$ (*) and $p < 0.005$ (**).

The results obtained for ρ^0 mutants (Figure 5.10) indicate a somewhat similar trend to that observed for the wildtype cells (Figure 5.9). The decrease (30%) in $\Delta\Psi_m$ observed after 24 hours of treatment with green rooibos could possibly be related to the corresponding cell cycle analysis results (5.3.2), due to the observed decrease in the amount of cells in the G1/G0 phase relative to untreated ρ^0 mutants (explained below). Once again, the observation of hyperpolarization after 48 and 72 hours of treatment could be associated with processes such as the activation of mitochekpoint, autophagy, or other metabolic processes. On the other hand, these effects might simply be due to improved mitochondrial health and activity, however further investigation into the effects of rooibos on specific mitochondrial bioenergetics will have to be done (as discussed in Chapter 6).

Fluctuations in $\Delta\Psi_m$ impact the functioning of the mitochondria with respect to energy metabolism, intracellular ion homeostasis, and perhaps most importantly the cell life – death transition (Perry *et al.*, 2011). A decrease in $\Delta\Psi_m$ is often an early indicator of apoptosis. However, considering that no changes in cell viability was observed, it indicated that the decreased $\Delta\Psi_m$ might be the result of decreased mitochondrial respiration which could occur during quiescence or ensuing cellular stress, leading to a transient mitochondrial membrane permeabilization. Although the exact mechanisms are still poorly understood, studies have shown that mitochondrial dynamics relating to morphology, mitochondrial membrane potential, oxidative phosphorylation activity, size, distribution and abundance, are important mediators in cell cycle progression (Arakaki *et al.*, 2006; Ferree & Shirihai, 2012; Koopman *et al.*, 2013; Mitra *et al.* 2009). As the cell progresses through the G1 phase, mitochondria convert from isolated, fragmented elements into a giant hyperfused and remarkably hyperpolarized, tubular network at the G1-S transition.

The decreased $\Delta\Psi_m$ observed after 24 hours of treatment with green rooibos could possibly be related to the corresponding cell cycle analysis results (5.3.2), given that the green rooibos treated cells could have proceeded through the G1-S transition faster than the untreated cells. This would not only account for the significantly decreased G1/G0 phase cell population along with the increased S phase cell population, but also the decreased $\Delta\Psi_m$, due to the fact that the highest $\Delta\Psi_m$ is observed at the G1-S transition (large hyperfused tubular network), after which the mitochondrial network fragments and separates in preparation for the G2/M phase. Similarly, the hyperpolarized $\Delta\Psi_m$ observed for green rooibos after 72 hours, and fermented rooibos after 48 and 72 hours, could also be related to the corresponding cell cycle analysis results (5.3.2).

However, seeing as the formation of the hyperpolarised, hyperfused tubular network at the G1-S transition is transient, and that the cell cycle analysis results indicated no significant changes in the distribution of cells throughout the cell cycle compared to untreated cells, it should be considered that the increased $\Delta\Psi_m$ could be associated with processes such as the activation of mitochekpoint, autophagy, or other metabolic processes. Additionally, hyperpolarisation of $\Delta\Psi_m$ has previously been shown to inhibit mitogenesis of lymphocytes and spleen cells (Chang *et al.*, 2001).

Interestingly, the green extract showed a more prominent effect on the cell cycle and cell growth characteristics compared to the fermented extract, however it exhibited a lesser effect on the mitochondrial membrane potential compared to the fermented extract, suggesting that these effects are independent, at least within the context of this experimental model, and that additional molecular mechanisms may also be involved. This discrepancy could be attributed to the varied antioxidant activities and the threshold required to initiate a particular cellular response.

5.3.5 Metabolic parameters: glucose utilization and lactate production

Given that glucose metabolism is strongly correlated to mitochondrial function, glucose utilization and lactate production was investigated as markers for changes in mitochondrial function upon treatment with rooibos using both wildtype and ρ^0 mutant cells. Considering the variation in cell growth characteristics (5.3.2), results were normalised to the respective cell densities. Results are expressed as a percentage of glucose utilization (Figure 5.11 and 5.13) and lactate production (Figure 5.12 and 5.14) relative to untreated cells.

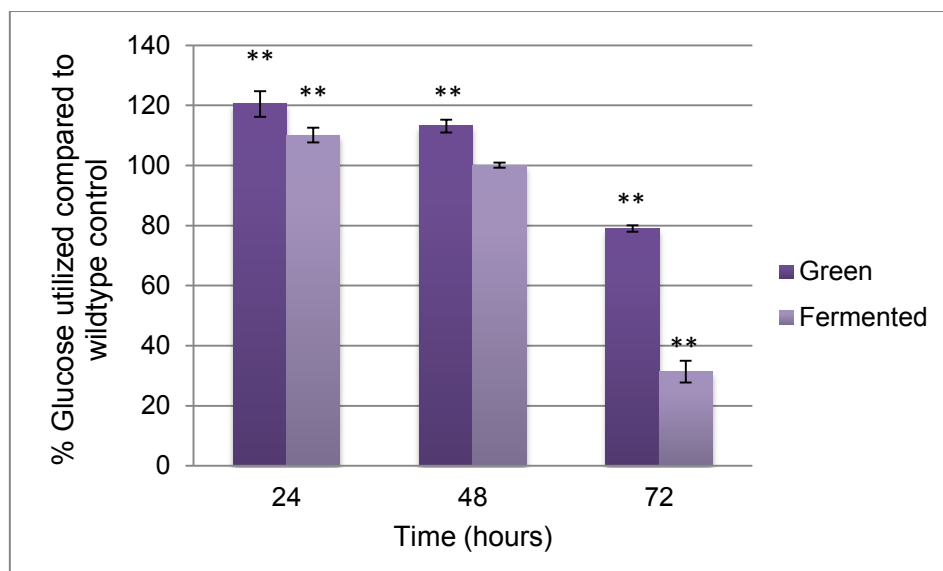


Figure 5.11: Normalised glucose utilization by rooibos treated (100 µg/mL) wildtype cells after 24, 48 and 72 hours, represented as a percentage of the untreated wildtype control (100%). Error bars represent SD of nine replicate values (n=3). Statistical significance was determined using the two-tailed Student *t*-test and is indicated for $p < 0.005$ (**) relative to untreated control.

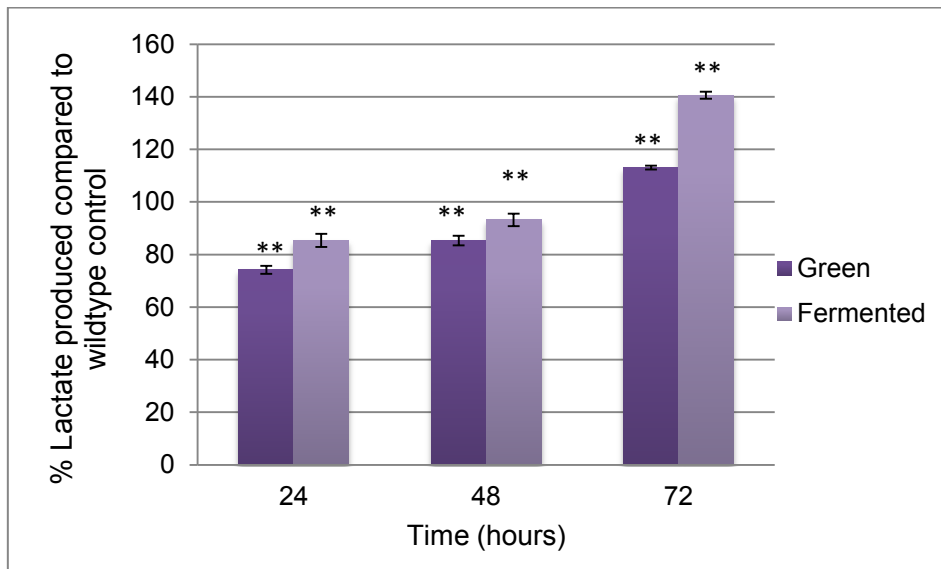


Figure 5.12: Normalised lactate production by rooibos treated (100 µg/mL) wildtype cells after 24, 48 and 72 hours, represented as a percentage of the untreated wildtype control (100%). Error bars represent SD of nine replicate values (n=3). Statistical significance was determined using the two-tailed Student *t*-test and is indicated for $p < 0.005$ (**) relative to untreated control.

Numerous studies have demonstrated that rooibos treatment increases glucose uptake (Joubert & de Beer, 2011; Muller *et al.*, 2012; Sanderson *et al.*, 2014). It is therefore not surprising that an increase in glucose utilization was observed after 24 and 48 hours of treatment with green and fermented rooibos. However after 72 hours of treatment, glucose utilization is significantly reduced relative to untreated cells. A progressive increase in lactate production can be observed as the green and fermented rooibos treatment time increases.

Mitochondrial respiration and oxidative phosphorylation is impaired in ρ^0 mutants, resulting in an overreliance on glycolysis to produce the required cellular ATP. Considering that only 2 ATP molecules are produced per glucose molecule during glycolysis, compared to a total of 36 produced through the complete mitochondrial respiration process, it is clear that a significant increase in glucose utilization is expected. The overreliance on glycolysis leads to an accumulation of NADH, which has to be regenerated to NAD^+ through the conversion of pyruvate to lactate via lactate dehydrogenase resulting in an increase in lactate production. Therefore, compared to wildtype cells, glucose utilization and lactate production are significantly increased in ρ^0 mutants (4.3.1.4).

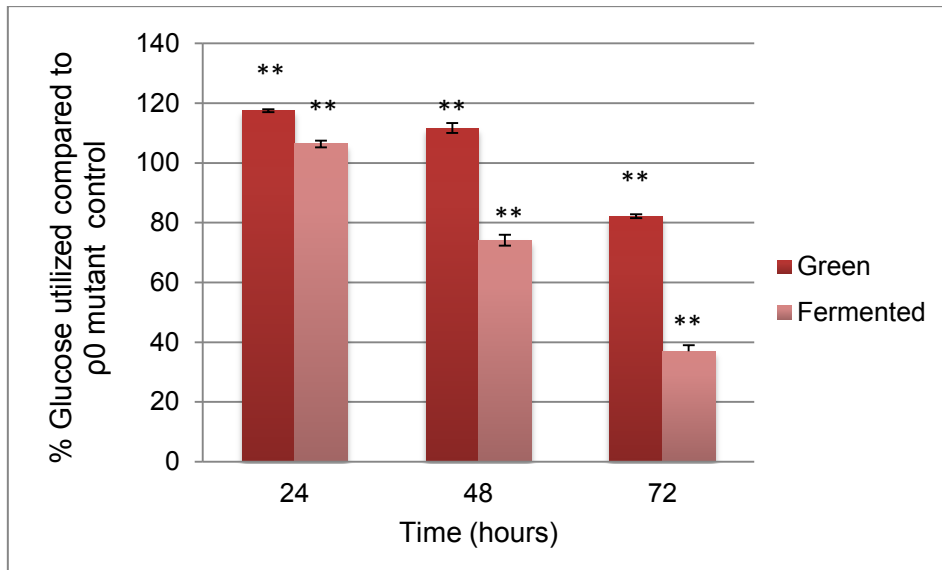


Figure 5.13: Normalised glucose utilization by rooibos treated (100 µg/mL) ρ^0 mutant cells after 24, 48 and 72 hours, represented as a percentage of the untreated ρ^0 mutant control (100%). Error bars represent SD of nine replicate values (n=3). Statistical significance was determined using the two-tailed Student *t*-test and is indicated for $p < 0.005$ (**) relative to untreated control.

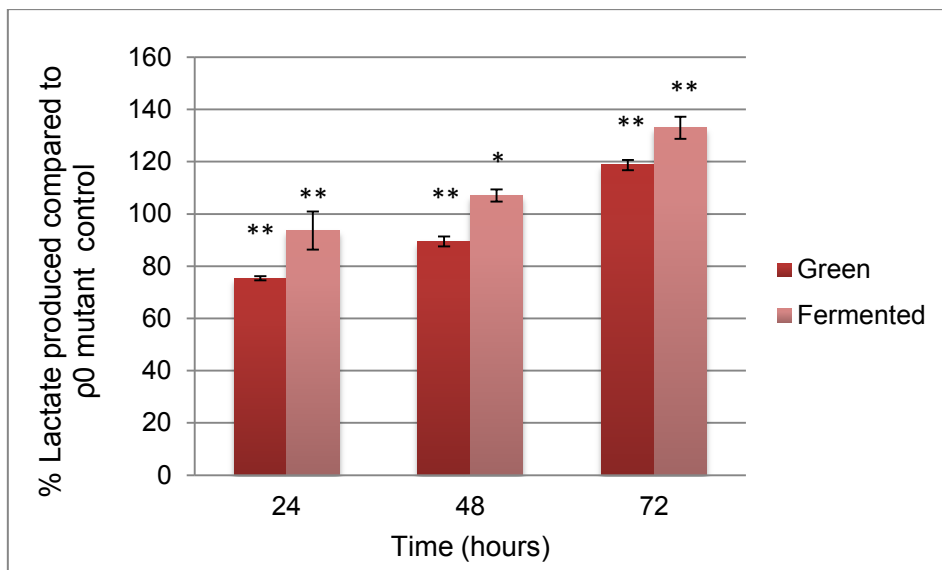


Figure 5.14: Normalised lactate production by rooibos treated (100 µg/mL) ρ^0 mutant cells after 24, 48 and 72 hours, represented as a percentage of the untreated ρ^0 mutant control (100%). Error bars represent SD of nine replicate values (n=3). Statistical significance was determined using the two-tailed Student *t*-test and is indicated for $p < 0.05$ (*) and $p < 0.005$ (**) relative to untreated control.

As shown in Figure 5.13 glucose utilization is increased after 24 hours of treatment with green and fermented rooibos, and progressively decreased as the treatment time increased. Lactate production (Figure 5.14) is decreased after 24 hours of rooibos treatment, and progressively increased as the treatment time increased. Overall, the increase in glucose utilization indicates an improvement in the mitochondrial function. However, the progressive decrease in glucose utilization, along with a concomitant increase in lactate production is quite unexpected considering that increased lactate production is usually associated with significantly increased glucose utilization.

These results could indicate that rooibos does not directly target mitochondrial function. Alternately, this could indicate that rooibos induces a metabolic shift in which carbon flow is directed away from mitochondrial metabolism, and more towards lactate production. Therefore, the cell would become resistant to mitochondrial dysfunction and subsequently an improvement in growth kinetics is observed. This is in accordance with results published on the anti-diabetic properties of rooibos, indicating an increase in glucose uptake concurrent to an activation of AMPK. Interestingly, studies have indicated that AMPK signalling controls energy metabolism, autophagic degradation, stress resistance, as well as the process of ageing, as indicated by a decreased sensitivity toward AMPK activation (Salminen & Kaarniranta, 2012). Additionally, results by Chen *et al.* (2013) indicated that treatments with aspalathin can extend the life span of *C. elegans* during stressed conditions through regulation of the DAF-16/FOXO insulin-like signalling pathway, in addition to enhancing resistance to oxidative stress through the up-regulation and expression of stress-response related genes. Considering the direct relation between AMPK signalling and DAF-16/FOXO activation, investigation of this with regards to possible conserved mammalian pathways could be a vital component to gain more understanding of the complex process of ageing (Salminen & Kaarniranta, 2012; Tullet *et al.*, 2014).

Adipocytes are particularly sensitive to oxidative stress, during which responses such as increased lactate production have been observed, which is subsequently involved in the development of insulin resistance (Soares *et al.*, 2005). This might provide an explanation for the above results, however the effects of rooibos in the treatment of insulin resistance has been extensively characterised, therefore making this observation highly unlikely.

Considering that resistance to oxidative stress is linked to lactate production, due to the fact that an increased glucose flux also stimulates glutathione production through the glucose-6-phosphate dehydrogenase reaction, the same argument can be offered as above, in that inducing a metabolic shift and redirecting the metabolism could provide resistance to oxidative stress.

The difference in treatment times could also be of significant importance, seeing as other studies report treatment times of only 3 – 6 hours (Muller *et al.*, 2012; Mazibuko *et al.*, 2013; Dlodla *et al.*, 2014), compared to the 24 to 72 hour treatment time used in this study. This could be attributed to an increase in the pro-oxidant properties of phenolic compounds due to their instability in culture medium however it should also be considered that, after extensive treatment time intervals such as the 72 hour treatment time used in this study, glucose consumption would no longer simply be restricted to energy homeostasis, and will also support cell growth etc., consequently the correlation between glucose utilization and lactate production becomes far more complex.

In support of the results obtained in this study, studies using the exact same rooibos extracts reported an increase in glucose uptake in C2C12 skeletal myotubes and Chang liver cells, which was attributed to the increased aspalathin content in the green relative to the fermented rooibos (Table 5.1).

Likewise, Mazibuko *et al.* (2013) reported that these rooibos extracts produced an increase in glucose uptake, mitochondrial activity and ATP production in insulin resistant C2C12 cells, with the green rooibos exhibiting an increased effectivity relative to the fermented rooibos. PPAG has also been shown to increase glucose uptake in 3T3-L1 adipocytes, and was present in green (0.491 g/100g) and fermented (0.713 g/100g) rooibos, and finally a synergistic effect has been reported for aspalathin and rutin, showing an improved hypoglycaemic activity (Muller *et al.*, 2012; Muller *et al.*, 2013).

However, it is also important to consider the different cell types, specifically with regards to the different glucose transporters, seeing as C2C12 myotubes express GLUT4 transporters, whereas undifferentiated 3T3-L1 cells would primarily express GLUT1, and Chang liver cells are capable of expressing both GLUT1 and GLUT2. Whilst this cannot provide an explanation as to the differences in the results obtained for green and fermented rooibos, it would provide insight into the mechanism of glucose uptake between different cell lines, and should perhaps be considered for future studies.

5.3.6 Confocal microscopy

To confirm and visualise the mitochondrial membrane potential ($\Delta\Psi_m$) changes observed using flow cytometry (5.3.3), rooibos treated wildtype and ρ^0 mutant cells were stained with JC-1 and viewed using confocal microscopy.

Using the confocal microscopy images obtained for JC-1 stained mitochondria, individual rooibos treated and untreated wildtype and ρ^0 mutant cells were isolated and analysed using Zen software post-acquisition processing. A ratio of red / green fluorescence intensity, indicating the $\Delta\Psi_m$, was determined for 10 randomly selected cells exposed to either green or fermented rooibos, for both the wildtype and ρ^0 mutant cell populations, as shown in Table 5.4.

Table 5.4: Results obtained from post-acquisition confocal microscopy image processing indicating the $\Delta\Psi_m$ for wildtype and ρ^0 mutant cells. Representing $\Delta\Psi_m$ as: a ratio of the mean fluorescence intensity of FL3 (red) to FL1 (green) \pm SD.

| | wildtype | ρ^0 mutants |
|------------------|------------------|------------------|
| untreated | 1.345 \pm 0.49 | 1.093 \pm 0.20 |
| green | 1.369 \pm 0.29 | 1.120 \pm 0.17 |
| fermented | 1.445 \pm 0.51 | 1.316 \pm 0.43 |

The above results are in agreement with results obtained for JC-1 staining and analysis using flow cytometry (5.3.4) indicating an increase in $\Delta\Psi_m$ after 48 hours of treatment with fermented rooibos for both the ρ^0 mutant and wildtype cells, relative to the negligible / small increase observed for green rooibos treated ρ^0 mutant and wildtype cells.

Representative images can be seen in Figure 5.15, where live cell imaging was performed using confocal microscopy after 48 hours of treatment with rooibos extracts (63x oil immersion magnification). Mitochondria were stained using the polychromatic $\Delta\Psi_m$ sensitive fluorescent probe JC-1, which exhibits a membrane potential dependent accumulation and aggregate formation within the mitochondria. Polarized (red) and depolarized (green) mitochondria are indicated with yellow colouration representing overlap. One representative of 15 images taken for each respective treatment, during a single experiment is shown.

During the progression of the cell cycle, mitochondria undergo changes in morphology, size, distribution and abundance (Ferree & Shirihai, 2012; Arakaki *et al.*, 2006). This morphological spectrum has been characterised according to the cell cycle progression into tubular, intermediate and fragmented conformations (Mitra *et al.* 2009; Margineantu *et al.*, 2002). As can be seen in Figure 5.15, green and fermented treated wildtype and ρ^0 mutant cells have a more intermediate mitochondrial arrangement, typical of proliferating cells (G1-S or S phase), with tubular elements clearly visible.

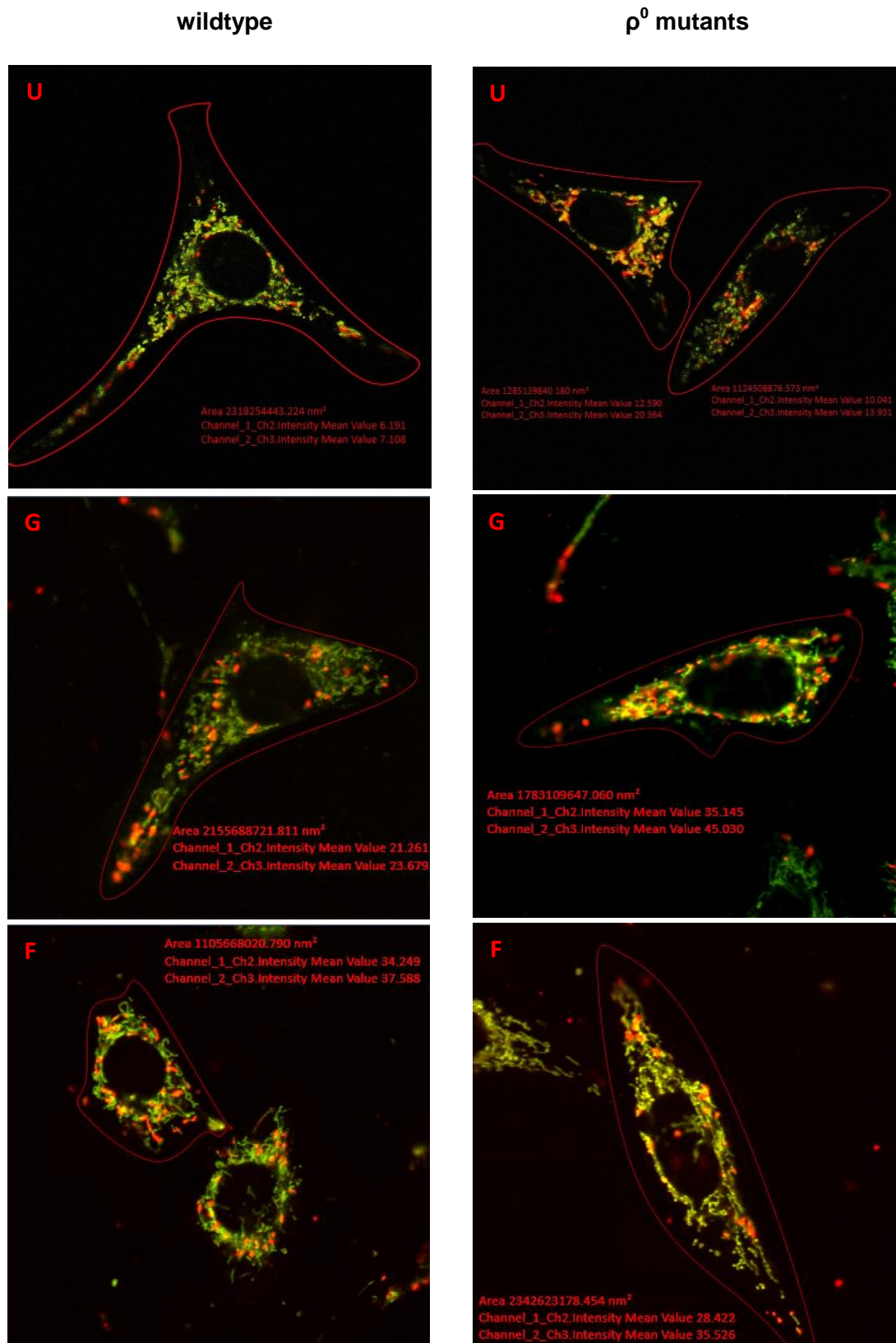


Figure 5.15: Representative confocal microscopy images of JC-1 stained mitochondria in individually characterised untreated (U) as well as green (G) and fermented (F) rooibos treated wildtype (left) and ρ^0 mutant cells (right).

5.4 Conclusion

Wildtype 3T3-L1 preadipocytes

The effects of rooibos in 3T3-L1 adipocytes have previously been reported with regards to its antidiabetic action as well as the potential to prevent obesity through the modulation of glucose uptake, leptin secretion etc. (Joubert & de Beer, 2011; Muller *et al.*, 2012; Mazibuko *et al.*, 2013; Sanderson *et al.*, 2014). No literature pertaining to the effect of rooibos on preadipocytes could however be found. The results obtained in this study indicated that treatment with green and fermented rooibos extracts had a positive effect on cell proliferation after 48 hours of treatment, which was associated with an increase in mitochondrial membrane potential. As expected, glucose utilization was increased after 24 and 48 hours of treatment with green rooibos in both the wildtype and ρ^0 mutant cells, whereas treatment with fermented rooibos only produced a significant increase in glucose utilization after 24 hours.

ρ^0 3T3-L1 preadipocytes

Throughout this study, rooibos treatments had a more significant effect on ρ^0 mutant cells relative to the wildtype cells. This was illustrated by the stimulation of cell growth after 24 and 48 hours of treatment, most notably with the green rooibos treatment – although subsequent experiments, as discussed in Chapter 6, need to be performed to confirm this observation. The same trend was observed for the effects of rooibos on the mitochondrial membrane potential, relative to wildtype cells. Once again, the expected increase in glucose utilization was observed after 24 hours, and decreased as the treatment time was increased.

Therefore the results obtained highlight the potential restorative effect of rooibos on the age associated mitochondrial dysfunction observed in preadipocytes, especially with regards to the possible metabolic shift, AMPK activation and DAF-16/FOXO activated signalling pathways as discussed previously (5.3.5), keeping in mind however, that the AMPK regulation of DAF-16 activation through the insulin/IGF signalling pathway has been identified in *C. elegans* (Chen *et al.*, 2014) and although evidence of activation of AMPK subunits in mammals suggests that such FOXO-AMPK interactions may be evolutionarily conserved, a great deal more research is required (Tullet *et al.*, 2014).

CHAPTER 6: Concluding remarks

The aim of this study was to investigate the potential anti-ageing properties of green and fermented rooibos (*Aspalathus linearis*) using an *in vitro* cell culture model representative of the age-related mitochondrial dysfunction observed in preadipocytes. Mitochondrial dysfunction was induced through mtDNA depletion as a result of long term exposure to sub lethal concentrations of EtBr, as described in Chapter 4. Compared to wildtype cells, p^0 mutants exhibited a much slower growth rate in culture, congruent with a significant delay in G1 phase cell cycle progression, as well as a significantly reduced mitochondrial membrane potential, an increased glucose utilization and lactate production. Treatment with green rooibos stimulated cell growth and proliferation, and attenuated the G1 phase delay. This was also observed in the fermented treated cells but to a lesser extent. Both fermented and green rooibos significantly improved the mitochondrial membrane potential, as well as demonstrating some ability to regulate glucose utilization in relation to lactate production. Although less apparent, a similar effect was observed in wildtype cells. In conclusion, the results obtained indicate that rooibos extracts exhibit effects which preserve the functional capacity of preadipocytes exposed to ageing related insults. Clearly, the health benefits of rooibos may be context dependent and thus require careful experimental design and data interpretation to ensure accurate conclusions.

Throughout this study, notable differences in activity were observed between the green and fermented rooibos treatments, with the former being more effective at improving cell growth and proliferation, as well as modulating glucose utilization and lactate production. Interestingly, compared to the green rooibos, treatment with the fermented extract exhibited a more prominent effect on mitochondrial health, as shown by the increased mitochondrial membrane potential. This can be attributed to the different phenolic compositions. Further conclusions can however not be made with regards to the activity of specific isolated compounds due to the limited amount of literature available on the activities of isolated compounds, as well as the effects of rooibos on ageing. Therefore, the isolation and identification of active compounds in relation to the anti-ageing potential of rooibos would be extremely beneficial.

Furthermore, the synergistic and antagonistic effects of a combination of active compounds should also be investigated. The importance of this lies not only in the fact that it would provide some much needed insight into the process of ageing, but also due to the fact that rooibos is well known for its perceived anti-ageing effects, with both green and fermented extracts being commonly used in skin care products and as dietary supplements, without much published research supporting these claims.

The ρ^0 3T3-L1 preadipocyte cell line developed and characterised in this study, represents a novel concept in the field of ageing research, specifically relating to mitochondrial dysfunction within ageing preadipocytes. Likewise, although other studies have previously investigated the anti-ageing properties of rooibos using the nematode *C. elegans* (Chen *et al.*, 2013), and Japanese quail (*Coturnix coturnix japonica*) hens (Juráni *et al.*, 2008), the ρ^0 3T3-L1 preadipocyte cell line represents the first *in vitro* cell culture model used in the investigation of the anti-ageing properties of rooibos on a cellular level.

Apart from the points discussed above, other considerations for improvement of this study are listed below.

Considerations for improvement of this study

- Investigate the effect of rooibos on AMPK signalling pathways and its interaction with FOXO, specifically with regards to its role as a possible anti-ageing mechanism.
- Repeat proliferation studies to more accurately determine S phase populations, using assays such as the 5-bromo-2-deoxyuridine (BrdU) labelling assay, for example. The uridine derivative BrdU, is a structural analogue of thymidine, and will be incorporated into DNA as a substitute for thymidine during S phase, thereby serving as a marker for proliferation.
- Measure ATP production to evaluate metabolic activity as well as cell viability.
- Further investigate effects of long term rooibos treatments / optimize treatment concentration and / or time.

- Mitochondrial function is regulated by autophagy (mitophagy). Segregation of damaged mitochondria depends on fission and fusion events which are altered in mitochondrial dysfunction (García-escudero *et al.*, 2013). Considering the potential of rooibos to induce autophagy (unpublished data) this could provide important information on the anti-ageing potential of rooibos – specifically relating to the development of age related neurodegenerative diseases.
- The time lapse confocal imaging performed in this study could not provide sufficient quantitative or qualitative information due to the non-specific nature of the experiment. Optimization could provide information on the effect of rooibos on mitochondrial dynamics including fission and fusion events (Detmer & Chan, 2007).
- Investigate the restorative effect of rooibos through the repletion of mtDNA (Biswas *et al.*, 1999; Park & Lee 2007).
- Investigate the capacity to differentiate, which is decreased during the ageing process.

Other molecular mechanisms involved in the age associated decline in preadipocyte function include oxidative stress, hypoxia, and inflammation. Due to time constraints however, only some initial investigations were made into the generation of a second *in vitro* cell culture model representative of oxidative stress in ageing preadipocytes.

Although promising results were obtained, these findings are not included in this document due to the fact that much more work was required to complete this model. Hopefully further investigations can be done in the future to complete the characterisation of this model, as well as evaluating the effects of rooibos on oxidative stress as observed in the age-related decline in preadipocyte function. Due to the anti-inflammatory activity of rooibos, as well as the effects of dietary polyphenols on signal transduction pathways, it would also be interesting to determine the effects of rooibos on the age related progression of inflammation in preadipocytes.

Prospective for future studies

Mitochondrial dysfunction is considered a critical component in the development of diabetes and insulin resistance (Lim *et al.*, 2006). Considering the well-known anti-diabetic activity of rooibos, similar models of mitochondrial dysfunction within appropriate cell lines such as C2C12 myotubes for example, could provide vital information on the anti-diabetic properties of rooibos.

Within the last decade or so, discovery of mitochondrial signalling mechanisms and the involvement of mitochondrial dysfunction in stress responses, has revolutionized the way in which we view mitochondria. Mitochondria are no longer just seen as ATP producing / apoptosis regulating organelles, and are now understood to be dynamic, mobile structures, constantly undergoing fusion and fission, and engaging in intimate interactions with other cellular compartments and structures, such as the endoplasmic reticulum, to modulate an extensive range of intracellular signalling (McInnes, 2013). Therefore, it is not surprising that an increasing number of human diseases have been associated with functional defects in mitochondria, and the processes they regulate. During this study, a new appreciation for the mitochondria was developed and of particular interest to the author were the pathophysiological outcomes in mitochondrial diseases. A brief overview of mitochondrial diseases is given in Appendix IV seeing as this is not technically within the scope of this study, however it has definitely provided a vital motivation for prospective studies.

Thank you

References

- Ajuwon, K.M., Banz, W., Winters, T. (2009) Stimulation with Peptidoglycan induces interleukin 6 and TLR2 expression and a concomitant downregulation of expression of adiponectin receptors 1 and 2 in 3T3-L1 adipocytes, *Journal of Inflammation*, **6**: 8.
- Alexeyev, M., Shokolenko, I., Wilson, G., LeDoux, S. (2013) The maintenance of mitochondrial DNA integrity - critical analysis and update, *Cold Spring Harbour Perspectives in Biology*, **5**: a012641.
- Alfadda, A. & Sallam, R. (2012) Reactive Oxygen Species in Health and Disease, *Journal of Biomedicine and Biotechnology*, **2012**: 1 – 14.
- Allen, J.F. (2003) Why chloroplasts and mitochondria contain genomes, *Comparative and Functional Genomics*, **4**: 31 – 36.
- Amuthan, G., Biswas, G., Ananadatheerthavarada, H.K., Vijayasarathy, C., Shephard, H.M. & Avadhani, N.G. (2002) Mitochondrial stress-induced calcium signaling , phenotypic changes and invasive behavior in human lung carcinoma A549 cells, *Oncogene*, **21**: 7839 – 7849.
- Arakaki, N., Nishihama, T., Owaki, H., Kuramoto, Y., Suenaga, M., Miyoshi, E., Emoto, Y., Shibata, H. (2006) Dynamics of mitochondria during the cell cycle, *Biological and Pharmaceutical Bulletin*, **29**: 1962 – 1965.
- Arduíno, D., Raquel Esteves, A., Cortes, L., Silva, D., Patel, B., Grazina, M., Swerdlow, R. & Oliveira, C. (2012) Mitochondrial metabolism in Parkinson's disease impairs quality control autophagy by hampering microtubule-dependent traffic, *Human Molecular Genetics*, **21**: 4680 – 4702.
- Armand, R., Channon, J.Y., Kintner, J., White, K., Miselis, K., Perez, R.P., Lewis, L.D. (2004) The effects of ethidium bromide induced loss of mitochondrial DNA on mitochondrial phenotype and ultrastructure in a human leukemia T-cell line (MOLT-4 cells), *Toxicology and Applied Pharmacology*, **196**: 68 – 79.

- Arnould, T., Vankoningsloo, S., Renard, P., Houbion, A., Ninane, N., Demazy, C., Remacle, J., Raes, M. (2002) CREB activation induced by mitochondrial dysfunction is a new signaling pathway that impairs cell proliferation, *The European Molecular Biology Organization (EMBO) Journal*, **21**: 53 – 63.
- Ashok, B.T. & Ali, R. (1999) The aging paradox: free radical theory of aging, *Experimental Gerontology*, **34**: 293 – 303.
- Barbieri, S.S., Eligini, S., Brambilla, M., Tremoli, E., Colli, S. (2003) Reactive oxygen species mediate cyclooxygenase-2 induction during monocyte to macrophage differentiation: critical role of NADPH oxidase, *Cardiovascular Research*, **60**: 187.
- Baret, P., Septembre-Malaterre, A., Rigoulet, M., Lefebvre d'Hellencourt, C., Priault, M., Gonthier, M.-P., Devin, A. (2013) Dietary polyphenols preconditioning protects 3T3-L1 preadipocytes from mitochondrial alterations induced by oxidative stress, *The International Journal of Biochemistry & Cell Biology*, **45**: 167 – 174.
- BD Biosciences (2000) *Introduction to Flow Cytometry: A Learning Guide*, Becton, Dickinson and Company, Available: <http://www.d.umn.edu/~biomed/flowcytometry/introflow-cytometry.pdf>. Accessed: 10 August 2014.
- Beckman Coulter (2010) *Beckman Coulter - FC 500 Series*, Beckman Coulter Inc. USA, Available: <http://www.beckmancoulter.com/wsrportal/wsr/diagnostics/clinicalproducts/flowcytometry/flowcytometers/fc500series/index.htm#2/10//0/25/1/0/asc/2/175487///0/1//0/>. Accessed: 10 August 2014.
- Beelders, T., Sigge, G.O., Joubert, E., De Beer, D., de Villiers, A. (2012) Kinetic optimisation of the reversed phase liquid chromatographic separation of rooibos tea (*Aspalathus linearis*) phenolics on conventional high performance liquid chromatographic instrumentation, *Journal of Chromatography A*, **1219**: 128 – 139.

- Beltrán-Debón, R., Rull, A., Rodríguez-Sanabria, F., Iswaldi, I., Herranz-López, M., Aragonès, G., Camps, J., Alonso-Villaverde, C., Menéndez, J.A., Micol, V., Segura-Carretero, A., Jovena, J. (2011) Continuous administration of polyphenols from aqueous rooibos (*Aspalathus linearis*) extract ameliorates dietary-induced metabolic disturbances in hyperlipidemic mice, *Phytomedicine*, **18**: 414 – 424.
- Benz, C. & Yau, C. (2008) Ageing, oxidative stress and cancer: paradigms in parallax, *Nature Reviews - Cancer*, **8**: 875 – 879.
- Berg, A.H., Lin, Y., Lisanti, M.P., Scherer, P.E. (2004) Adipocyte differentiation induces dynamic changes in NF-kappaB expression and activity, *American journal of physiology - Endocrinology and Metabolism*, **287**: E1178 – E1188.
- Biswas, G., Adebajo, O.A., Freedman, B.D., Anandatheerthavarada, H.K., Vijayasathy, C., Zaidi, M., Kotlikoff, M., Avadhani, N.G. (1999) Retrograde Ca²⁺ signaling in C2C12 skeletal myocytes in response to mitochondrial genetic and metabolic stress : a novel mode of inter-organelle crosstalk, *The European Molecular Biology Organization (EMBO) Journal*, **18**: 522 – 533.
- Boland, M.L., Chourasia, A.H., Macleod, K.F. (2013) Mitochondrial dysfunction in cancer, *Frontiers in Oncology*, **3**: 292.
- Bramati, L. Aquilano, F., Pietta, P. (2003) Unfermented rooibos tea: quantitative characterization of flavonoids by HPLC-UV and determination of the total antioxidant activity, *Journal of Agricultural and Food Chemistry*, **51**: 7472 – 7474.
- Brand, M.D. & Nicholls, D.G. (2011) Assessing mitochondrial dysfunction in cells, *Biochemical Journal*, **435**: 297 – 312.
- Bratic, A. & Larsson, N. (2013) The role of mitochondria in aging, *Journal of Clinical Investigation*, **123**: 951 – 957.
- Brotherick, I. (2006) Basic DNA Measurement by Flow Cytometry, In: *Guide to Flow Cytometry*, 2nd Edition, Dako, USA.

- Brown, M. & Wittwer, C. (2000) Flow Cytometry : Principles and Clinical Applications in Hematology, *Clinical Chemistry*, **8**: 1221 – 1229.
- Buchet, K. & Godinot, C. (1998) Functional F1-ATPase Essential in Maintaining Growth and Membrane Potential of Human Mitochondrial DNA-depleted Cells, *Journal of Biological Chemistry*, **273**: 22983 – 22989.
- Calabrese, V., Cornelius, C., Dinkova-Kostova, A.T., Iavicoli, I., Di Paola, R., Koverech, A., Cuzzocrea, S., Rizzarelli, E., Calabrese, E.J. (2011) Cellular stress responses, hormetic phytochemicals and vitagenes in aging and longevity, *Biochimica et Biophysica Acta (BBA) - Molecular Basis of Disease*, **1822**: 753 – 783.
- Cartwright, M.J., Tchkonja, T., Kirkland, J.L. (2007) Aging in adipocytes: potential impact of inherent, depot-specific mechanisms, *Experimental Gerontology*, **42**: 463 – 471.
- Chandel, N.S. (2014) Mitochondria as signaling organelles, *BioMed Central (BMC) Biology*, **12**: 34.
- Chang, M.C., Ho, Y.S., Lee, P.H., Chan, C.P., Lee, J.J., Hahn, L.J., Wang, Y.J., Jeng, J.H. (2001) Areca nut extract and arecoline induced the cell cycle arrest but not apoptosis of cultured oral KB epithelial cells: Association of glutathione, reactive oxygen species and mitochondrial membrane potential, *Carcinogenesis*, **22**: 1527 – 1535.
- Chatterjee, N., Kiran, S., Rama, B.M., Islam, N., Ramasarma, T., Ramakrishna, G. (2011) Diperoxovanadate can substitute for H₂O₂ at much lower concentration in inducing features of premature cellular senescence in mouse fibroblasts (NIH3T3), *Mechanisms of Ageing and Development*, **132**: 230 – 239.
- Chen, W., Resmala, I., Wang, E., Joubert, E., van Wyk, B., Wink, M. (2013) Phytomedicine Ameliorative effect of aspalathin from rooibos (*Aspalathus linearis*) on acute oxidative stress in *Caenorhabditis elegans*, *European Journal of Integrative Medicine*, **20**: 380 – 386.

- Chen, X.J. (2013) Mechanism of homologous recombination and implications for aging-related deletions in mitochondrial DNA, *Microbiology and Molecular Biology Reviews*, **77**: 476 – 496.
- Chinnery, P.F. (2014) Mitochondrial Disorders Overview, In: *GeneReviews*[®] [Internet], Pagon, R.A., Adam, M.P., Ardinger, H.H. et al., Editors, Available: <http://www.ncbi.nlm.nih.gov/books/NBK1224/?report=reader>. Accessed: 26 September 2014.
- Chirumbolo, S., Franceschetti, G., Zoico, E., Bambace, C., Cominacini, L., Zamboni, M. (2014) LPS response pattern of inflammatory adipokines in an *in vitro* 3T3-L1 murine adipocyte model, *Inflammation Research*, **63**: 495 – 507.
- Copeland, W.C. & Longley, M.J. (2014) Mitochondrial genome maintenance in health and disease, *DNA Repair*, **19**: 190 – 198.
- Cottet-Rousselle, C., Ronot, X., Lerverve, X., Mayol, J. (2011) Cytometric assessment of mitochondria using fluorescent probes, *Cytometry Part A*, **6**: 405 – 425.
- Crozier, A., Jaganath, I.B., Clifford, M.N. (2009) Dietary phenolics: chemistry, bioavailability and effects on health, *Natural Product Reports*, **26**: 1001 – 1043.
- Cullberg, K.B., Larsen, J.Ø., Pedersen, S.B., Richelsen, B. (2014) Effects of LPS and dietary free fatty acids on MCP-1 in 3T3-L1 adipocytes and macrophages *in vitro*, *Nutrition & Diabetes*, **4**: e113.
- Das, S., Parveen, S., Pradhan, A.B. (2014) An insight into the interaction of phenanthridine dyes with polyriboadenylic acid: spectroscopic and thermodynamic approach, *Spectrochimica Acta - Part A, Molecular and Biomolecular Spectroscopy*, **118**: 356 – 366.
- Davinelli, S., Sapere, N., Visentin, M., Zella, D., Scapagnini, G. (2013) Enhancement of mitochondrial biogenesis with polyphenols: combined effects of resveratrol and equol in human endothelial cells, *Immunity & Ageing*, **10**: 28.

- Dawson, M. (1998) *The significance of endotoxin to cell culture and biotechnology*, Associates of Cape Cod Inc., Available: <http://www.acciusa.com/pdfs/newsletter/updt0398.pdf>. Accessed: 08 December 2014.
- Demine, S., Reddy, N., Renard, P., Raes, M., Arnould, T. (2014) Unraveling biochemical pathways affected by mitochondrial dysfunctions using metabolomic approaches, *Metabolites*, **4**: 831 – 878.
- Detmer, S. & Chan, D.C. (2007) Functions and dysfunctions of mitochondrial dynamics, *Nature Reviews - Molecular Cell Biology*, **8**: 870 – 879.
- Dludla, P. V, Muller, C.J.F., Louw, J., Joubert, E., Salie, R., Opoku, A.R., Johnson, R. (2014) The cardioprotective effect of an aqueous extract of fermented rooibos (*Aspalathus linearis*) on cultured cardiomyocytes derived from diabetic rats, *Phytomedicine*, **21**: 595 – 601.
- Dudkina, N.V, Kouril, R., Peters, K., Braun, H.-P., Boekema, E.J. (2010) Structure and function of mitochondrial supercomplexes, *Biochimica et Biophysica Acta*, **1797**: 664 – 670.
- Erickson, L. (2003) Rooibos tea: Research into antioxidant and antimutagenic properties, *The Journal of the American Botanical Council*, **59**: 34 – 45.
- Felber, S. & Brand, M. (1982) Valinomycin can depolarize mitochondria in intact lymphocytes without increasing plasma membrane potassium fluxes, *Federation of European Biochemical Societies (FEBS) Letters*, **150**: 122 – 124.
- Feria-Morales, A. (2002) Examining the case of green coffee to illustrate the limitations of grading systems/expert tasters in sensory evaluation for quality control, *Food Quality and Preference*, **13**: 355 – 367.
- Ferree, A. & Shirihai, O. (2012) Mitochondrial dynamics: the intersection of form and function, *Advances in Experimental Medicine and Biology*, **748**: 13 – 40.

- Findeisen, H.M., Pearson, K.J., Gizard, F., Zhao, Y., Qing, H., Jones, K.L., Cohn, D., Heywood, E.B., de Cabo, R., Bruemmer, D. (2010) Oxidative Stress Accumulates in Adipose Tissue during Aging and Inhibits Adipogenesis, *PLoS ONE*, **6**: e18532.
- Finkel, T. & Hwang, P.M. (2009) The Krebs cycle meets the cell cycle: mitochondria and the G1-S transition, *Proceedings of the National Academy of Sciences of the United States of America*, **106**: 11825 – 11826.
- Fontana, L., Kennedy, B.K., Longo, V.D. (2014) Clinical studies: Prepare for human testing, *Nature*, **511**: 405 – 407.
- Forejtníková, H., Lunerová, K., Kubínová, R., Jankovská, D., Marek, R., Kares, R., Suchý, V., Vondráček, J. (2005) Chemoprotective and toxic potentials of synthetic and natural chalcones and dihydrochalcones *in vitro*, *Toxicology*, **208**: 81 – 93.
- Giada, M. (2013) Food Phenolic Compounds: Main Classes, Sources and Their Antioxidant Power, In: *Oxidative Stress and Chronic Degenerative Diseases - A Role for Antioxidants*, 1st Edition, Morales-González, J., Editor, Rijeka: InTech.
- Gibellini, L., Pinti, M., Nasi, M., De Biasi, S., Roat, E., Bertocelli, L., Cossarizza, A. (2010), Interfering with ROS Metabolism in Cancer Cells: The Potential Role of Quercetin, *Cancers*, **2**: 1288 – 1311.
- Gilkerson, R., Margineantu, D., Capaldi, R., Selker, J. (2000) Mitochondrial DNA depletion causes morphological changes in the mitochondrial reticulum of cultured human cells, *Federation of European Biochemical Societies (FEBS) Letters*, **474**: 1 – 4.
- Green, H. & Kehinde, O. (1975) An established preadipose cell line and its differentiation in culture. II. Factors affecting the adipose conversion, *Cell*, **1**: 19 – 27.

- Grüner-Richter, S., Otto, F., Weinreich, B. (2008) Rooibos extract with increased aspalathin content, process for the preparation of such a rooibos extract, and cosmetic agent containing such a rooibos extract, U.S. Patent Application No. US2008/0247974 A1.
- Habu, T., Flath, R.A., Mon, T.R., Morton, J.F. (1985) Volatile compounds of rooibos tea (*Aspalathus linearis*), *Journal of Agricultural and Food Chemistry*, **33**: 249 – 254.
- Han, X., Shen, T., Lou, H. (2007) Dietary Polyphenols and Their Biological Significance, *International Journal of Molecular Sciences*, **8**: 950 – 988.
- Haque, A., Nishikawa, M., Qian, W., Mashimo, M., Hirose, M., Nishiguchi, S., Inoue, M. (2006) Lack of mitochondrial DNA enhances growth of hepatocellular carcinoma *in vitro* and *in vivo*, *Hepatology Research*, **36**: 209 – 216.
- Harkins, J.M., Moustaid-moussa, N., Chung, Y., Penner, K.M., Pestka, J.J., North, C.M., Claycombe, K.J. (2004) Expression of Interleukin-6 is greater in preadipocytes than in adipocytes of 3T3-L1 cells and C57BL/6J and *ob/ob* mice, *Journal of Nutrition*, **134**: 2673 – 2677.
- Harman, D. (1956) Aging: a theory based on free radical and radiation chemistry, *The Journals of Gerontology*, **11**: 298 – 300.
- Harman, D. (1972) The biological clock: the mitochondria?, *Journal of the American Geriatrics Society*, **20**: 145 – 147.
- Havens, C., Ho, A., Yoshioka, N., Dowdy, S. (2006) Regulation of Late G1/S Phase Transition and APC^{Cdh1} by Reactive Oxygen Species, *Molecular and Cellular Biology*, **26**: 4701 – 4711.
- Heilbronn, L., Smith, S.R., Ravussin, E. (2004) Failure of fat cell proliferation, mitochondrial function and fat oxidation results in ectopic fat storage, insulin resistance and type II diabetes mellitus, *International Journal of Obesity and Related Metabolic Disorders*, **28**: S12 – S21.

- Hillis, W.E. & Inoue, T. (1967) The polyphenols of *Nothofagus* species. II. The heartwood of *Nothofagus fusca*, *Phytochemistry*, **6**: 59 – 67.
- Holmuamedov, E., Jahangir, A., Bienengraeber, M., Lewis, L.D., Terzic, A. (2003) Deletion of mtDNA disrupts mitochondrial function and structure, but not biogenesis, *Mitochondrion*, **1**: 13 – 19.
- Hu, M.L. (2011) Dietary polyphenols as antioxidants and anticancer agents: more questions than answers, *Chang Gung Medical Journal*, **34**: 449 – 460.
- Inanami, O., Asanuma, T., Inukai, N., Jin, T., Shimokawa, S., Kasai, N., Nakano, M., Sato, F., Kuwabara, M. (1995) The suppression of age-related accumulation of lipid peroxides in rat brain by administration of rooibos tea (*Aspalathus linearis*), *Neuroscience Letters*, **196**: 85 – 88.
- Jaganath, I. & Crozier, A. (2010) Dietary Flavonoids and Phenolic Compounds, In: *Plant phenolics and human health: biochemistry, nutrition, and pharmacology*, 1st Edition, Fraga, C., Editor, John Wiley & Sons, Inc.
- Jelley, E. (1936) Spectral Absorption and Fluorescence of Dyes in the Molecular State, *Nature*, **138**: 1009 – 1010.
- Joubert, E. & de Beer, D. (2011) Rooibos (*Aspalathus linearis*) beyond the farm gate: From herbal tea to potential phytopharmaceutical, *South African Journal of Botany*, **77**: 869 – 886.
- Joubert, E. & Schulz, H. (2006) Production and quality aspects of rooibos tea and related products. A review, *Journal of Applied Botany and Food Quality*, **80**: 138 – 144.
- Joubert, E. (1994) Processing of rooibos tea under controlled conditions (*Aspalathus linearis*), Ph.D. (Food Science), Stellenbosch University, Stellenbosch, South Africa.
- Joubert, E. (1998) Effect of controlled conditions during deep bed fermentation and drying on rooibos tea (*Aspalathus linearis*) quality, *Journal of Food Processing and Preservation*, **22**: 405 – 417.

- Joubert, E., Beelders, T., de Beer, D., Malherbe, C.J., de Villiers, A.J., Sigge, G.O. (2012) Variation in phenolic content and antioxidant activity of fermented rooibos herbal tea infusions: role of production season and quality grade, *Journal of Agricultural and Food Chemistry*, **60**: 9171 – 9179.
- Joubert, E., Gelderblom, W.C., Louw, A., de Beer, D. (2008) South African herbal teas: *Aspalathus linearis*, *Cyclopia* spp. and *Athrixia phylicoides* - A review, *Journal of Ethnopharmacology*, **119**: 376 – 412.
- Joubert, E., Winterton, P., Britz, T.J., Gelderblom, W.C. (2005) Antioxidant and pro-oxidant activities of aqueous extracts and crude polyphenolic fractions of rooibos (*Aspalathus linearis*), *Journal of Agricultural and Food Chemistry*, **53**: 10260 – 10267.
- Juráni, M., Lamosová, D., Mácajová, M., Kostál, L., Joubert, E., Greksák, M. (2008) Effect of rooibos tea (*Aspalathus linearis*) on Japanese quail growth, egg production and plasma metabolites, *British Poultry Science*, **49**: 55 – 64.
- Kawakami, M., Kobayashim, A., Kator, K. (1993) Volatile constituents of rooibos tea as affected by extraction process, *Journal of Agricultural and Food Chemistry*, **41**: 633 – 636.
- Khamaisi, M., Kavel, O., Rosenstock, M., Porat, M., Yuli, M., Kaiser, N., Rudich, A. (2000) Effect of inhibition of glutathione synthesis on insulin action: in vivo and in vitro studies using buthionine sulfoximine, *Biochemical Journal*, **349**: 579 – 586.
- Khan, S.M., Smigrodzki, R.M., Swerdlow, R.H. (2007) Cell and animal models of mtDNA biology: progress and prospects, *American Journal of Physiology: Cell Physiology*, **292**: C658 – C669.
- Kim, H.-S., Quon, M.J., Kim, J.-A. (2014) New insights into the mechanisms of polyphenols beyond antioxidant properties; lessons from the green tea polyphenol, epigallocatechin 3-gallate, *Redox Biology*, **2**: 187 – 195.
- King, M.P. & Attardi, G. (1989) Human cells lacking mtDNA: repopulation with exogenous mitochondria by complementation, *Science*, **246**: 500 – 503.

- King, M.P. & Attardi, G. (1996) Isolation of human cell lines lacking mitochondrial DNA, *Methods in Enzymology*, **264**: 304 – 313.
- Kirkland, J.L., Tchkonina, T., Pirtskhalava, T., Han, J., Karagiannides, I. (2002) Adipogenesis and aging: does aging make fat go MAD? *Experimental Gerontology*, **37**: 757 – 767.
- Kolesar, J.E., Safdar, A., Abadi, A., MacNeil, L.G., Crane, J.D., Tarnopolsky, M. Kaufman, B. (2014) Defects in mitochondrial DNA replication and oxidative damage in muscle of mtDNA mutator mice, *Free Radical Biology & Medicine*. **75**: 241 – 251.
- Koolman, J. & Roehm, K. (2005) *Color atlas of biochemistry*, 2nd Edition, Thieme, Germany.
- Koopman, W.J.H., Distelmaier, F., Smeitink, J.M., Willems, P.H.G.M. (2013) OXPHOS mutations and neurodegeneration, *The European Molecular Biology Organization (EMBO) Journal*, **32**: 9 – 29.
- Krafczyk, N. & Glomb, M.A. (2008) Characterization of phenolic compounds in rooibos tea, *Journal of Agricultural and Food Chemistry*, **56**: 3368 – 3376.
- Krafczyk, N., Heinrich, T., Porzel, A. & Glomb, M.A. (2009) Oxidation of the dihydrochalcone aspalathin leads to dimerization, *Journal of Agricultural and Food Chemistry*, **57**: 6838 – 6843.
- Kukat, A., Kukat, C., Brocher, J., Schäfer, I., Krohne, G., Trounce, I., Villani, G., Seibel, P. (2008) Generation of rho0 cells utilizing a mitochondrially targeted restriction endonuclease and comparative analyses, *Nucleic Acids Research*, **36**: e44.
- Kumar, S. & Pandey, A. (2013) Chemistry and Biological Activities of Flavonoids: An Overview, *The Scientific World Journal*, **2013**: 1 – 16.
- Lagouge, M. & Larsson, N.G. (2013) The role of mitochondrial DNA mutations and free radicals in disease and ageing, *Journal of Internal Medicine*, **273**: 529 – 543.

- Lamošová, D., Juráni, M., Greksák, M., Nakano, M., Vaneková, M. (1997) Effect of Rooibos Tea (*Aspalathus linearis*) on Chick Skeletal Muscle Cell Growth in Culture, *Comparative Biochemistry and Physiology Part C: Pharmacology, Toxicology & Endocrinology*, **116**: 39 – 45.
- Lauri, A., Pompilio, G., Capogrossi, M.C. (2014) The mitochondrial genome in aging and senescence, *Ageing Research Reviews*, **18C**: 1 – 15.
- Le Bras, M., Clément, M.V., Pervaiz, S., Brenner, C. (2005) Reactive oxygen species and the mitochondrial signaling pathway of cell death, *Histology and Histopathology*, **20**: 205 – 220.
- Leibowitz, R.D. (1971) The effect of ethidium bromide on mitochondrial DNA synthesis and mitochondrial DNA structure in HeLa cells, *The Journal of Cell Biology*, **51**: 116 – 122.
- Leslie, G. (2006) *Flow Cytometry: A basic guide*, Available: www.flowcytometri.dk/literature/Leslie-FCBasic.pdf. Accessed: 07 October 2014.
- Life Technologies™ (2015) Propidium Iodide ReadyProbes® Reagent, Life Technologies™, Thermo Fisher Scientific Inc. USA, Available: <https://www.lifetechnologies.com/order/catalog/product/R37108>. Accessed: 03 January 2015.
- Lim, J.H., Lee, J.I., Suh, Y.H., Kim, W., Song, J.H., Jung, M.H. (2006) Mitochondrial dysfunction induces aberrant insulin signalling and glucose utilisation in murine C2C12 myotube cells, *Diabetologia*, **49**: 1924 – 1936.
- Lin, Y., Lee, H., Berg, H., Lisanti, M.P., Shapiro, L., Scherer, P.E. (2000) The lipopolysaccharide-activated toll-like receptor (TLR)-4 induces synthesis of the closely related receptor TLR-2 in adipocytes, *The Journal of Biological Chemistry*, **275**: 24255 – 24263.
- Lombès, A., Auré, K., Bellanné-Chantelot, C., Gilleron, M., Jardel, C. (2014) Unsolved issues related to human mitochondrial diseases, *Biochimie*, **100**: 171 – 176.

- Lopez-Mejia, I.C. & Fajas, L. (2015) Cell cycle regulation of mitochondrial function, *Current Opinion in Cell Biology*, **33**: 19 – 25.
- Lui, J.C., Chen, W., Barnes, K.M., Baron, J. (2010) Changes in gene expression associated with aging commonly originate during juvenile growth, *Mechanisms of Ageing and Development*, **131**: 641 – 649.
- Magcwebeba, T. (2013) Chemopreventive properties of South African herbal teas, rooibos (*Aspalathus Linearis*) and honeybush (*Cyclopia* spp.): mechanisms against skin carcinogenesis, Ph.D (Biochemistry), Stellenbosch University, Stellenbosch, South Africa.
- Magda, D., Lecane, P., Prescott, J., Thiemann, P., Ma, X., Dranchak, P.K., Toleno, D.M., Ramaswamy, K. (2008) mtDNA depletion confers specific gene expression profiles in human cells grown in culture and in xenograft, *BioMed Central (BMC) Genomics*, **9**: 521.
- Malik, J., Szakova, J., Drabek, O., Balik, J., Kokoska, L. (2008) Determination of certain micro and macroelements in plant stimulants and their infusions, *Food Chemistry*, **111**: 520 – 525.
- Margineantu, D., Gregory Cox, W., Sundell, L., Sherwood, S., Beechem, J., Capaldi, R. (2002) Cell cycle dependent morphology changes and associated mitochondrial DNA redistribution in mitochondria of human cell lines, *Mitochondrion*, **1**: 425 – 435.
- Marnewick, J., Joubert, E., Joseph, S., Swanevelder, S., Swart, P., Gelderblom, W. (2005) Inhibition of tumour promotion in mouse skin by extracts of rooibos (*Aspalathus linearis*) and honeybush (*Cyclopia intermedia*), unique South African herbal teas, *Cancer Letters*, **224**: 193 – 202.
- Marnewick, J.L., Gelderblom, W.C.A., Joubert, E. (2000) An investigation on the antimutagenic properties of South African herbal teas, *Mutation Research*, **471**: 157 – 166.
- Masaki, H. (2010) Role of antioxidants in the skin: Anti-aging effects, *Journal of Dermatological Science*, **58**: 85 – 90.

- Mazibuko, S.E., Muller, C.J.F., Joubert, E., de Beer, D., Johnson, R., Opoku, A.R., Louw, J. (2013) Amelioration of palmitate-induced insulin resistance in C2C12 muscle cells by rooibos (*Aspalathus linearis*), *Phytomedicine*, **20**: 813 – 819.
- McInnes, J. (2013) Mitochondrial-associated metabolic disorders: foundations, pathologies and recent progress, *Nutrition & Metabolism*, **10**: 63.
- McKay, D.L. & Blumberg, J.B. (2007) A Review of the Bioactivity of South African Herbal Teas: Rooibos (*Aspalathus linearis*) and Honeybush (*Cyclopia intermedia*), *Phytotherapy Research*, **21**: 1 – 16.
- Meyer, J.N., Leung, M.C.K., Rooney, J.P., Sendoel, A., Hengartner, M.O., Kisby, G.E., Bess, A.S. (2013) Mitochondria as a Target of Environmental Toxicants, *Toxicological Sciences*, **134**: 1 – 17.
- Minamikawa, T., Sriratana, A., Williams, D.A., Bowser, D.N., Hill, J.S., Nagley, P. (1999) Chloromethyl-X-rosamine (MitoTracker Red) photosensitises mitochondria and induces apoptosis in intact human cells, *Journal of Cell Science*, **2430**: 2419 – 2430.
- Mitra, K. & Lippincott-Schwartz, J. (2010) Analysis of Mitochondrial Dynamics and Functions Using Imaging Approaches, *Current Protocols in Cell Biology*, **46**: 4.25.1 – 4.25.21.
- Mitra, K., Wunder, C., Roysam, B., Lin, G., Lippincott-Schwartz, J. (2009) A hyperfused mitochondrial state achieved at G1-S regulates cyclin E buildup and entry into S phase, *Proceedings of the National Academy of Sciences of the United States of America*, **106**: 11960 – 11965.
- Molecular Probes® (2008) *MitoTracker® Mitochondrion-Selective Probes*, Life Technologies™, Thermo Fisher Scientific Inc. USA, Available: <https://tools.lifetechnologies.com/content/sfs/manuals/mp07510.pdf>. Accessed: 15 November 2014.
- Morton, J.F. (1983) Rooibos tea, *Aspalathus linearis*, a caffeine-less, low-tannin beverage, *Economic Botany*, **37**: 164 – 173.

- Muller, C., Joubert, E., Pfeiffer, C., Ghoor, S., Sanderson, M., Chellan, N., Fey, S. & Louw, J. (2013) Z-2-(β -d-glucopyranosyloxy)-3-phenylpropenoic acid, an α -hydroxy acid from rooibos (*Aspalathus linearis*) with hypoglycemic activity, *Molecular Nutrition & Food Research*, **57**: 2216 – 2222.
- Muller, C.J.F., Joubert, E., de Beer, D., Sanderson, M., Malherbe, C.J., Fey, S.J., Louw, J. (2012) Acute assessment of an aspalathin-enriched green rooibos (*Aspalathus linearis*) extract with hypoglycemic potential, *Phytomedicine*, **20**: 32 – 39.
- Nelson, D. & Cox, M. (2008) *Lehninger principles of biochemistry*, 5th Edition, W.H. Freeman, New York, USA.
- Nijveldt, R.J., van Nood, E., van Hoorn, D.E., Boelens, P.G., van Norren, K., van Leeuwen, P.A. (2001) Flavonoids: a review of probable mechanisms of action and potential applications, *The American Journal of Clinical Nutrition*, **74**: 418 – 425.
- Núñez-Sellés, A.J. (2005) Antioxidant therapy: myth or reality?, *Journal of the Brazilian Chemical Society*, **16**: 699 – 710.
- Nunnari, J. & Suomalainen, A. (2012) Mitochondria: in sickness and in health, *Cell*, **148**: 1145 – 1159.
- Ormerod, M.G. (2000) *Flow Cytometry: A practical approach*, 3rd Edition, Oxford University Press, New York, USA.
- Page, M.M., Robb, E.L., Salway, K.D., Stuart, J.A. (2010) Mitochondrial redox metabolism: aging, longevity and dietary effects, *Mechanisms of Ageing and Development*, **131**: 242 – 252.
- Park, C.B. & Larsson, N.G. (2011) Mitochondrial DNA mutations in disease and aging, *The Journal of Cell Biology*, **193**: 809 – 818.
- Park, S.Y. & Lee, W. (2007) The depletion of cellular mitochondrial DNA causes insulin resistance through the alteration of insulin receptor substrate-1 in rat myocytes, *Diabetes Research and Clinical Practice*, **77**: S165 – S171.

- Patel, Y. & Lane, M. (2000) Mitotic Clonal Expansion during Preadipocyte Differentiation: Calpain-mediated Turnover of p27, *Journal of Biological Chemistry*, **275**: 17653 – 17660.
- Pellegrino, M., Nargund, A., Haynes, C. (2012) Signaling the mitochondrial unfolded protein response, *Biochimica et Biophysica Acta (BBA) - Molecular Cell Research*, **1833**: 410 – 416.
- Pendergrass, W., Wolf, N., Poot, M. (2004) Efficacy of MitoTracker Green™ and CMXRosamine to measure changes in mitochondrial membrane potentials in living cells and tissues, *Cytometry Part A*, **61**: 162 – 169.
- Pereira, D., Valentão, P., Pereira, J., Andrade, P. (2009) Phenolics: From Chemistry to Biology, *Molecules*, **14**: 2202 – 2211.
- Perry, S.W., Norman, J.P., Barbieri, J., Brown, E.B., Gelbard, H.A. (2011) Mitochondrial membrane potential probes and the proton gradient: a practical usage guide, *Biotechniques*, **50**: 98 – 115.
- Petrova, A. (2009) Modulation of ultraviolet light- induced skin carcinogenesis by extracts of rooibos and honey bush using a mouse model: elucidating possible photo protective mechanisms, M.Tech. (Biomedical Technology), Cape Peninsula University of Technology, Bellville, South Africa.
- Phuoc, L., Laveille, P., Chamouleau, F., Renard, G., Drone, J., Coq, B., Fajula, F., Galarneau, A. (2010) Phospholipid-templated silica nanocapsules as efficient polyenzymatic biocatalysts, *Dalton Transactions*, **39**: 8511.
- Pieczenik, S.R. & Neustadt, J. (2007) Mitochondrial dysfunction and molecular pathways of disease, *Experimental and Molecular Pathology*, **83**: 84 – 92.
- Poquet, L., Clifford, M., Williamson, G. (2010) Bioavailability of Flavanols and Phenolic Acids, In: *Plant phenolics and human health: Biochemistry, Nutrition, and Pharmacology*, 1st Edition, Fraga, C., Editor, Hoboken, John Wiley & Sons, Inc., USA.

- Procházková, D., Boušová, I., Wilhelmová, N. (2011) Antioxidant and pro-oxidant properties of flavonoids, *Fitoterapia*, **82**: 513 – 523.
- Promega (2013) *CellTiter-Blue™ Cell Viability Assay*, Promega Inc. USA, Available: <https://worldwide.promega.com/~media/files/resources/protocols/technical%20bulletins/101/celltiterblue%20cell%20viability%20assay%20protocol.pdf>. Accessed: 19 January 2014.
- Qian, W. & van Houten, B. (2010) Alterations in bioenergetics due to changes in mitochondrial DNA copy number, *Methods*, **51**: 452 – 457.
- Queen, B. & Tollefsbol, T. (2010) Polyphenols and Aging, *Current Ageing Science*, **3**: 34 – 42.
- Quintero-Fabián, S., Ortuño-Sahagún, D., Vázquez-Carrera, M., López-Roa, R.I. (2013) Alliin, a garlic (*Allium sativum*) compound, prevents LPS-induced inflammation in 3T3-L1 adipocytes, *Mediators of Inflammation*, **2013**: 381815.
- Raffaello, A. & Rizzuto, R. (2011), Mitochondrial longevity pathways, *Biochimica et Biophysica Acta (BBA) - Molecular Cell Research*, **1813**: 260 – 268.
- Rooibos Ltd. (2015) *Rooibos country*, Available: <http://www.rooibosLtd.co.za/rooibos-background-cederberg.php>. Accessed: 03 January 2015.
- Rottenberg, H. & Wu, S. (1998) Quantitative assay by flow cytometry of the mitochondrial membrane potential in intact cells, *Biochimica et Biophysica Acta (BBA) - Molecular Cell Research*, **1404**: 393 – 404.
- Ryan, J. (2008) *Endotoxins and cell culture*, Corning Inc. USA, Available: http://csmedia2.corning.com/LifeSciences//media/pdf/cc_endotoxins_tc_305_rev1.pdf. Accessed: 08 December 2014.
- Sagan, L. (1967) On the Origin of Mitosing Cells, *Journal of Theoretical Biology*, **14**: 225 – 274.
- Salminen, A. & Kaarniranta, K. (2012) AMP-activated protein kinase (AMPK) controls the aging process via an integrated signaling network, *Ageing Research Reviews*, **11**: 230 – 241.

- Sanderson, M., Mazibuko, S.E., Joubert, E., de Beer, D., Johnson, R., Pfeiffer, C., Louw, J., Muller, C.J.F. (2014) Effects of fermented rooibos (*Aspalathus linearis*) on adipocyte differentiation, *Phytomedicine*, **21**: 109 – 117.
- Sandle, T. (2012) Pyrogens, Endotoxin and the LAL test: An Introduction in Relation to Pharmaceutical Processing, Global BioPharmaceutical Resources (GBPR) Inc., May 2012 Newsletter.
- Scalbert, A., Johnson, I.T., Saltmarsh, M. (2005) Polyphenols: antioxidants and beyond, *The American Journal of Clinical Nutrition*, **81**: 215S – 217S.
- Schäffler, A. & Schölmerich, J. (2010) Innate immunity and adipose tissue biology, *Trends in Immunology*, **31**: 228 – 235.
- Schapira, A.H.V. (2012) Mitochondrial diseases, *Lancet*, **379**: 1825 – 1834.
- Schon, E.A., DiMauro, S., Hirano, M. (2012) Human mitochondrial DNA: roles of inherited and somatic mutations, *Nature Reviews - Genetics*, **13**: 878 – 890.
- Schroeder, P., Gremmel, T., Berneburg, M., Krutmann, J. (2008) Partial depletion of mitochondrial DNA from human skin fibroblasts induces a gene expression profile reminiscent of photoaged skin, *The Journal of Investigative Dermatology*, **128**: 2297 – 2303.
- Schulz, H., Joubert, E., Schütze, W. (2003) Quantification of quality parameters for reliable evaluation of green rooibos (*Aspalathus linearis*), *European Food Research and Technology*, **216**: 539 – 543.
- Seo, A.Y., Joseph, A., Dutta, D., Hwang, J.C.Y., Aris, J.P., Leeuwenburgh, C. (2010) New insights into the role of mitochondria in aging : mitochondrial dynamics and more, *Journal of Cell Science*, **123**: 2533 – 2542.
- Sepe, A., Tchkonja, T., Thomou, T., Zamboni, M. & Kirkland, J.L. (2011) Aging and regional differences in fat cell progenitors - A mini-review, *Gerontology*, **57**: 66 – 75.
- Sigma-Aldrich (2015a) *JC-1*, Available: <http://www.sigmaaldrich.com/catalog/product/sigma/t4069?lang=en®ion=ZA>. Accessed: 03 January 2015.

- Sigma-Aldrich (2015b) *Propidium iodide*, Available: <http://www.sigmaaldrich.com/catalog/product/sigma/p4170?lang=en®ion=ZA>. Accessed: 03 January 2015.
- Sigma-Aldrich (2015c) *Trypan Blue*, Available: <http://www.sigmaaldrich.com/catalog/product/sigma/t6146?lang=en®ion=ZA>. Accessed: 03 January 2015.
- Singh, K.K. (2004) Mitochondria damage checkpoint in apoptosis and genome stability, *Federation of European Microbiological Societies (FEMS) Yeast Research*, **5**: 127 – 132.
- Siu, K.T., Rosner, M.R., Minella, A.C. (2012) An integrated view of cyclin E function and regulation, *Cell Cycle*, **11**: 57 – 64.
- Snijman, P.W., Joubert, E., Ferreira, D., Li, X.-C., Ding, Y., Green, I.R., Gelderblom, W.C. (2009) Antioxidant activity of the dihydrochalcones Aspalathin and Nothofagin and their corresponding flavones in relation to other Rooibos (*Aspalathus linearis*) Flavonoids, Epigallocatechin Gallate, and Trolox, *Journal of Agricultural and Food Chemistry*, **57**: 6678 – 6684.
- Soares, F., Guichardant, M., Cozzone, D., Bernoud-Hubac, N., Bouzaïdi-Tiali, N., Lagarde, M. (2005) Effects of oxidative stress on adiponectin secretion and lactate production in 3T3-L1 adipocytes, *Free Radical Biology & Medicine*, **38**: 882 – 889.
- Sohal, R.S., Mockett, R.J., Orr, W.C. (2002) Mechanisms of aging: an appraisal of the oxidative stress hypothesis, *Free Radical Biology & Medicine*, **33**: 575 – 586.
- Song, M.J., Kim, K.H., Yoon, J.M., Kim, J.B. (2006) Activation of Toll-like receptor 4 is associated with insulin resistance in adipocytes, *Biochemical and Biophysical Research Communications*, **346**: 739 – 745.
- South African National Biodiversity Institute (2007) *Aspalathus linearis* (Burm.f.) R. Dahlgren, Available: <http://www.plantzafrica.com/plantab/aspallinearis.htm>. Accessed: 06 December 2014.

- Spelbrink, J.N. (2010) Functional organization of mammalian mitochondrial DNA in nucleoids: history, recent developments, and future challenges, *International Union of Biochemistry and Molecular Biology (IUBMB) Life*, **62**: 19 – 32.
- Standley, L., Winterton, P., Marnewick, J.L., Gelderblom, W.C.A., Joubert, E., Britz, T.J. (2001) Influence of processing stages on antimutagenic and antioxidant potentials of rooibos tea, *Journal of Agricultural and Food Chemistry*, **49**: 114 – 117.
- Stankov, M.V., Das, A.M., Schmidt, R.E. (2007) Relationship of mitochondrial DNA depletion and respiratory chain activity in preadipocytes treated with nucleoside reverse transcriptase inhibitors, *Antiviral Therapy*, **12**: 205 – 216.
- Stankov, M.V, Lücke, T., Das, A.M., Schmidt, R.E., Behrens, G.M.N. (2010) Mitochondrial DNA depletion and respiratory chain activity in primary human subcutaneous adipocytes treated with nucleoside analogue reverse transcriptase inhibitors, *Antimicrobial Agents and Chemotherapy*, **54**: 280 – 287.
- Stats SA (Statistics South Africa) (2014) Mortality and causes of death in South Africa, 2013: findings from death notification - P0309.3, Pretoria, Statistics South Africa, Available: www.statssa.gov.za, Accessed: 10 January 2015.
- Strober, W. (1997) Trypan Blue Exclusion Test of Cell Viability, *Current Protocols in Immunology*, Appendix **3**: 2 – 3.
- Taylor, R.W. & Turnbull, D.M. (2005) Mitochondrial DNA mutations in human disease, *Nature Reviews - Genetics*, **6**: 389 – 402.
- Tchkonia, T., Morbeck, D.E., von Zglinicki, T., van Deursen, J., Lustgarten, J., Scrable, H., Khosla, S., Jensen, M.D., Kirkland, J.L. (2010) Fat tissue, aging, and cellular senescence, *Aging Cell*, **1**: 1 – 18.
- Thermo Scientific (2013) *Pierce® LAL Chromogenic Endotoxin Quantitation Kit*, Thermo Scientific, Thermo Fisher Scientific Inc. USA, Available: <https://www.piercenet.com/instructions/2162445.pdf>. Accessed: 12 November 2014.

- Thermo Scientific (2015) *Pierce® LAL Chromogenic Endotoxin Quantitation Kit reaction scheme*. Available: <http://www.piercenet.com/product/pierce-lal-chromogenic-endotoxin-quantitation-kit>. Accessed: 03 January 2015.
- The World Factbook (2013) *Central Intelligence Agency, USA*, Available: <https://www.cia.gov/library/publications/download/download-2013/index.html> Accessed: 04 January 2015.
- Trifunovic, A. & Larsson, N. (2008) Mitochondrial dysfunction as a cause of ageing, *Journal of Internal Medicine*, **263**: 167 – 178.
- Trinder, P. (1969) Determination of glucose in blood using glucose oxidase with an alternative oxygen acceptor, *Annals of Clinical Biochemistry: An International Journal of Biochemistry and Laboratory Medicine*, **6**: 24 – 27.
- Tullet, J., Araiz, C., Sanders, M., Au, C., Benedetto, A., Papatheodorou, I., Clark, E., Schmeisser, K. (2014) DAF-16/FoxO Directly Regulates an Atypical AMP-Activated Protein Kinase Gamma Isoform to Mediate the Effects of Insulin/IGF-1 Signaling on Aging in *Caenorhabditis elegans*, *PLoS Genetics*, **10**: e1004109.
- Twig, G., Hyde, B., Shirihai, O. (2008) Mitochondrial fusion, fission and autophagy as a quality control axis: The bioenergetic view, *Biochimica et Biophysica Acta (BBA) - Bioenergetics*, **1777**: 1092 – 1097.
- Ungvari, Z., Sonntag, W.E., de Cabo, R., Baur, J.A., Csiszar, A. (2011) Mitochondrial protection by resveratrol, *Exercise and Sports Sciences Reviews*, **39**: 128 – 132.
- Unger, R.H. (2005) Longevity, lipotoxicity and leptin: the adipocyte defense against feasting and famine, *Biochimie*, **87**: 57 – 64.
- van Heerden, F.R., van Wyk, B.-E., Viljoen, A.M., Steenkamp, P.A. (2003) Phenolic variation in wild populations of *Aspalathus linearis* (rooibos tea), *Biochemical Systematics and Ecology*, **31**: 885 – 895.

- van Niekerk, C. & Vijloen, A. (2008) Indigenous South African Medicinal Plants - Part 11: *Aspalathus linearis* ('Rooibos'), *South African Pharmaceutical Journal*, **75**: 41 – 42.
- Vannuvel, K., Renard, P., Raes, M., Arnould, T. (2013) Functional and morphological impact of ER stress on mitochondria, *Journal of Cellular Physiology*, **228**: 1802 – 1818.
- von Gadow, A., Joubert, E., Hansmann, C.F. (1997) Comparison of the antioxidant activity of Aspalathin with that of other plant phenols of rooibos tea (*Aspalathus linearis*), α -Tocopherol, BHT, and BHA, *Journal of Agricultural and Food Chemistry*, **45**: 632 – 638.
- Wallace, D.C. & Chalkia, D. (2013) Mitochondrial DNA Genetics and the Heteroplasmy Conundrum in Evolution and Disease, *Cold Spring Harbour Perspectives in Biology*, **5**: a021220.
- Wallace, D.C. (2005) A Mitochondrial Paradigm of Metabolic and Degenerative Diseases, Aging, and Cancer: A Dawn for Evolutionary Medicine, *Annual Review of Genetics*, **39**: 359.
- Wilson-Fritch, L., Burkart, A., Bell, G., Mendelson, K., Leszyk, J., Nicoloso, S., Czech, M., Corvera, S. (2003) Mitochondrial Biogenesis and Remodelling during Adipogenesis and in Response to the Insulin Sensitizer Rosiglitazone, *Molecular and Cellular Biology*, **3**: 1085 – 1094.
- Wisman, K.N., Perkins, A.A., Jeffers, M.D., Hagerman, A.E. (2008) Accurate assessment of the bioactivities of redox-active polyphenolics in cell culture, *Journal of Agricultural and Food Chemistry*, **56**: 7831 – 7837.
- Würthner, F., Kaiser, T.E., Saha-Möller, C.R. (2011) J-aggregates: from serendipitous discovery to supramolecular engineering of functional dye materials, *Angewandte Chemie (International ed. in English)*, **50**: 3376 – 3410.

- Yakes, F.M. & Van Houten, B. (1997) Mitochondrial DNA damage is more extensive and persists longer than nuclear DNA damage in human cells following oxidative stress, *Proceedings of the National Academy of Sciences of the United States of America*, **94**: 514 – 519.
- Yu, M., Shi, Y., Wei, X., Yang, Y., Zhou, Y., Hao, X., Zhang, N., Niu, R. (2007) Depletion of mitochondrial DNA by ethidium bromide treatment inhibits the proliferation and tumorigenesis of T47D human breast cancer cells, *Toxicology Letters*, **170**: 83 – 93.
- Yu, M. (2011) Generation, function and diagnostic value of mitochondrial DNA copy number alterations in human cancers, *Life Sciences*, **89**: 65 – 71.
- Zamboni, M., Rossi, A.P., Fantin, F., Zamboni, G., Chirumbolo, S., Zoico, E., Mazzali, G. (2014) Adipose tissue, diet and aging, *Mechanisms of Ageing and Development*, **136-137**: 129 – 137.
- Zamzami, N. (2000) Quantitation of mitochondrial transmembrane potential in cells and in isolated mitochondria, *Methods in Enzymology*, **322**: 208 – 213.
- Zen-Bio (2010) *3T3-L1 Cell Care Manual Maintenance and Differentiation of 3T3-L1 Preadipocytes to Adipocytes*, ZenBio, Inc. USA, Available: <http://www.zen-bio.com/pdf/ZBM0009.013T3L1CareprotocolRV08.08.pdf>. Accessed: 21 February 2013.
- Zu, L., He, J., Jiang, H., Xu, C., Pu, S., Xu, G. (2009) Bacterial endotoxin stimulates adipose lipolysis via toll-like receptor 4 and extracellular signal-regulated kinase pathway, *The Journal of Biological Chemistry*, **284**: 5915 – 5926.

APPENDIX I: Materials list

The following table lists the materials referred to in Chapter 3, as well as the relevant method and material sections 4.2 and 5.2. Consumables are listed according to the manufacturer, and product or catalogue numbers are provided.

| product | catalogue / product # |
|---|-----------------------|
| GE Healthcare Life Sciences (Logan, Utah, USA) | |
| HyClone™ DMEM (High glucose, with L-glutamine and sodium pyruvate) | SH30243 |
| HyClone™ DMEM (High glucose, with L-glutamine, without sodium pyruvate) | SH30249 |
| HyClone™ Foetal Bovine Serum | SV30160 |
| Lonza (Walkersville, MD, USA) | |
| BioWhittaker® Dulbecco's phosphate buffered saline (DPBS) with Ca ²⁺ and Mg ²⁺ | 17-513F |
| BioWhittaker® Dulbecco's phosphate buffered saline (DPBS) without Ca ²⁺ and Mg ²⁺ | 17-512F |
| Trypsin-EDTA | CC-5012 |
| Sigma-Aldrich (St. Louis, MO, USA) | |
| Penicillin / Streptomycin (P/S) | P4333 |
| Uridine | U3003 |
| Trypan blue | T6146 |
| Ethidium Bromide | E8751 |
| Phenol | P3653 |
| Glucose oxidase | G0543 |
| Lactate oxidase | L0638 |
| Peroxidase | P8375/8250 |
| 4-Aminoantipyrene | 06800 |
| JC-1 | T4069 |
| Valinomycin | V3639 |
| Thermo Scientific - Thermo Fisher Scientific (Logan, Utah, USA) | |
| Pierce® LAL Chromogenic Endotoxin Quantitation Kit | 88282 |
| Promega (Madison, WI, USA) | |
| CellTiter-Blue™ cell viability assay | G8081 |
| Beckman Coulter (CA, USA) | |
| Coulter® DNA Prep™ kit | 6607055 |
| Molecular Probes® - Life technologies - Thermo Fisher Scientific (Logan, Utah, USA) | |
| MitoTracker® Green FM | M7514 |
| Click-iT® EdU Alexa Fluor® 488 Kit | C-10425 |

APPENDIX II: Reagent preparation

The glucose oxidase and lactate oxidase assay reagents were prepared as follows:

| | |
|-------------------------|--|
| Phosphate buffer | Solution A (7 g NaH ₂ PO ₄ in 100 mL water) |
| | Solution B (18.4 g Na ₂ HPO ₄ in 400 mL water) |

Add 10 mL (A) to 40 mL (B) and dilute to final volume of 1.3 L (pH 7.4)

Assay reagent

Into 100 mL phosphate buffer add:

- 0.028 g phenol
- 0.008 g 4-aminoantipyrine
- 0.074 g EDTA
- 65 µL glucose oxidase
- 0.001 g peroxidase

Prepare fresh before use. Alternatively, store at 4°C and add enzymes just before use. The lactate oxidase assay reagent was prepared in exactly the same manner, the only difference being the substitution of the glucose oxidase enzyme for the lactate oxidase enzyme.

APPENDIX III: Project outputs and awards

International conferences:

Delivered as a poster presentation at the 62rd International Congress and Annual Meeting of the Society for Medicinal Plant and Natural Product Research (GA), in Portugal (September, 2014).

Hattingh, A., van De Venter, M., Joubert, E. & Koekemoer, T. (2014) The anti-ageing potential of Rooibos (*Aspalathus linearis*): Preserving preadipocyte function, *Planta Medica*, **80** (16).

National conferences:

Delivered as a poster presentation at the 17th annual conference of the Indigenous Plant Use Forum (IPUF) and received a Best poster presentation award (June, 2014).

Hattingh, A., van De Venter, M., Joubert, E. & Koekemoer, T. (2014) The anti-ageing potential of Rooibos (*Aspalathus linearis*): Preserving preadipocyte function, In *IPUF, 17th Annual Conference: Green Gold*, Available: http://www.uj.ac.za/EN/Faculties/science/departments/botany/research/ipuf/Documents/IPUF2014_PRogramme_and_abstracts.pdf

Others:

Delivered as an oral presentation, throughout the duration of this study, at the NMMU Masters and Doctoral (M&D) Research day to fellow students and academic staff members of the Department of Biochemistry, Microbiology and Physiology (2012, 2013 and 2014).

APPENDIX IV: Mitochondrial dysfunction and diseases

Since the first documented case of mitochondrial disease in 1962, numerous pathological conditions associated with mitochondrial dysfunction have been identified. Human mitochondrial diseases are an extremely diverse and complex group of diseases predominantly defined as any disease caused by alteration in oxidative phosphorylation (Chinnery, 2014; Lombès *et al.*, 2014). Mitochondrial diseases can present at any age and can affect multiple organ systems simultaneously, or present in a tissue specific manner within which different target cells may be involved - thereby creating an extremely diverse disease phenotype (Chinnery, 2014; Taylor & Turnbull, 2005, Nunnari & Suomalainen, 2012).

Mitochondrial diseases are extremely difficult to diagnose due to the considerable clinical variability caused by the numerous combinations of a myriad of symptoms, including: migraine, epilepsy, dementia, spasticity, dysphagia, cardiomyopathy, exercise intolerance, diabetes, thyroid disease, ptosis, optic atrophy, sensorineural deafness, as well as mid- and late stage pregnancy loss (Schapira, 2012; Alexeyev *et al.*, 2013; Chinnery, 2014). Currently only symptomatic treatment is available.

Etiology of disease is predominantly attributed to any number of mutations in mitochondrial and / or nuclear DNA implicated in mitochondrial function, and can therefore be inherited maternally, from an autosome, or X chromosome (Chinnery, 2014; Taylor & Turnbull, 2005, Nunnari & Suomalainen, 2012). Additionally, environmental factors can also contribute to mitochondrial disease as well as interact and intensify predisposed genetic risk factors (Meyer *et al.*, 2013). Changes in cellular energy demands, poor diet and lifestyle (excessive alcohol consumption, smoking and lack of exercise), as well as adverse side effects of drugs (Aminoglycoside antibiotics, doxorubicin, nucleoside analogue reverse transcriptase inhibitors (NRTI)) are just some environmental factors that can contribute to mitochondrial dysfunction and disease (Taylor & Turnbull, 2005; Wallace, 2013; Meyer *et al.*, 2013, Stankov, 2010; Greaves *et al.*, 2012)

mtDNA mutations:

Mutations in mtDNA, including: point mutations, rearrangements and deletions, are considered the primary cause of mitochondrial diseases, and more than 300 pathogenic mutations have been identified (Greaves *et al.*, 2011; Chinnery, 2014; Schapira, 2012). Mitochondrial point mutations and rearrangements are inherited maternally, whereas mtDNA deletions generally occur *de novo* and often due to mutations in nDNA encoding mitochondrial maintenance genes (Chinnery, 2014; Schapira, 2012). Somatic mutations caused by faulty repair or free radical mediated damage, also play an important role in mitochondrial disease and ageing (Schapira, 2012).

nDNA mutations:

Nuclear gene mutations can be inherited in an autosomal (recessive / dominant) or X-linked manner and have been implicated in mtDNA instability leading to alterations in: mtDNA content (deletion / depletion), structural subunits, as well as assembly and translation factors involved in mitochondrial function and maintenance (Nunnari & Suomalainen, 2012; Copeland & Longley, 2014; Chinnery, 2014). At least 13 nuclear genes affecting mtDNA stability have been identified in mitochondrial disease patients, most important of which is *POLG* which encodes the only replicative DNA polymerase known to function in the mitochondria, Pol γ (Copeland & Longley, 2014).

Pol γ is exclusively responsible for mtDNA replication and repair, therefore it is not surprising that any alteration in its function will have profound effects on mtDNA stability. Currently more than 200 mutations in *POLG* are associated with mitochondrial diseases, and spontaneous replication errors made by Pol γ account for almost all of the base substitutions in mtDNA (pathogenic or neutral variants), and subsequently contributes to mtDNA deletions and depletions that occur over time (Copeland & Longley, 2014). Accordingly Pol γ activity is also considered to be involved in the natural process of ageing (Copeland & Longley, 2014; Schapira, 2012).

Considering that tissues with a high energy demand such as the brain, heart, muscles, kidneys and endocrine systems are more commonly and severely affected by mitochondrial diseases, and that the same genetic mutation may not lead to the same disease phenotype in affected individuals, it becomes clear that the nature of the genetic mutation is not the only contributing factor to the clinically heterogeneous nature of mitochondrial diseases (Lombès *et al.*, 2014; Wallace & Chalkia, 2013). Factors such as the target tissues' metabolic requirements, capacity to subsequently develop compensatory responses as well as the heteroplasmic nature of mtDNA should also be considered (Lombès *et al.*, 2014; Wallace & Chalkia, 2013).

In conclusion, the definition of mitochondrial disease has been extended to include any disease associated with alterations in any mitochondrial component since mitochondrial dysfunction has also been implicated in many other acquired and age related diseases such as: diabetes, cancer, neurodegenerative diseases (Huntington's, Alzheimer's and Parkinson's) cardiovascular disease, atherosclerosis, as well as the general process of ageing and senescence (Schapira, 2012; Alexeyev *et al.*, 2013). Therefore, when considering the strong antioxidant properties of plant phenolic compounds as well as their capacity to influence various signal transduction pathways, together with the significance of oxidative stress etc. on mitochondrial dysfunction, a clear direction for various prospective studies can be identified.

References:

- Alexeyev, M., Shokolenko, I., Wilson, G. & LeDoux, S. (2013) The maintenance of mitochondrial DNA integrity--critical analysis and update, *Cold Spring Harbor Perspectives in Biology*, **5**: a012641.
- Chinnery, P.F. (2014) Mitochondrial Disorders Overview, In: *GeneReviews*[®] [Internet], Pagon, R.A., Adam, M.P., Ardinger, H.H. *et al.*, Editors, Available: <http://www.ncbi.nlm.nih.gov/books/NBK1224/?report=reader>. Accessed: 26 September 2014.
- Copeland, W.C. & Longley, M.J. (2014) Mitochondrial genome maintenance in health and disease, *DNA Repair*, **19**: 190 – 198.

- Greaves, L.C., Reeve, A.K., Taylor, R.W., Turnbull, D.M. (2012) Mitochondrial DNA and disease, *The Journal of pathology*, **226**: 274 – 286.
- Lombès, A., Auré, K., Bellanné-Chantelot, C., Gilleron, M., Jardel, C. (2014) Unsolved issues related to human mitochondrial diseases, *Biochimie*, **100**: 171 – 176.
- Meyer, J.N., Leung, M.C.K., Rooney, J.P., Sendoel, A., Hengartner, M.O., Kisby, G.E., Bess, A.S. (2013) Mitochondria as a target of environmental toxicants, *Toxicological Sciences*, **134**: 1 – 17.
- Nunnari, J. & Suomalainen, A. (2012) Mitochondria: in sickness and in health, *Cell*, **148**: 1145 – 1159.
- Schapira, A.H.V. (2012) Mitochondrial diseases, *Lancet*, **379**: 1825 – 1834.
- Stankov, M., Lücke, T., Das, A.M., Schmidt, R.E., Behrens, G.M.N. (2010) Mitochondrial DNA depletion and respiratory chain activity in primary human subcutaneous adipocytes treated with nucleoside analogue reverse transcriptase inhibitors, *Antimicrobial Agents and Chemotherapy*, **54**: 280 – 287.
- Taylor, R.W. & Turnbull, D.M. (2007) Mitochondrial DNA mutations in human disease, *Europe PubMed Central (PMC) Funders Group*, **6**: 389 – 402.
- Wallace, D.C. (2013) Science in medicine: A mitochondrial bioenergetic etiology of disease, *Journal of Clinical Investigation*, **123**: 1405 – 1412.
- Wallace, D.C. & Chalkia, D. (2013) Mitochondrial DNA genetics and the heteroplasmy conundrum in evolution and disease, *Cold Spring Harbor Perspectives in Biology*, **5**: a021220 – a021220.